Titre: Title:	Exploring the Impact of Anatomical References for Quantifying Spinal Cord Morphometrics Using Magnetic Resonance Imaging
Auteur: Author:	Sandrine Bédard
Date:	2024
Type:	Mémoire ou thèse / Dissertation or Thesis
Référence: Citation:	Bédard, S. (2024). Exploring the Impact of Anatomical References for Quantifying Spinal Cord Morphometrics Using Magnetic Resonance Imaging [Master's thesis, Polytechnique Montréal]. PolyPublie. https://publications.polymtl.ca/58308/

URL de PolyPublie: PolyPublie URL:	https://publications.polymtl.ca/58308/
Directeurs de recherche: Advisors:	Julien Cohen-Adad
Programme: Program:	Génie biomédical

POLYTECHNIQUE MONTRÉAL
affiliée à l'Université de Montréal

Exploring the impact of anatomical references for quantifying spinal cord morphometrics using magnetic resonance imaging

SANDRINE BÉDARD
Institut de génie biomédical

Mémoire présenté en vue de l'obtention du diplôme de *Maîtrise ès sciences appliquées*
Génie biomédical
Avril 2024

POLYTECHNIQUE MONTRÉAL
affiliée à l'Université de Montréal

Ce mémoire intitulé :

Exploring the impact of anatomical references for quantifying spinal cord morphometrics using magnetic resonance imaging

présenté par **Sandrine BÉDARD**
en vue de l'obtention du diplôme de *Maîtrise ès sciences appliquées*
a été dûment accepté par le jury d'examen constitué de :

Marco BONIZZATO, président
Julien COHEN-ADAD, membre et directeur de recherche
Josefina MARANZANO, membre externe

ACKNOWLEDGEMENTS

I would first like to thank my director, Julien Cohen-Adad, for all his help, his advice, his encouragement, and mainly his trust. During my degree, I learned a lot, and have grown into a confident young researcher, and this, particularly because of Julien! I would also like to thank my colleagues at Neuropoly Lab, particularly Jan Valošek and Naga Kartik, with whom I collaborated closely in various projects. I would like to thank all my other colleagues for their support and contributions: Nathan Molinier, Nilser Laines Medina, Uzay Macar, Joshua Newton, Nick Guenther, Alexandru Foias, Charley Gros, Andjela Dimitrijevic, Nadia Blostein, Alexandre D'Astous, Mathieu Guay-Paquet, and Daniel Papp.

During my master's, I had the opportunity to do a 5-month internship at Stanford's Systems Neuroscience and Pain Lab. I would like to thank my supervisor, Kenneth Weber for his advice, his kindness and trust. I would like to thank my other colleagues Valeria Oliva, Merve Kaptan, Dario Pfyffer, and Christine Law, who made this experience memorable and enriching for me.

I would also like to thank Marco Bonizzato and Josefina Maranzano for being a part of my master's thesis jury. I thank all the funding agencies that supported my master's degree and internship at Stanford: FRQNT, NSERC, Maxime Fortin, and Fondation et Alumni de Polytechnique Montréal, Polytechnique Montréal International, and the Quebec Bio-imaging Network.

Thank you to all my friends from the cross-country ski club for their support, for listening, and for motivating me to stay active! Thank you to my parents for their constant encouragement and daily support. Thank you to my father for all his advice and discussions about my projects and particularly about statistics. Thank you to my sisters, Aurélie and Éliane, for their support and distraction. Thank you to Paul for his advice and daily support.

RÉSUMÉ

Contexte: L'évaluation de l'atrophie de la moelle épinière par l'analyse de sa morphologie est pertinente pour comprendre diverses pathologies neurodégénératives, telles que la sclérose en plaques. Un indicateur clé de cette dégénérescence est l'aire de la section transversale de la moelle épinière, mesurable via l'imagerie par résonance magnétique (IRM). Toutefois, cette mesure possède une importante variabilité inter-individuelle, limitant son utilité comme biomarqueur. Habituellement, l'aire de la section transversale est calculée en référence à un niveau vertébral précis, facilitant ainsi les comparaisons temporelles et inter-individuelles. Cependant, l'approximation des niveaux spinaux par les niveaux vertébraux n'est pas précise, augmentant la variabilité des mesures d'aire de section transversale. Bien que d'autres points de référence, tels que le sillon ponto-médullaire, aient été suggérés, ils n'ont jamais été utilisé pour mesurer l'aire de la section transversale.

Objectif: Ce projet vise à élaborer une méthode automatique pour le calcul de l'aire de la section transversale de la moelle épinière en se référant au sillon ponto-médullaire. Plus précisément, nous développons un pipeline automatique permettant de déterminer l'aire de section trasnversale à une distance spécifique du sillon ponto-médullaire, et évaluons l'efficacité de cette nouvelle référence pour minimiser la variabilité inter-individuelle dans un vaste ensemble d'images IRM de sujets sains. Ensuite, nous étudions la contribution de divers facteurs confondants sur la variabilité de l'aire de la section transversale. Finalement, nous mesurons l'impact de cette nouvelle référence sur la variabilité intra-individuelle, avec différentes positions du cou, sur des images IRM structurelles.

Méthodes: Tout d'abord, un pipeline automatique a été développé pour calculer l'aire de la section transversale à une distance définie du sillon ponto-médullaire, calculée le long de la ligne centrale de la moelle épinière. Cette méthode a été appliquée sur un large échantillon d'images IRM pondérée T1 de la base de données UK Biobank (n = 804). Nous avons comparé l'aire de la section transversale obtenue avec celle calculée en se référant aux niveaux vertébraux C2-C3, et exploré divers facteurs confondants afin d'établir un modèle de normalisation.

Ensuite, nous avons évalué la pertinence de l'aire de section transversale basée sur le sillon ponto-médullaire dans un contexte d'étude longitudinale. Pour ce faire, nous avons acquis des images pondérées T2 de haute résolution sur 10 adultes sains avec 3 différentes positions du cou. Les niveaux spinaux ont été manuellement annotés en se basant sur les racines nerveuses spinales. Nous avons comparé l'estimation de la position des niveaux spinaux en

utilisant le sillon ponto-médullaire vs les niveaux vertébraux. Ensuite, pour quantifier la variabilité intra-individuelle, nous avons calculé l'aire de section transversale en utilisant 3 références: le sillon ponto-médullaire, les niveaux vertébraux et les niveaux spinaux.

Résultats: La variabilité inter-individuelle de l'aire de section transversale sur les images du UK Biobank était de 10,09 % basée sur le sillon ponto-médullaire et de 9,96 % basée sur les niveaux vertébraux C2-C3. Pour les deux références, le volume du thalamus, le volume cérébral, le sexe et l'interaction entre le volume cérébral et le sexe contribuaient significativement à la variabilité de l'aire de section transversale. La variabilité intra-individuelle de l'aire de section transversale entre les positions du cou était de 3,99 ± 2,96 % basée sur le sillon ponto-médullaire vs 4,02 ± 3,01 % basée sur les niveaux spinaux manuels vs 4,46 ± 3,10 % basée sur niveaux vertébraux, sans différence significative entre les méthodes. L'écart-type de l'estimation de la position des niveaux spinaux était de 1,06 ± 0,33 mm avec le sillon ponto-médullaire par rapport à 1,40 ± 0,26 mm avec les niveaux vertébraux, sans différence significative.

Conclusions: Dans cette étude, nous avons développé un pipeline automatique pour calculer l'aire de section transversale de la moelle épinière en prenant comme référence le sillon ponto-médullaire. Son utilisation n'a pas montré de différence de variabilité inter- et intra-individuelle de l'aire de section transversale par rapport aux niveaux vertébraux. Utiliser le sillon ponto-médullaire pourrait servir d'alternative aux niveaux vertébraux dans les cas où l'identification des vertèbres est difficile, notamment pour des patients avec des fusions vertébrales ou des malformations. Cependant, des recherches supplémentaires sont nécessaires pour identifier fiablement et automatiquement les niveaux spinaux. Une telle méthdode pourrait être bénéfique non seulement pour le calcul de l'aire de section transversale, mais aussi pour les analyses de groupe en IRM fonctionnelle et pour la normalisation des images vers un espace standard.

ABSTRACT

Context: Analysing the shape of the spinal cord is relevant to assess atrophy in various neurodegenerative diseases like multiple sclerosis. Typically, spinal cord cross-sectional area (CSA), derived from magnetic resonance imaging (MRI), is computed as a measure of atrophy and is a relevant biomarker. However, spinal cord CSA suffers from considerable inter-subject variability limiting its use. CSA is typically computed in reference to a specific vertebral level to infer the positions of the spinal levels and allowing comparison through time and individuals. However, the vertebral levels do not provide a precise estimation of the spinal levels, contributing to the observed CSA variability. Other references were proposed to bypass the use of the vertebral levels like the pontomedullary junction (PMJ), but were never used to compute CSA.

Objective: The main goal of this project is to develop an automatic pipeline to compute CSA using the PMJ as a reference and to validate its relevance to reduce CSA variability. More precisely, we develop an automatic pipeline to compute CSA using a new reference part of the central nervous system, the PMJ, instead of the vertebral levels. We first investigate the relevance of using the PMJ as a reference for CSA computation to reduce inter-subject variability. To do so, we use a large dataset of healthy controls, and we examine additional factors that contribute to CSA variability. Then, we explore the relevance of PMJ-based CSA on intra-subject variability by varying neck positions.

Methods: First, we developed an automatic pipeline to compute spinal cord CSA at a specified distance from the PMJ, measured along the spinal cord centerline using arc-length. The method was applied to T1-weighted MRI images from a subset of the UK Biobank database (n = 804). PMJ-based CSA was compared to CSA computed at the C2-C3 vertebral levels. We explored other confounding factors contributing to CSA variability and developed a normalization model.

Second, we evaluated the relevance of PMJ-based CSA in a longitudinal context. To do so, we acquired high resolution T2-weighted MRI images on 10 healthy adult volunteers with 3 neck positions. The spinal levels were manually labeled using the spinal nerve rootlets. We estimated their position using the PMJ vs. vertebral levels. We also computed CSA using 3 different references – the PMJ, vertebral levels, spinal levels – to assess intra-subject variability.

Results: In images from the UK Biobank, spinal cord CSA inter-subject variability was 10.09 % for PMJ-based CSA compared to 9.96 % for CSA at C2-C3 vertebral levels. Regression

analysis revealed that thalamus volume, brain volume, sex, and the interaction between brain volume and sex significantly contributed to CSA variability for both references. Intra-subject variability across neck positions was 3.99 ± 2.96 % for PMJ-based CSA, 4.02 ± 3.01 % for manual spinal-based CSA, and 4.46 ± 3.10 % for vertebral-based CSA, with no significant differences observed. The estimated position of the spinal segment across neck position had a standard deviation of 1.06 ± 0.33 mm using the PMJ compared to 1.40 ± 0.26 mm using the vertebral levels. However, statistical analysis showed no significant difference.

Conclusions: In this study, we developed an automatic pipeline to compute spinal cord CSA at a specified distance from the PMJ. This approach did not show any significant differences in terms of inter- and intra-subject variability compared to CSA measurements based on vertebral levels. Using the PMJ to measure spinal cord CSA could serve as a valuable alternative to the vertebral levels in cases where identifying the vertebrae is more challenging, such as in patients with spinal fusions or malformations. Further research is needed to develop other automatic and reliable spinal segment identification methods. This holds potential not only for CSA computation but also for broader applications such as functional MRI group-level analysis and image spatial normalization.

TABLE OF CONTENTS

ACKNOWLEDGEMENTS iii

RÉSUMÉ iv

ABSTRACT vi

TABLE OF CONTENTS viii

LIST OF TABLES xi

LIST OF FIGURES xii

LIST OF SYMBOLS AND ACRONYMS xv

LIST OF APPENDICES xvi

CHAPTER 1 INTRODUCTION 1
- 1.1 Problematic 1
- 1.2 Research Objectives 2
- 1.3 Thesis Outline 3

CHAPTER 2 LITERATURE REVIEW 4
- 2.1 Spine and Spinal Cord Anatomy 4
  - 2.1.1 Spinal Cord and Nerve Rootlets 4
  - 2.1.2 Spinal Cord Morphometry 7
- 2.2 Imaging the Spinal Cord with MRI 9
- 2.3 Cross-sectional Area (CSA) 10
  - 2.3.1 Computing CSA with MRI 10
  - 2.3.2 Sources of CSA variability 12
  - 2.3.3 Normalization Methods 14

CHAPTER 3 METHODS 16
- 3.1 Objective 1: Develop a PMJ-based Approach for CSA Computation 16
- 3.2 Objective 2: Quantify Inter-subject Variability of PMJ-based CSA 16
- 3.3 Objective 3: Quantify Intra-subject Variability of PMJ-based CSA 16
- 3.4 Scientific Publications 17

CHAPTER 4 ARTICLE 1: AUTOMATIC MEASURE AND NORMALIZATION OF SPINAL CORD CROSS-SECTIONAL AREA USING THE PONTOMEDULLARY JUNCTION 18
4.1 Introduction 19
4.2 Material and methods 21
4.2.1 Demography 21
4.2.2 Image acquisition 22
4.2.3 Data processing 22
4.2.4 Quality control 25
4.2.5 Statistical Analyses 25
4.3 Results 27
4.3.1 Spinal cord CSA 27
4.3.2 Statistical Analyses 28
4.3.3 Normalization 32
4.4 Discussion 35
4.4.1 CSA results 35
4.4.2 PMJ-based CSA method 36
4.4.3 Correlation with spinal cord CSA 37
4.4.4 Normalization methods 38
4.4.5 SCT normalization feature 40
4.5 Conclusions 40
4.6 Acknowledgements 41
4.7 Conflict of Interest 41
4.8 Supplementary Material 41
4.8.1 Supplementary Figures and Tables 41

CHAPTER 5 ARTICLE 2: PONTOMEDULLARY JUNCTION AS A REFERENCE FOR SPINAL CORD CROSS-SECTIONAL AREA: VALIDATION ACROSS NECK POSITIONS 47
5.1 Introduction 48
5.2 Material and Methods 49
5.2.1 Data processing 50
5.3 Results 54
5.3.1 Spinal segment labeling 54
5.3.2 Distance with PMJ, spinal segment and discs 54
5.3.3 CSA computation 57

5.3.4 Neck angle . . . 59
5.4 Discussion . . . 59
5.4.1 Spinal segment manual labeling . . . 60
5.4.2 Distance with PMJ, spinal segments and discs . . . 60
5.4.3 CSA computation . . . 60
5.4.4 Limitations & Perspective . . . 61
5.5 Conclusion . . . 61
5.6 Acknowledgements . . . 62
5.7 Author contributions . . . 62
5.8 Data availability statement . . . 62
5.9 Additional Information . . . 63
5.9.1 Competing interests . . . 63
5.10 Supplementary material . . . 63

CHAPTER 6 GENERAL DISCUSSION . . . 68
6.1 Research Objectives & Hypotheses . . . 68
6.2 PMJ based-CSA Method . . . 68
6.3 CSA Measurements . . . 69
6.4 Impact of PMJ Reference on CSA Variability . . . 70
6.5 Spinal Segment Labeling . . . 71
6.6 Data and Code Availability . . . 72
6.7 Perspectives . . . 72

CHAPTER 7 CONCLUSION . . . 73
7.1 Summary of Works . . . 73
7.2 Limitations . . . 73
7.3 Future Research . . . 74

REFERENCES . . . 75

APPENDICES . . . 89

LIST OF TABLES

Table 4.1	Pearson's correlation among spinal cord CSA, physical and brain measures.	29
Table 4.2	Multilinear Regression Analysis for spinal cord CSA(PMJ) (N = 804 participants).	31
Table 4.3	Multilinear Regression Analysis for spinal cord CSA(C2-C3) (N=804 participants).	32
Table 5.1	STD of distance between spinal segments and PMJ or discs per level.	56
Table 5.2	Paired Two-way ANOVA of STD of distance PMJ-spinal segment and disc-spinal segment across neck positions.	56
Table 5.3	Mean COV of CSA per level across participants using PMJ, spinal segments and Discs as a reference and averaged on 3 slices.	58
Table 5.4	Paired Three-way ANOVA on spinal cord CSA.	59
Table 5.5	Spinal cord CSA results across neck positions per method and level.	66
Table 5.6	Neck angle of the 3 neck positions per participant.	66
Table 5.7	Correlation between neck angle variation and variation of distance of the spinal segment and PMJ/discs between neck flexion and extension.	66
Table 5.8	Correlation between neck angle variation and distance of the spinal segment variation between neck flexion and extension for PMJ and discs per level.	67

LIST OF FIGURES

Figure 2.1 Spinal cord morphology. Illustration of the spinal segments and nerve rootlets with their exit through the intervertebral foramina. Adapted from https://nba.uth.tmc.edu/neuroscience/m/s2/chapter03.html . . 5

Figure 2.2 T2w image and illustration of spinal cord, vertebrae, nerve rootlets, and PMJ. (A) illustrate the spinal segment C3 delimited from the rostral-caudal nerve rootlets. 6

Figure 2.3 CSA measures across vertebral levels. 7

Figure 2.4 Cross section of the spinal cord in the PAM50 T1w MRI template for various spinal levels. 8

Figure 2.5 Example of an image affected by gradient non-linearity distortion (A) and the same image after correction (B). Notice the bottom part of the image, where the integrity of the spinal cord shape is recovered in the corrected image. 11

Figure 2.6 Spinal cord CSA measurement at C2-C3 vertebral levels. 11

Figure 4.1 Overview of the processing pipeline. Correction for gradient non-linearities was applied on the T1w image and spinal cord was segmented automatically. Vertebral levels were identified and spinal cord CSA was computed at C2-C3 levels. The PMJ was labeled and the centerline was extracted to compute spinal cord CSA from the PMJ . 23

Figure 4.2 **a)** spinal cord centerline from PMJ. The spinal cord centerline was extracted from spinal cord segmentation and the PMJ label using linear interpolation and smoothing. The distance from PMJ is measured along the centerline following the arc-length. **b)** Extent mask to average spinal cord CSA. At 64 mm from PMJ, CSA was computed slice-wise, corrected for angulation and averaged within a 20 mm extent. The extent mask is centered at 64 mm from PMJ. 24

Figure 4.3 **a)** Scatterplot of PMJ-based CSA at 64 mm and vertebral-based CSA at C2-C3 vertebral levels. **b)** Scatterplot of the distance between the PMJ and the C2-C3 disc. 28

Figure 4.4 **A)** Violin plot of spinal cord CSA at 64 mm from the PMJ for female and male with mean (μ) and STD (σ) for each sex. **B)** Violin plot of spinal cord CSA at C2-C3 disc for female and male with mean (μ) and STD (σ) for each sex. 30

Figure 4.5 **A)** Linear fit for CSA at 64 mm from the PMJ as a function of age. **B)** Linear fit for CSA at C2-C3 disc as a function of age. 31
Figure 4.6 Scatterplots of CSA(PMJ) as a function of brain volume and thalamus volume separated for sex with linear fit. 34
Figure 4.7 Scatterplots of CSA(C2-C3) as a function of brain volume and thalamus volume separated for sex with linear fit. 35
Figure 4.8 Scatterplot of CSA at 64 mm from the PMJ as a function of age. . . 42
Figure 4.9 Scatterplot of CSA at 64 mm from the PMJ as a function of brain GM volume. 42
Figure 4.10 Scatterplot of CSA at 64 mm from the PMJ as a function of brain WM volume. 43
Figure 4.11 Scatterplot of CSA at 64 mm from the PMJ as a function of brain volume. 43
Figure 4.12 Scatterplot of CSA at 64 mm from the PMJ as a function of brain volume normalized for head size. 44
Figure 4.13 Scatterplot of CSA at 64 mm from the PMJ as a function of height. . 44
Figure 4.14 Scatterplot of CSA at 64 mm from the PMJ as a function of weight. . 45
Figure 4.15 Scatterplot of CSA at 64 mm from the PMJ as a function of thalamus volume. 45
Figure 4.16 Scatterplot of CSA at 64 mm from the PMJ as a function of ventricular CSF volume 46
Figure 4.17 Scatterplot of CSA at 64 mm from the PMJ as a function of Vscale . 46
Figure 5.1 Example of the head positioning in the MRI's head coil for neck extension **(A)**, neutral **(B)** and flexion **(C)**. The bottom row shows localizers. (One of the authors is in the scanner). 50
Figure 5.2 Spinal segment labeling pipeline. **(1)** spinal cord centerline is detected, **(2)** spinal cord is straightened, **(3)** denoised, and manually labeled in the coronal view. **(4)** The inverse transformation is applied on the labels. The distances between the PMJ and each spinal segment (green), and between each spinal segment and corresponding disc (pink) were computed. 51
Figure 5.3 Spinal cord CSA computed with 3 references: **(A)** mean distance of each spinal rootlet from participant's PMJ, **(B)** each spinal segment, **(C)** each intervertebral disc. 53

Figure 5.4 Example of challenging **(A)** and easy **(B)** spinal segment labeling in the straightened space in two representative participants. In the more challenging participants, motion and CSF flow likely contributed to the less apparent nerve rootlets. 55

Figure 5.5 Boxplots (25-75 percentiles) of STD across neck positions per participant of the distance between the spinal segment and PMJ (green) and spinal segment and corresponding discs (yellow). Green triangles show the mean and gray diamonds outliers. No post-hoc analysis was performed beyond the ANOVA described in Table 5.4. 57

Figure 5.6 Boxplot of CSA COV per level based on discs C1-C2 to C7-T1, on spinal segments C2 to C8, and on the mean distance between the PMJ and each spinal segment. Green triangles represent the mean, and gray diamonds represent outliers. 58

Figure 5.7 Neck angle measurement. The neck angle was computed in the right-left direction between the C1-C2 and C4-C5 intervertebral discs. . . . 64

Figure 5.8 STD across neck positions of the distance between the PMJ and spinal segments (a) and between each disc and spinal segment (b) per participant. 64

Figure 5.9 a) Scatterplot of COV of CSA perlevel based on intervertebral discs C1-C2 to C7-T1. b) Scatterplot of COV of CSA per level based on spinal segments C3 to T1. c) Scatterplot of COV of CSA per level based on the mean distance between the PMJ and each spinal segment. CSA is averaged on 3 slices. 65

Figure 5.10 Each dot corresponds to a participant position and angle. For each participant, we calculated the angle between the spinal cord centerline at C2-C3 and C4-C5 levels, and we took the difference of that angle between the neck extension and flexion: this is what is represented in the abscissa. The ordinate represents the difference of distance, between extension and flexion, between the PMJ and the corresponding spinal segment (PMJ-segment C2 ; PMJ-segment C3, etc.) (a) and the difference of distance between the corresponding disc and the corresponding spinal segment (disc C2 - segment C2; disc C3 - segment C3, etc.) (b). 65

LIST OF SYMBOLS AND ACRONYMS

BMI	Body Mass Index
COV	Coefficient of Variation
CSA	Cross-Sectional Area
CSF	Cerebrospinal Fluid
GM	Gray Matter
MRI	Magnetic Resonnance Imaging
MS	Multiple Sclerosis
PMJ	Pontomedullary Junction
SCT	Spinal Cord Toolbox
STD	Standard Deviation
T1w	T1-weighted
T2w	T2-weighted
Vscale	Scaling factor for brain normalization due to differences in head size (SIENAX)
WM	White Matter

LIST OF APPENDICES

Appendix A MY CONTRIBUTIONS 89

CHAPTER 1 INTRODUCTION

Various neurodegenerative diseases, such as multiple sclerosis (MS), manifest through a series of distinct pathological changes, such as the degeneration of myelin, neurons, and axons, leading to the atrophy of the spinal cord. [1–3]. MS is a leading cause of non-traumatic disability in young adults and affects about 90 000 Canadians (2020) [4, 5]. Magnetic resonance imaging (MRI) provides a reliable and non-invasive technique for visualizing soft tissues, such as the spinal cord. From MRI, quantitative measurements like spinal cord cross-sectional area (CSA) can be derived. Specifically, CSA of the upper cervical spinal cord holds significant value for the prognosis and monitoring of MS. There is a notable correlation between spinal cord atrophy and clinical outcomes, particularly the severity of disability and the progression of the disease [6, 7].

1.1 Problematic

Changes in spinal cord CSA typically occur at a very slow rate, approximately 2 % per year, making it challenging to detect minor variations during the early stages of the disease and over brief periods of time. Furthermore, the utility of spinal cord CSA measurements is currently limited by considerable variability observed among healthy individuals, with differences reported to be between 7.5 % and 10 % [8–12]. Research efforts have elucidated that certain demographic factors, notably sex, significantly contribute to this observed variability [9, 10, 13]. Moreover, factors related to MRI acquisition protocols, MRI contrast, MRI vendor, and segmentation methods, further contribute to CSA variability [13–15].

To compare CSA measurements across time and individuals, it is important to determine the location of the measurements and to use a common referential. Typically, CSA is computed using the vertebral levels as a reference, such as C2-C3 vertebral levels. However, the vertebral levels do not precisely align with the spinal levels, leading to potential inaccuracies in identifying the positions of the spinal segments, thus contributing to CSA variability [16]. Additionally, head flexion and extension were shown to vary the correspondence between vertebral and spinal levels. Although labeling the spinal nerve rootlets to identify the spinal levels could offer a more accurate approach, this method is limited by the requirement for high-resolution MRI scans and an expert-rater.

Previous studies have introduced other anatomical references to bypass the use of the vertebral levels, such as the pontomedullary junction (PMJ) [16–18] or the conus medullaris [19].

However, these alternatives references have never been used for CSA measurement.

Overall, reducing CSA variability is important to increase sensitivity of CSA as a biomarker, and to decrease the required sample size for detecting atrophy in cross-sectional studies [20].

1.2 Research Objectives

The main objective of this project is to evaluate the impact of using the PMJ as an anatomical reference for spinal cord CSA measurements on CSA variability.

Hypothesis: The PMJ, as part of the central nervous system, will provide more precise estimations of the spinal levels than the traditional vertebral level reference.

The specific objectives of this study include:

- **(O1)**: Develop an automatic pipeline for computing CSA in MRI images using the PMJ as a reference.
  - **(H1.1)**: The automatic measurement of arc-length distance from the PMJ will yield a more accurate estimation of spinal levels than the vertebral levels for CSA computation.
- **(O2)**: Assess the impact of using the PMJ as a reference for CSA computation in comparison to the vertebral levels on CSA inter-subject variability.
  - **(H2.1)**: The anatomical reference of vertebral levels contributes to inter-subject variability in CSA measurements.
  - **(H2.2)**: Using the PMJ as a reference for CSA measurements is expected to reduce CSA inter-subject variability compared to the vertebral levels.
- **(O3)**: Quantify the impact of using the PMJ as a reference for CSA measurements on CSA intra-subject variability across different neck positions compared to the vertebral levels and manual spinal segments.
  - **(H3.1)**: Using the PMJ as a reference will increase the reproducibility of CSA measurements across different neck positions within individuals, in contrast to vertebral levels.

1.3 Thesis Outline

The chapters of this thesis are organized as follows. **Chapter 2** presents a literature review exploring various factors contributing to CSA variability, **Chapter3** presents the chosen methodology, **Chapter 4** presents the article on the normalization of CSA using the PMJ as a reference to reduce inter-subject variability, **Chapter 5** presents an article exploring the relevance of the PMJ as a reference for CSA measurements in the context of varying neck positions. **Chapter 6** presents a global discussion of results, and **Chapter 7** discusses future steps and concludes.

CHAPTER 2 LITERATURE REVIEW

2.1 Spine and Spinal Cord Anatomy

2.1.1 Spinal Cord and Nerve Rootlets

The spinal cord is an organized cylindrical structure located in the spinal canal and part of the central nervous system. It elongates from the medulla oblongata through the foramen magnum at the base of the skull [21]. **Figure 2.1** provides a visual representation of the spinal cord, nerve rootlets, and vertebrae.

The spinal cord is organized in 31 spinal segments: 8 cervical, 12 thoracic, 5 lumbar, 5 sacral and 1 coccygeal segments [21]. These spinal segments correspond specifically with the topology of motor efference and sensory afference. For each spinal cord segment, a pair of spinal nerves, consisting of dorsal and ventral rootlets, emerge from the spinal cord and exit through the intervertebral foramina (**Figure 2.1**). Ventral nerve rootlets, carrying motor neuron axons, exit the spinal cord via the anterolateral sulcus. Dorsal nerve rootlets, carrying sensory neuron axons, emerge from the posterolateral sulcus [22]. Interestingly, the presence of the C1 dorsal nerve rootlets varies among individuals [23, 24]. A spinal cord segment is defined by the entry points of the nerve rootlets, ranging from the most rostral to the most caudal rootlets of that level, as illustrated in **Figure 2.2**. At the C2 cervical level, the nerve rootlets emerge almost perpendicularly from the spinal cord and angle downward progressively in lower segments [25]. Additionally, at lower levels, the rootlets tend to overlap with one another, further complicating the identification of specific spinal levels.

The spinal cord is composed mainly of two different tissue types: white matter (WM) and gray matter (GM). Unlike in the brain, the spinal cord's WM is located at the periphery, with GM centrally positioned in a "butterfly" shape. WM is mainly composed of ascending and descending myelinated axons and GM is mainly composed of neuron cell bodies. In the GM, we can distinguish ventral and dorsal horns [4].

The spinal cord is surrounded by the pia mater, the arachnoid mater, and the dura mater. It is also protected by the vertebral column. For flexibility, the column is divided into 7 cervical, 12 thoracic and 5 lumbar bony segments. On average, in adults, the spinal cord terminates at vertebral levels L1-L2, although the caudal termination of the spinal cord relative to the vertebrae varies among individuals [22, 26, 27].

There is a correspondence between vertebral and spinal segments: spinal nerves of each spinal

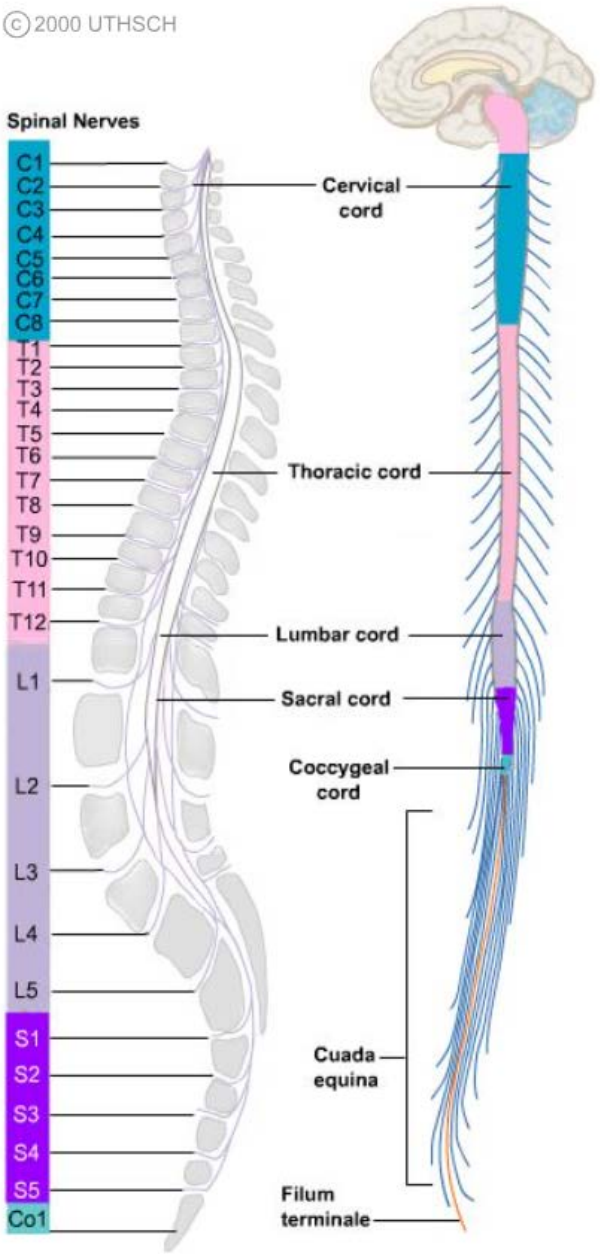

Figure 2.1 Spinal cord morphology. Illustration of the spinal segments and nerve rootlets with their exit through the intervertebral foramina. Adapted from https://nba.uth.tmc.edu/neuroscience/m/s2/chapter03.html

segment enter the intervertebral foramina adjacent to the caudal end of each vertebral body as illustrated in **Figure 2.2**. The position of a spinal segment is typically estimated using its rostral vertebral body [28]. For example, in **Figure 2.2**, the spinal level C4 is rostral to the C4 vertebral body.

However, significant inter-subject variability exists in the relative positioning between vertebral and spinal segments [16]. To address this limitation, several normalization strategies were introduced. Frostell et al. introduced a normalization strategy that defines the relative positioning of spinal and vertebral segments using the distance from the C3 vertebral level to the C3 spinal level and the end of the spinal cord [29]. Other landmarks, such as the PMJ [16–18] and the conus medullaris [19], are also used to estimate spinal segment positions. In cervical spinal cord MRI, the PMJ would be a preferable reference because of its proximity to the cervical area. Additionally, the PMJ is easy to identify (**Figure 2.2**) and can be automatically labeled on MRI images using the Spinal Cord Toolbox (SCT)'s `sct_detect_pmj` function [30, 31].

Another important consideration is the movement of the spinal cord relative to the vertebral column. Bilston & Thibault demonstrated that, during neck extension, the C3 spinal segment shifts caudally by 5 mm, in contrast to a 2 mm shift at the C5 level [32]. Additionally, it was observed that the spinal cord elongates and its CSA reduces when the neck is flexed, as opposed to a neutral neck position. [33].

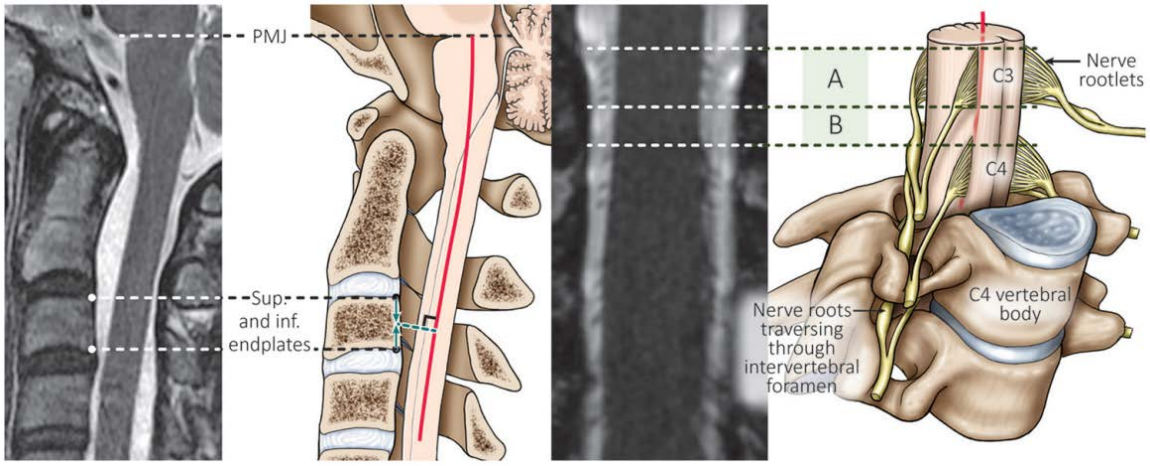

Figure 2.2 T2w image and illustration of spinal cord, vertebrae, nerve rootlets, and PMJ. (A) illustrate the spinal segment C3 delimited from the rostral-caudal nerve rootlets.

Figure adapted from [16].

2.1.2 Spinal Cord Morphometry

The shape and size of the spinal cord varies along the superior-inferior axis. Notably, there is a visible increase in spinal cord CSA at the cervical (C4-C5) and lumbar (L3) enlargements [8,27,29,34–37]. **Figure 2.3** displays CSA measurements across the entire spinal cord from 50 healthy volunteers. In **Figure 2.3**, the locations of the cervical and lumbar enlargements, where CSA is higher, are noticeable. Compared to the cervical enlargement, there is significant variation in the positioning of the lumbar enlargement relative to the vertebral levels among individuals. [27].

Furthermore, the spinal cord does not have a perfect cylindrical shape throughout its length. It transitions from a circular shape at C1-C2 to an elliptical shape around C4-C5, and reverting to a more circular shape at lower levels, as shown in **Figure 2.4** [21].

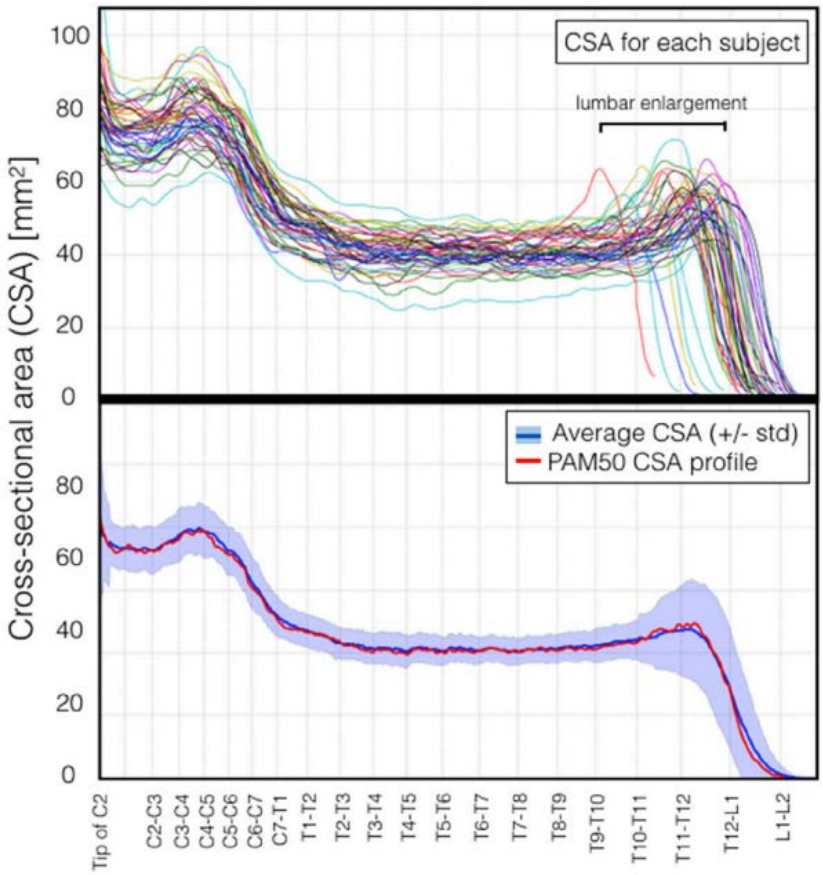

Figure 2.3 CSA measures across vertebral levels.

Figure adapted from [27].

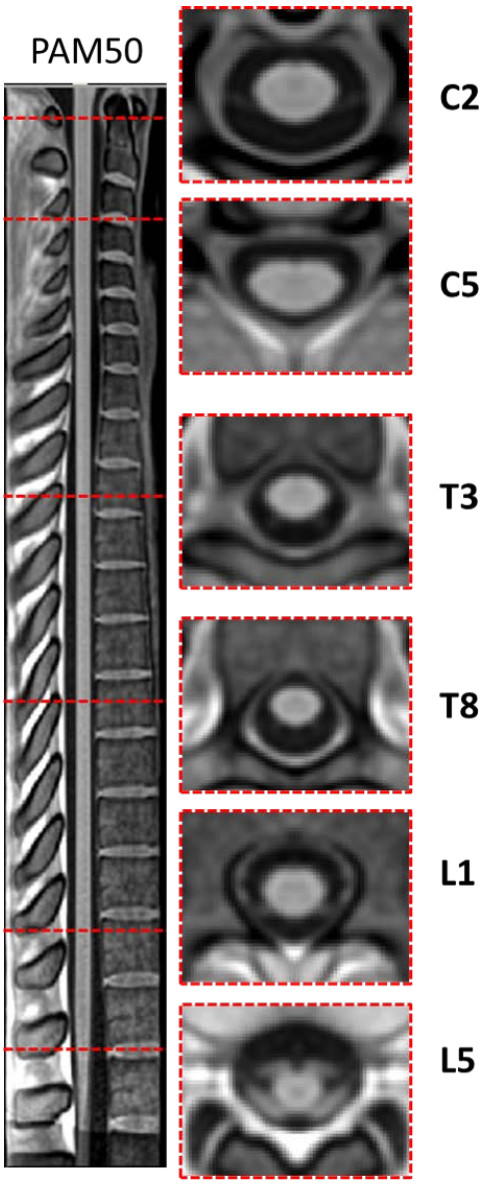

Figure 2.4 Cross section of the spinal cord in the PAM50 T1w MRI template for various spinal levels.

2.2 Imaging the Spinal Cord with MRI

MRI is a non-invasive technique that can image soft tissues. Its resolution allows for the imaging of small structures such as the spinal cord. Imaging the spinal cord with MRI consists of exposing the human body to a high static magnetic field (B0) and exciting hydrogen protons with radiofrequencies. These protons emit radiofrequency signals, enabling the construction of a detailed map of hydrogen proton distribution across various tissues. MRI distinguishes between tissues based on two types of relaxation processes: longitudinal (T1) and transverse (T2), each providing unique tissue signatures [38].

In this project, we concentrate on T1-weighted (T1w) and T2-weighted (T2w) image contrast which are typically the structural images acquired for standard MRI assessments. In T1w images, the spinal cord appears bright, whereas the surrounding cerebrospinal fluid (CSF) is darker due to its long T1 relaxation time. In T2w images, the contrast is reversed, with the spinal cord appearing darker than the CSF due to the CSF's long T2 relaxation time [4]. Specific MRI sequences can be used to obtain structural images of the spinal cord for CSA computation. Common MRI sequences for obtaining structural images include T2w fast spin echo and T1w MPRAGE (magnetization-prepared rapid gradient echo), the later includes an inversion pulse to nullify signal in the CSF [12, 39].

In high resolution T2w MRI scans (e.g., 0.8 mm isotropic), spinal nerve rootlets can be visualized as hypo-intense region in contrast to the CSF (**Figure 2.2**). Alternative MRI sequences, including dual-echo steady-state [40] and multi-echo gradient-echo [41], can also be used for visualizing spinal nerve rootlets. Despite advancements in imaging techniques, clearly visualizing nerve rootlets remains challenging due to their small size and the angles at which they intersect the CSF in all 3 dimensions [25, 42]. Isotropic acquisitions, which provide uniform resolution in all three dimensions, facilitate the visualization of these structures.

Imaging the spinal cord is challenging due to its small size and proximity to structures like vertebrae, intervertebral discs, and the lungs, each with different magnetic susceptibilities that can cause magnetic field inhomogeneities. This can result in signal loss and image distortions. Movements from surrounding tissues, including those caused by respiration, heartbeats, swallowing, tongue motion, and CSF flow, can introduce motion and susceptibility variations, leading to signal blurring and ghosting [4, 43].

In structural brain MRI, the upper cervical spinal cord is often captured within the field of view. However, since it is located at the extremity of the field of view, it is often affected by distortions caused by gradient non-linearity. Such distortions can significantly affect the accuracy of spinal cord morphometric measures from the cervical region, as shown in **Figure**

2.5 [44]. Typically, gradient non-linearities are corrected either using a vendor implemented algorithm, fitted phantom data, or using the gradient coefficients from the scanner model [44].

2.3 Cross-sectional Area (CSA)

Spinal cord cross sectional area is a relevant biomarker for the prognosis and monitoring of various neurodegenerative diseases, including MS [45], as well as traumatic and non-traumatic spinal injury [3, 46, 47]. In the context of MS, there is a significant association between spinal cord atrophy and both clinical disability and disease progression [6, 7]. Moreover, in cases of degenerative cervical myelopathy, CSA measurements at the compression site demonstrated substantial diagnostic value, correlating closely with clinical impairments [48].

2.3.1 Computing CSA with MRI

Spinal cord CSA is typically derived from MRI structural images by segmenting the spinal cord. A variety of automatic and semi-automatic segmentation techniques were developed, using strategies based on intensity, surface, image features, and deep learning [49].

The accuracy of CSA measurements is constrained by the axial resolution of MRI images. To counteract partial volume effects, CSA is commonly averaged over several slices. Additionally, to account for the spinal cord's curvature, angle correction may be applied to CSA measurements, ensuring they are computed orthogonally to the spinal cord's centerline.

For consistency and comparability across different subjects and over time, CSA measurements are aligned with vertebral levels [13, 50]. For instance, in monitoring atrophy in MS, CSA is usually averaged across the C2-C3 vertebral levels [39]. Vertebral serve as proxies for determining spinal segment positions, as they are easily identifiable on MRI structural images. Several methods exist to automatically label the vertebrae in MRI images [51–57], including `sct_label_vertebrae` function [51] in SCT [30]. **Figure 2.6** illustrates how to compute CSA, averaged across C2-C3 vertebral levels, using spinal cord segmentation and vertebral labels.

Spinal cord CSA can be derived from T1w or T2w structural MRI scans. Parameters such as image resolution directly impact the precision of CSA measures. Given the small size and curvature of the spinal cord, a 3D scan with an isotropic resolution ($\sim$ 1 mm) is preferred for deriving shape metrics. It also provides high signal to noise ratio [4, 12]. Anisotropic axial scans with thicker slices provide less precision in both CSA measurements, and in the labeling of vertebral levels.

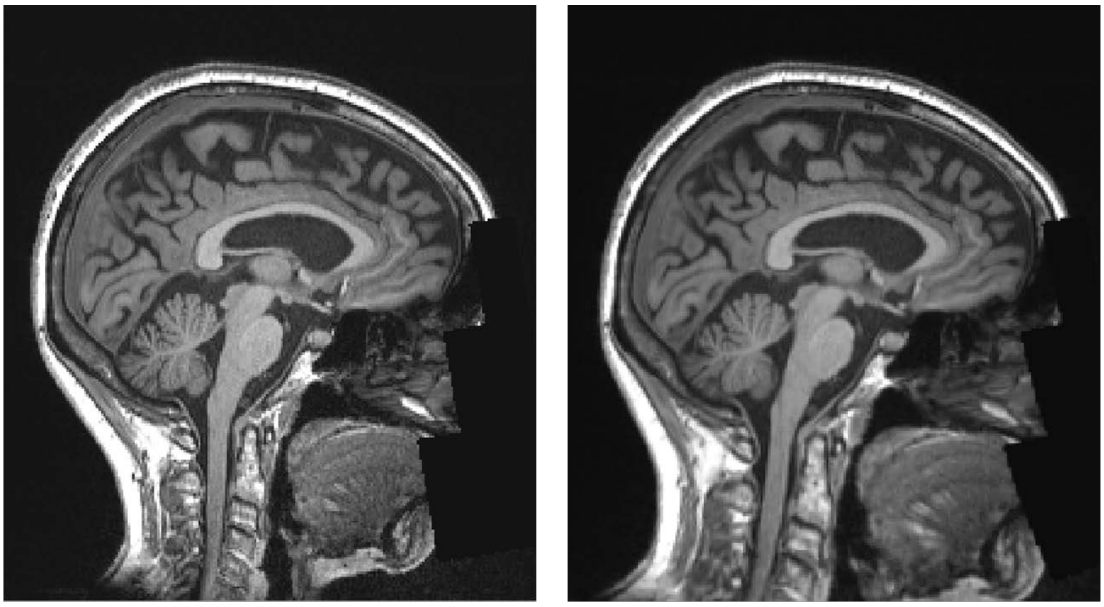

Figure 2.5 Example of an image affected by gradient non-linearity distortion (A) and the same image after correction (B). Notice the bottom part of the image, where the integrity of the spinal cord shape is recovered in the corrected image.

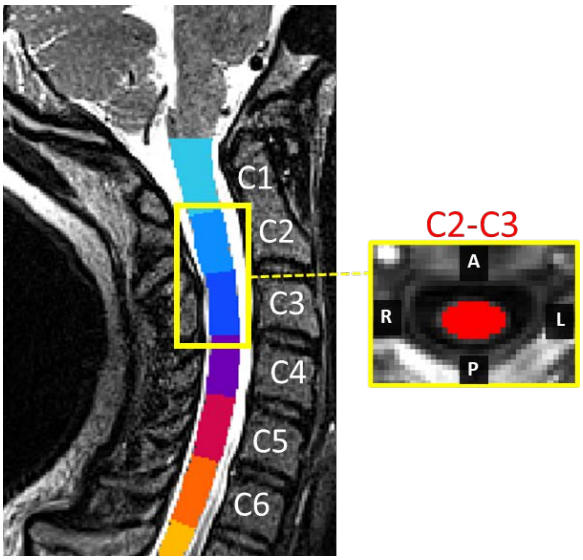

Figure 2.6 Spinal cord CSA measurement at C2-C3 vertebral levels.

Additionally, various image artifacts can degrade image quality, thereby affecting the reliability of CSA measurements. Movements such as patient swallowing can lead to ghosting artifacts at upper cervical levels, compromising the clarity of the spinal cord's boundaries. This may reduce the accuracy of both the segmentation and the subsequent CSA measurements.

2.3.2 Sources of CSA variability

CSA among healthy individuals faces considerable inter-subject variability. The coefficient of variation (COV) is typically reported as an indicator of variability and is calculated as the standard deviation (STD) divided by the mean, multiplied by 100 %, as showed in the following equation:

$$COV = \frac{STD}{mean} \cdot 100\% \tag{2.1}$$

Cohen-Adad et al. [12] reported a COV of 7.8 % for CSA at the C2-C3 vertebral levels among 267 healthy adults. Similar studies by Papinutto et al. [9], Yiannakas et al. [11], and Solstrand Dahlberg et al. [10] reported COVs of 9.47 %, 9.81 %, and 7.87 %, respectively, underscoring the variability within this measurement. Furthermore, Valošek et al. [8] showed an increase in CSA COV at lower vertebral levels.

Variations in CSA measurements were also observed across different MRI vendors [12, 14]. Notably, Cohen-Adad et al. [12] highlighted significant differences of CSA between MRI scanner from GE, Siemens, and Philips, particularly on T1w images from a study involving a single subject scanned across 19 sites. Casserly et al. [39], in a systematic review, pointed out the wide range of imaging protocols and contrasts used in MS atrophy research, further contributing to CSA variability. To foster standardization and ensure consistent image quality across research sites, the *Spine Generic* acquisition protocol was introduced [13], incorporating isotropic structural sequences: a T2w scan with 0.8 mm isotropic resolution and a T1w scan with 1 mm isotropic resolution.

Various imaging factors were shown to increase CSA intra-subject variability, including motion in the neck region (e.g., due to swallowing or head tilting), the presence of mouth metal implants, or the neck position (e.g., extreme lordosis makes it harder to acquire slices perpendicular to the spinal cord axis, inducing excessive partial volume effect), [15]. Moreover, certain MRI sequences, like gradient echo (GRE) sequences, are more sensitive to motion, making them more susceptible to CSA variability in comparison to spin-echo sequences [12].

The choice of segmentation method also plays a critical role in the accuracy of CSA measurements. Chien et al. [15] showed that CSA values obtained using the semi-automatic method from JIM (http://www.xinapse.com/Manual/cord_intro.html) were consistently higher than those derived using the automatic segmentation tool `sct_deepseg_sc` provided in SCT [58].

Furthermore, CSA is known to vary across MRI contrasts [12, 59]. Specifically, CSA measurments derived from T2w images are generally larger than those derived from T1w images [12,60]. This discrepancy is attributed to the contrast-dependent nature of segmentation methods, as the delineation between the CSF and the spinal cord can appear differently in various contrasts, thereby influencing CSA measures [61].

While factors such as MRI vendor, image contrast, and segmentation method can be controlled within single-center studies, other confounding factors still play a role in inter-subject CSA variability.

Demographic factors, for example, were shown to significantly influence CSA measurements. Higher values were consistently observed in males compared to females across various studies [8–10, 34, 62–65].

The relationship between age and the spinal cord's CSA is less clear compared to that for sex. Although some research indicates a decline in CSA with advancing age [9, 62, 65–68], this effect was not significant. Papinutto et al. [9] observed an increase of CSA until the age of 45, followed by a decrease. Additionally, Terao et al. [69] reported a decline of small fiber density associated with age, particularly in cervical and lumbar segments.

Regarding height, weight and body mass index (BMI), some studies identified moderate correlations with CSA [9,65]. However, other studies did not find any significant correlations between these factors and CSA measurements [9, 10, 70].

Significant correlations were identified between the size of the spinal canal and spinal cord CSA measurements [9, 71]. However, the inclusion of spinal canal metrics in studies remains limited, primarily due to the absence of reliable automated techniques for segmenting the CSF.

Moreover, metrics derived from brain imaging demonstrated substantial correlations with spinal cord CSA. Notably, the volume of brain WM is significantly associated with CSA, whereas GM volume shows a weak correlation, and no significant relationship was observed between brain CSF volume and CSA [62,66,72]. Additionally, research by Soltrand Dahlberg et al. [10] highlighted a significant correlation between thalamus volume and cervical spinal cord CSA.

2.3.3 Normalization Methods

To mitigate the impact of the various factors influencing CSA measures discussed previously, researchers can implement several normalization strategies. These include the proportional or residual methods, which are commonly applied in the normalization of cerebral volumes [70, 73].

The proportional method calculates normalized CSA values by dividing each subject's CSA by a chosen normalization factor, as illustrated in equation 2.2. This approach does not require any group correction. However, it does not account for the variability of the normalization factor, potentially leading to increased variability in the normalized CSA values [70]. Additionally, this method may introduce systematic and random errors associated with the normalization factor into the calculated results.

$$CSA_{norm} = \frac{CSA_{meas}}{X_{meas}} \tag{2.2}$$

Alternatively, the regression-based residual method uses a linear regression model to adjust CSA values by accounting for various factors and their average group values. This method offers a more comprehensive normalization approach, by simultaneously considering multiple factors. Unlike the proportional method, the residual normalization method does not incorporate the variability of the normalization factor and its systematic bias. However, its application requires a group dataset.

The regression-based residual normalization aims to remove the relationships between CSA and selected normalization factors, as demonstrated in the following equation: [9, 70]:

$$CSA_{norm} = CSA_{meas} + c_1 \cdot (X_{1,mean} - X_{1,meas}) + c_2 \cdot (X_{2,mean} - X_{2,meas}) + ... + c_n \cdot (X_{n,mean} - X_{n,meas}) \tag{2.3}$$

Where CSA^i_{norm} is the adjusted CSA, CSA_{meas} is the measured CSA of a given subject, c_i is the slope between CSA and the corresponding factor, $X_{i,mean}$ is the mean of this factor in the population and $X_{i,meas}$ is the measured value of that factor for a given subject. Multiple factors can be included.

Several studies proposed normalization strategies for spinal cord upper cervical CSA [9, 66, 71, 74–76]. Among these, some studies identified spinal cord length as a useful strategy for normalizing spinal cord volume [74,75]. Previous research has primarily used as normalization factors sex, spinal cord length, brain WM volume, spinal canal area, intracranial volume

(ICV), and age [7, 9, 66, 71, 76]. Some studies used ICV instead of brain volume, as brain volume can vary with certain pathology such as MS [71]. Brain/skull metrics and sex are important factors to consider for normalizing CSA.

CHAPTER 3 METHODS

This chapter presents an overview of the selected method and the role of each article to achieve the objectives presented in **Chapter 1**.

3.1 Objective 1: Develop a PMJ-based Approach for CSA Computation

To overcome limitations associated with the use of a vertebral reference, we propose using the PMJ as a reference for spinal cord CSA measurements. The CSA is computed using an arc-length distance from the PMJ following the spinal cord centerline. The first objective of this Master thesis is to propose an automatic method to compute spinal cord CSA from a distance from the PMJ. In the paper entitled *Automatic measure and normalization of spinal cord CSA using the pontomedullary junction* presented in **Chapter 4**, we propose an automatic method to enhance PMJ automatic labeling and to compute CSA from a distance from the PMJ. The method is available through the open-source Software SCT. We apply the method on a subset of the UK Biobank dataset (n = 804) and compare CSA results with CSA computed at C2-C3 vertebral levels.

3.2 Objective 2: Quantify Inter-subject Variability of PMJ-based CSA

The second objective of this thesis is to quantify inter-subject variability of CSA when using the PMJ as a reference. In **Chapter 4**, we explore various demographic and anatomical factors contributing to spinal cord CSA variability and develop a normalization method on a subset of the UK Biobank. We compare the inter-subject variability and normalization methods for both PMJ-based CSA and vertebral-based CSA at C2-C3.

3.3 Objective 3: Quantify Intra-subject Variability of PMJ-based CSA

The third objective of the thesis is to quantify intra-subject variability of PMJ-based CSA. To do so, in the article *Pontomedullary junction as a reference for spinal cord CSA: validation across neck positions* (**Chapter 5**), we compute PMJ-based CSA on images with varying neck positions where the correspondence between spinal and vertebral levels is hypothesised to vary. We acquire high resolution T2w scans on 10 healthy volunteers with 3 different neck positions (flexion, neutral and extension). We compare CSA intra-subject variability across neck positions using the PMJ, intervertebral discs and spinal segments (manually labeled).

We also estimate the spinal segments positions using the PMJ vs. inter vertebral discs and assess the variability across neck positions.

3.4 Scientific Publications

From this work, two papers were published. The paper *Automatic measure and normalization of spinal cord cross-sectional area using the pontomedullary junction* was published in 2022 in Frontiers in Neuroimaging. The paper *Pontomedullary junction as a reference for spinal cord cross-sectional area: validation across neck positions* was published in 2023 in Scientific Reports.

CHAPTER 4 ARTICLE 1: AUTOMATIC MEASURE AND NORMALIZATION OF SPINAL CORD CROSS-SECTIONAL AREA USING THE PONTOMEDULLARY JUNCTION

Published the 2nd of November 2022 in Frontiers in Neuroimaging, 1:1031253. doi: 10.3389/fnimg.2022.1031253

Title: Automatic measure and normalization of spinal cord cross-sectional area using the pontomedullary junction.

Authors: Sandrine Bédard[1], Julien Cohen-Adad[1,2,3]

Affiliations:

1. NeuroPoly Lab, Institute of Biomedical Imaging, Polytechnique Montréal, Montreal, Quebec, Canada.
2. Functional Neuroimaging Unit, CRIUGM, University of Montreal, Montreal, QC, Canada.
3. Mila - Quebec AI Institute, Montreal, QC, Canada.

Abstract

Spinal cord CSA is a relevant biomarker to assess spinal cord atrophy in neurodegenerative diseases. However, the considerable inter-subject variability among healthy participants currently limits its usage. Previous studies explored factors contributing to the variability, yet the normalization models required manual intervention and used vertebral levels as a reference, which is an imprecise prediction of the spinal levels. In this study we implemented a method to measure CSA automatically from a spatial reference based on the central nervous system (the PMJ), we investigated factors to explain variability, and developed normalization strategies on a large cohort (N = 804).

Following automatic spinal cord segmentation, vertebral labeling and PMJ labeling, the spinal cord CSA was computed on T1w MRI scans from the UK Biobank database. The CSA was computed using two methods. For the first method, the CSA was computed at the level of the C2-C3 vertebral disc. For the second method, the CSA was computed at 64 mm caudally from the PMJ, this distance corresponding to the average distance between the PMJ and the C2-C3 disc across all participants. The effect of various demographic and anatomical factors was explored, and a stepwise regression found significant predictors; the coefficients of the best fit model were used to normalize CSA.

CSA measured at C2-C3 disc and using the PMJ differed significantly (paired t-test, *p-value* = 0.0002). The best normalization model included thalamus, brain volume, sex and the interaction between brain volume and sex. The COV went down for PMJ CSA from 10.09 % (without normalization) to 8.59 %, a reduction of 14.85 %. For CSA at C2-C3, it went down from 9.96 % to 8.42 %, a reduction of 15.13 %.

This study introduces an end-to-end automatic pipeline to measure and normalize cord CSA from a neurological reference. This approach requires further validation to assess atrophy in longitudinal studies. The inter-subject variability of CSA can be partly accounted for by demographics and anatomical factors.

Keywords: Spinal cord, MRI, Normalization, Inter-subject variability, Biomarker.

4.1 Introduction

Various neurodegenerative diseases such as MS are associated with spinal cord atrophy, which is caused by demyelination, neuronal and/or axonal loss [1, 77]. New techniques have now become available through recent advancement in MRI and are relevant to assess spinal cord atrophy [50].

Spinal cord atrophy at the upper cervical levels can be defined within its CSA [1,6]. The use of this metric is yet still limited due to considerable inter-subject variability. Finding factors that contribute to the observed variability is important to improve the spinal cord CSA's sensitivity and specificity.

Various studies have explored the correlation between spinal cord CSA and demographic, anatomical and biological factors. Sex was a relevant factor to explain spinal cord CSA variability, with females having significantly smaller spinal cord CSA than males [9, 10, 62]. While the majority of studies have reported this significant effect, Fradet et al. [78] found it to be an irrelevant factor and Papinutto et al. [66] did observe the trend, but no statistical difference was found. However, the absence of a statistical difference could be explained by the relatively small sample size (30 participants).

Regarding the effect of age, a decrease of spinal cord CSA was previously reported [9,62,66–68]. However, the effect was not significant [9, 62, 66]. This trend is accentuated for older populations, but the effect of age is still small [62]. An increase of spinal cord CSA values followed by a decrease at 45 years old was also reported, but the effect was not significant [9]. The effect of age on spinal cord CSA needs further investigation, small sample size and narrow range of age are limiting factors to assess the effect of age on spinal cord CSA.

As for height and body weight, no significant effect on spinal cord CSA was found according

to recent studies [9,10,66]. The effect of height may be driven by sex differences [9]. BMI was also tested as a normalization strategy for spinal cord volume, but results were inconclusive as inter-subject variability was increased [70]. In another study, no correlation was found with BMI by [10].

Strong correlation between brain metrics and spinal cord CSA were reported in prior studies [9,10,62,66]. WM volume significantly explains upper cervical area variability as opposed to CSF volume, which was not significant according to [62]. In addition, brain volume correlated strongly with spinal cord CSA as for intracranial volume [10, 66]. Papinutto et al. [9] also found this effect with Vscale (scaling factor for head size normalization) and considered it as the most promising factor for normalization strategies. Intracranial volume was also considered for normalization of spinal cord volume but had limited utility since it generally diminished the ability to detect clinical-radiological correlations [74, 75]. Since spinal cord CSA is a useful metric to assess spinal cord atrophy and brain volume changes have also been associated with those pathologies, intracranial volume would be a better factor to consider for normalization strategies [71]. A strong correlation was also found between thalamus volume and spinal cord CSA by [10]. Axial canal area was also a significant factor and promising for normalization strategies but has not been explored yet by many [9, 71]. A notable difficulty for computing the axial canal area is the ability to properly segment it.

Only a few of the previous cited works have explored normalization strategies for spinal cord CSA. spinal cord length was a relevant factor for spinal cord volume normalization compared to intracranial volume [74, 75]. Mean spinal cord volume in healthy participants was also used to normalize spinal cord volume of patients with MS [76]. Regarding spinal cord CSA, age, intracranial volume, and sagittal vertebral area were the most promising independent variables found by [66], but the method was based on 30 participants only. Another model later including Vscale, axial canal product (product of maximum axial anterior-posterior and lateral diameters of the cervical spinal cord) based on 129 participants significantly reduced spinal cord CSA variability [9]. Brain WM volume, sex and spinal canal area formed a relevant normalization strategy. Total intracranial volume can also replace brain WM volume for subjects with diseases affecting WM. The main limitation here was the relatively small number of participants (N = 61) [71]. As we can observe, brain/skull metrics and sex are important factors to consider in a possible normalization method. Also, the mentioned normalization methods are only reported in the related papers; they are not easily reusable to integrate directly within analysis pipelines.

In addition to the biological-derived normalization strategy, previous studies have reported a variability in CSA measures associated with the MRI acquisition parameters, and segmen-

tation method [12, 14, 15, 59].

The majority of the studies regarding spinal cord CSA use vertebral levels as an anatomical reference [39,50]. However, inferring the position of the spinal segments using vertebral levels is imprecise, adding variability to CSA measures [16]. Inferring neuroanatomic positions with vertebral bodies doesn't consider neck flexion and extension. In addition, because of the intrinsic intersubject variability, the vertebral bodies only give a rough approximation of the spinal segments [16]. Segmental nerve rootlets would provide a proper identification of the spinal segments, it is however difficult to identify and requires high resolution T2w scans and an expert rater to identify them. A few studies have attempted to bypass the vertebral-based limitation using the distance from an anatomical landmark, such as the PMJ [16–18], and the *conus medullaris* [19]. However, these methods require manual intervention limiting large-scale applications. In addition, the PMJ was not used in the context of measuring spinal cord CSA [16–19]. For cervical cord measures, the PMJ is a more appropriate landmark due to its proximity to the cervical spinal cord, hence limiting the required field of view in MRI scans, compared to *conus medullaris* which could be more appropriate for lumbar spinal cord measures.

While spinal cord CSA variability across participants was shown to be associated with multiple demographic, anatomical and biological factors [9, 10, 66, 71], no previous studies have addressed the variability associated with limitation of vertebral based spinal cord CSA measurement in the search for a normalization method of spinal cord CSA at a large scale.

In this study we quantify the contribution of various factors on the inter-subject variability in cervical spinal cord CSA measurements. We notably introduce a method to replace the commonly used vertebral-based referencial system [50] by an anatomical reference from the central nervous system to overcome the imprecise prediction of the spinal segments. More precisely, we (1) establish a fully-automatic MRI data processing pipeline to compute spinal cord CSA, (2) process MRI data from a subset (N = 804) of the UK Biobank database, (3) introduce a method to automatically use the PMJ as a referential system to measure spinal cord CSA, (4) develop a statistical model and normalization method for spinal cord CSA measurements.

4.2 Material and methods

4.2.1 Demography

1,000 participants (48 to 80 years old, 56.3 % female) were selected from the UK Biobank database. Not knowing the effect size we were after, we could not base this number on any

reliable power analysis. Hence, the number of participants was selected as a compromise between the statistical power we wanted to achieve in comparison with the previously-published studies addressing similar scientific questions (typically < 300 participants) and the time required to manually validate each step of the processing pipeline (visual inspection, manual correction of spinal cord segmentation and/or PMJ labeling and/or vertebral labeling). Participants with a history of neurological diseases were excluded from the study. Fields from the UK Biobank dataset included in the category *Nervous system disorders*[1] were used to identify these participants. This brought the number of participants from 1,000 to 972.

4.2.2 Image acquisition

Data used for this study were unprocessed NIfTI T1w structural scans from the UK Biobank Brain Imaging dataset [79]. Images were acquired in four different assessment centers on a Siemens Skyra 3T running VD13A SP4 with a standard Siemens 32-channel receive head coil. T1w structural scan has a field of view of 208×256×256 with an isotropic resolution of 1 mm^3. The superior-inferior field of view of 256 mm typically covers down to C3 vertebral level, which is relevant for the present study as spinal cord CSA was measured around the C2-C3 vertebral level. The UK Biobank data includes preprocessed data (corrected for gradient non-linearity and masked), however we could not use these data because the spinal cord was masked out. We therefore used the unprocessed T1w images as input of the processing pipeline described in the next section.

4.2.3 Data processing

Data processing pipeline is based on spine-generic v2.6 pipeline[2] [12] and SCT v5.4[3] [30]. The processing pipeline and its documentation are both available on GitHub[4].

Figure 4.1 presents an overview of the processing pipeline. First, all images were reoriented to right-inferior-posterior orientation. Since spinal cord CSA is computed using T1w brain images and spinal cord is in the periphery of the images' field of view, gradient non-linearity distortions have a considerable effect on CSA measures, depending on participant positioning [44]. Gradient non-linearity correction was applied by the UK Biobank after brain extraction and was therefore not possible for us to use since the cervical spine is the subject of investigation in this study. Thus, correction for gradient non-linearities was applied

[1] https://biobank.ndph.ox.ac.uk/showcase/label.cgi?id=2406

[2] https://github.com/spine-generic/spine-generic/releases/tag/v2.6

[3] https://github.com/neuropoly/spinalcordtoolbox/releases/tag/5.4

[4] https://github.com/sct-pipeline/ukbiobank-spinalcord-csa/tree/v1.1#cord-csa-on-uk-biobank-brain-mri-database

to the unprocessed images using *gradunwrap* from the HCP project [80] and the coefficient file for the Siemens Skyra 3T gradient system. Then, the spinal cord was segmented automatically using SCT's `sct_deepseg_sc` [58]. spinal cord CSA was computed using SCT's `sct_process_segmentation` with two different methods further explained below.

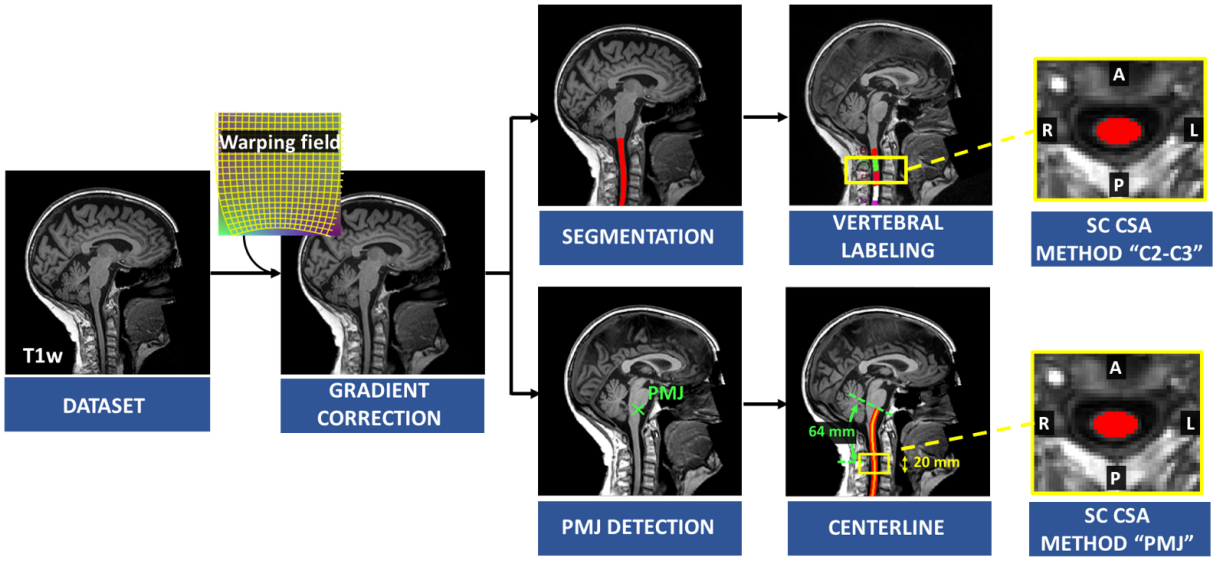

Figure 4.1 Overview of the processing pipeline. Correction for gradient non-linearities was applied on the T1w image and spinal cord was segmented automatically. Vertebral levels were identified and spinal cord CSA was computed at C2-C3 levels. The PMJ was labeled and the centerline was extracted to compute spinal cord CSA from the PMJ

CSA based on distance from neurological reference: pontomedullary junction

To overcome the limitation of spinal cord segment prediction with vertebral bodies, spinal cord CSA was measured from a distance of a neurological reference; we chose the PMJ [16,17]. First, the PMJ was identified using SCT'S `sct_detect_pmj`. Briefly, a 2D support vector machine trained with histogram of oriented gradient features (HOG+SVM 2D classifier) was run on the mid-sagittal slice to detect the PMJ [31]. However, the mid-sagittal slice does not necessarily correspond to the anatomical medial plane if the participant's head is slightly tilted in the scanner for example. We used a sliding window centered on the first estimated PMJ coordinate based on the mid-sagittal plane and computed cross-correlation within the window and its mirror image in the right-left orientation. We assumed that the maximum cross-correlation corresponds to the right-left symmetry slice. The HOG+SVM 2D classifier was run again on the updated medial plane. Since the spinal cord curvature associated with

cervical lordosis varies across individuals, the distance from the PMJ was computed along the spinal cord centerline following the arc-length. spinal cord segmentation normally doesn't go as high as the PMJ. The PMJ coordinate was then added to the spinal cord segmentation prior to extracting the spinal cord centerline. Linear interpolation and smoothing were used to extract the spinal cord centerline. spinal cord CSA was computed at the mean distance between the C2-C3 disc and the PMJ across all participants, which corresponds to 64 mm. spinal cord CSA was computed along the spinal cord centerline and then averaged on a 20 mm extent as presented in **Figure 4.2**.

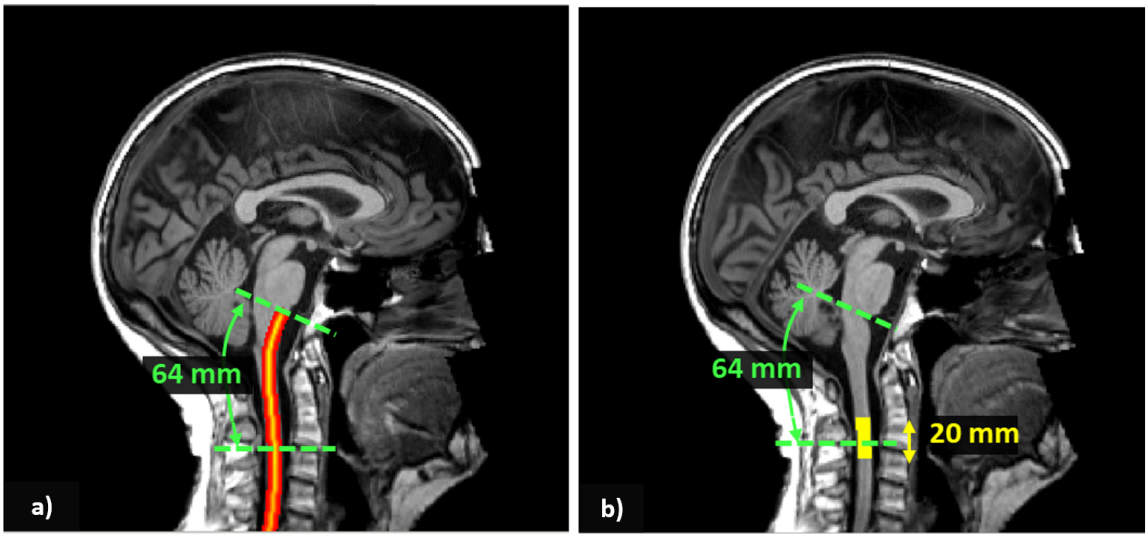

Figure 4.2 **a)** spinal cord centerline from PMJ. The spinal cord centerline was extracted from spinal cord segmentation and the PMJ label using linear interpolation and smoothing. The distance from PMJ is measured along the centerline following the arc-length. **b)** Extent mask to average spinal cord CSA. At 64 mm from PMJ, CSA was computed slice-wise, corrected for angulation and averaged within a 20 mm extent. The extent mask is centered at 64 mm from PMJ.

CSA based on C2-C3 vertebral levels

The second and more commonly used method to compute the spinal cord CSA was to use C2-C3 vertebral levels as an anatomical reference for spinal segments [39, 50]. We proceeded to vertebral labeling using `sct_label_vertebrae` [51]. spinal cord CSA was then averaged across C2-C3.

4.2.4 Quality control

After running a first pass of the automatic analysis pipeline, we inspected results of the spinal cord segmentations and of the PMJ and vertebral labeling using SCT's quality report (`sct_qc`). For more details about the procedure, see: https://github.com/sct-pipeline/ukbiobank-spinalcord-csa/blob/master/README.md#quality-control . Segmentation and labeling errors typically occurred if there were important artifacts in the image, such as ghosting caused by poor shimming and/or participant motion (e.g.: swallowing, head tilting). PMJ and vertebral labeling errors also sometimes happened if the field of view was improperly positioned (e.g.: excessive rotation about the right-left axis). If images were too artefacted to produce reliable morphometric measures (see examples at https://github.com/sct-pipeline/ukbiobank-spinalcord-csa/issues/61), these images were excluded from the statistical analysis. This brought the number of participants from 972 to 826. For less severe artifacts, manual corrections were done on the segmentation and/or labeling. Making these corrections ensured that the derived CSA measures are reliable. Segmentations were corrected using ITK-SNAP by adding or removing voxels when appropriate. To correct vertebral labeling, we manually labeled the posterior tip of the intervertebral discs C1-C2, C2-C3 and C3-C4 using SCT's `sct_label_utils`. A similar approach was done for the PMJ. All manual corrections were added to the dataset under the folder '/derivatives/labels' that follows the BIDS convention. The whole analysis was then re-run and when existing, the corrected segmentations/labels were used in lieu of the automatic segmentations/labels. Processing was distributed across 40 CPU cores (one participant per CPU core) using `sct_run_batch` on a 64-core CPU cluster. Processing took 01h53m59s.

4.2.5 Statistical Analyses

Comparison of CSA measure with both methods

To study the relationship between the PMJ-based and vertebral-based CSA measures, we built a scatterplot and derived a model. We also computed the distance between the C2-C3 disc and PMJ. Mean, STD, median and COV for both CSA measures were computed. We performed a two-sided paired T-test to assess if there is a statistically significant difference between PMJ-based CSA vs C2-C3-based CSA. All subsequent analyses were done on both CSA at 64 mm from the PMJ and at the C2-C3 disc.

Correlations with physical and brain measures

In this study, the effect of sex, age, physical measures, and brain measures on spinal cord CSA was explored by calculating Pearson's correlation coefficients. Physical measures included height and weight. Brain measures included brain WM volume, brain GM volume, brain volume, brain volume normalized for head size, thalamus volume and ventricular CSF volume. All data (images and demographic measures) were acquired at the same time for each participant and were available in the UK Biobank database. The brain metrics were computed by the UK Biobank team as part of their processing pipeline [81].

Effect of sex and age

To assess the effect of sex on spinal cord CSA, a T-test for two independent samples was performed to establish if the mean CSA for male and female has a significant difference. We fitted a linear and quadratic regression to assess the effect of age on spinal cord CSA. R^2 was reported.

Multilinear regression

The effect of all candidate predictors was evaluated using a multilinear analysis. Sex was included as a dichotomous variable to the regression. Any participant missing a parameter was excluded from this analysis. This brought the number of participants from 826 to 804. To select the relevant predictors of the multilinear regression, a stepwise method was used. The predictors are added to the model from the highest correlation with CSA to the lowest if they are significant ($p\text{-}value < 0.05$). After each addition of predictors, the significance of the current parameters was computed again, and parameters with a $p\text{-}value > 0.05$ were excluded from the model [82]. The level of significance was the same for both entry and exit tests. To validate the model, we proceeded to a residual analysis and computed R^2. Pearson's correlation coefficient between candidate predictors was used to choose which parameter to include in the stepwise model due to possible collinearity between parameters.

Normalization method

With the best multilinear regression fit, a regression-based residual method [9, 70] was developed using the significant predictors, as described in the following equation:

$$CSA^i_{norm} = CSA^i_{meas} + c_1 \cdot (X_{1,mean} - X^i_{1,meas}) + c_2 \cdot (X_{2,mean} - X^i_{2,meas}) + ... + c_n \cdot (X_{n,mean} - X^i_{n,meas}) \tag{4.1}$$

Where CSA^i_{meas} is the computed spinal cord CSA value from a given participant i, CSA^i_{norm} is the normalized CSA value, c_j are the coefficients of the multilinear regression, X_j, mean are the mean values of all significant predictors, $X^i_{j,meas}$ are values for the given participant's predictors, for j predictors [9].

Since this method assumes that the regression line slopes are parallel for both groups for sex [70], the interaction between significant predictors and sex was also explored afterward. If the interaction term was significant, it was added to the model. The interaction term corresponds to the predictor multiplied by sex (0 or 1) as we can see in the following equation:

$$y = c_1 \cdot X_1 + c_2 \cdot sex + c_3 \cdot X_1 \cdot sex \tag{4.2}$$

The effect of normalization was then evaluated by comparing the COV of the normalized spinal cord CSA (CSA^i_{norm}) and the measured CSA (CSA^i_{meas}). We also present the mean (μ_{norm}) and STD (σ_{norm}) of the normalized CSA measures (CSA^i_{norm}) and the *z-score* equation:

$$z\text{-}score = \frac{CSA_{norm} - \mu_{norm}}{\sigma_{norm}} \tag{4.3}$$

4.3 Results

4.3.1 Spinal cord CSA

In this study we compared spinal cord CSA measured using the PMJ as a reference or the C2-C3 disc as a reference (more popular). When using the PMJ as a reference (64 mm caudal to the PMJ), the CSA ranged between 51.9 and 95.6 mm^2 (mean ± STD: 66.2 mm^2 ± 6.69 mm^2). The COV was 10.09 %. When using C2-C3 vertebral levels as a reference, the CSA ranged between 51.5 and 96.9 mm^2 (mean ± STD: 66.4 mm^2 ± 6.61. mm^2). The COV was 9.96 %.

Figure 4.3a) shows the relationship between CSA at 64 mm from the PMJ and CSA at C2-C3 vertebral levels. The linear regression led to a R^2 of 0.97. **Figure 4.3b)** shows a scatterplot of the distance from the PMJ and C2-C3 disc. Mean distance from the PMJ to the C2-C3 disc is 64.37 ± 5.53 mm. We found a significant difference between the CSA calculated at 64 mm from the PMJ and the CSA measured at the C2-C3 disc (paired *t-test*, t = -3.71, *p-value* = 0.0002).

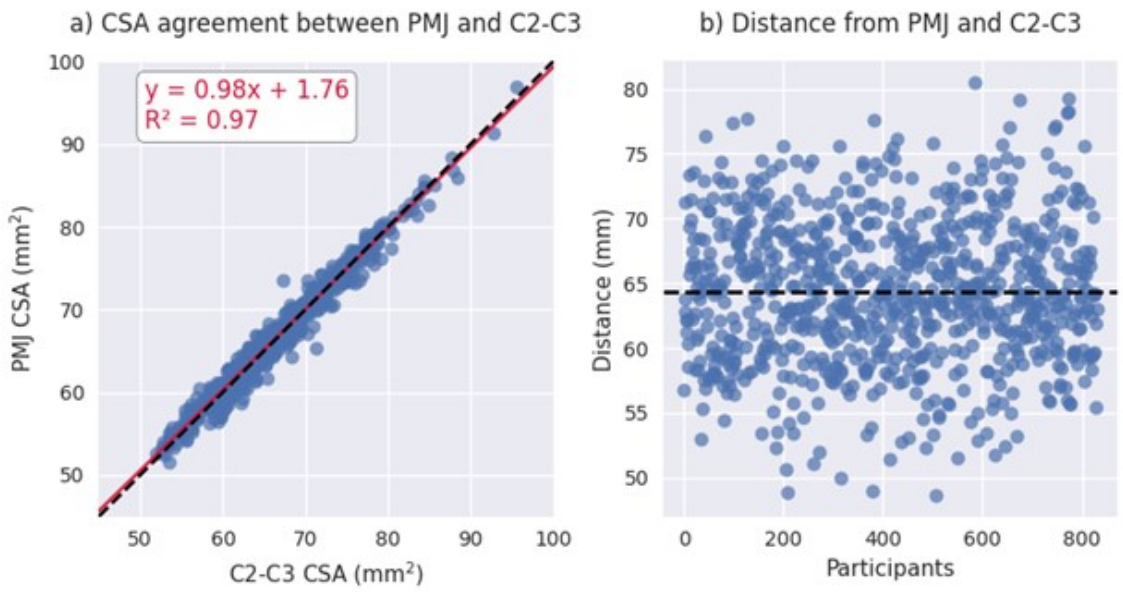

Figure 4.3 **a)** Scatterplot of PMJ-based CSA at 64 mm and vertebral-based CSA at C2-C3 vertebral levels. **b)** Scatterplot of the distance between the PMJ and the C2-C3 disc.

4.3.2 Statistical Analyses

Correlations with physical and brain measures

We investigated the relationship of spinal cord CSA with sex, age, physical and brain measures. Results of the correlation analysis (Pearson's) are reported in **Table 4.1**. Note that this correlation matrix is not corrected for multiple comparisons because its purpose was only to explore existing correlations. In subsequent analysis (see *Multilinear regression*), a multivariate analysis will account for the number of regressors in the estimated *p-values*. Scatterplots of CSA(PMJ) and all parameters are shown in supplementary material (4.8-4.17). Ventricular CSF volume was the only parameter to present a non-significant correlation coefficient with both spinal cord CSA measures ($p\text{-}value > 0.05$). Thalamus, brain, brain WM and brain GM volume present the highest correlations out of all parameters (*Pearson's* $r > 0.4$). Among parameters, we notice in particular a very strong correlation between thalamus volume and brain, brain WM and brain GM volume.

Effect of sex and age

Participants in this study include 43.7 % of males and 56.3 % of females. **Figure 4.4** presents spinal cord CSA violin plots for female and male with mean and STD. We found a significant

Table 4.1 Pearson's correlation among spinal cord CSA, physical and brain measures.

	Sex	Age	Height	Weight	Vscale	Ventricular CSF volume	Brain GM volume	Brain WM Volume	Brain volume norm	Brain volume	Thalamus volume	CSA (PMJ)	CSA (C2-C3)
Sex	1.0	0.07*	0.71***	0.48***	-0.59***	0.33***	0.39***	0.53***	-0.2***	0.49***	0.36***	0.19***	0.18***
Age		1.0	-0.07*	-0.05	-0.05	0.41***	-0.35***	-0.12***	-0.56***	-0.24***	-0.33***	-0.18***	-0.18***
Height			1.0	0.57***	-0.58***	0.21***	0.45***	0.51***	-0.13***	0.51***	0.42***	0.2***	0.19***
Weight				1.0	-0.41***	0.16***	0.3***	0.39***	-0.09**	0.36***	0.25***	0.13***	0.12***
Vscale					1.0	-0.46***	-0.78***	-0.84***	0.24***	-0.85***	-0.61***	-0.32***	-0.32***
Ventricular CSF volume						1.0	0.08*	0.25***	-0.53***	0.18***	-0.09**	-0.02	-0.04
Brain GM volume							1.0	0.81***	0.33***	0.94***	0.75***	0.4***	0.4***
Brain WM volume								1.0	0.22***	0.96***	0.76***	0.45***	0.46***
Brain volume norm									1.0	0.29***	0.36***	0.24***	0.25***
Brain volume										1.0	0.79***	0.45***	0.45***
Thalamus volume											1.0	0.51***	0.52***
CSA (PMJ)												1.0	0.99***
CSA (C2-C3)													1.0

p-value: *$0.01 < P < 0.05$, **$0.001 < P < 0.01$, *** $P < 0.001$

difference for CSA between female and male for both CSA at 64 mm from the PMJ and at C2-C3 disc (**CSA(PMJ)**: t = -5.37, *p-value* $< 10^{-7}$, **CSA(C2-C3)**: t = -5.17, *p-value* $< 10^{-7}$).

To explore the relationship between age and spinal cord CSA, we calculated a linear and quadratic fit. The age of the participants ranged between 48 and 80 years old. The linear fits are presented at **Figure 4.5**. The equations for the quadratic fit are:

$$\textbf{CSA(PMJ)} : y = 72.93 - 0.0469 \cdot x - 0.000907 \cdot x^2; R^2 = 0.031 \tag{4.4}$$

$$\textbf{CSA(C2-C3)} : y = 75.17 - 0.1076 \cdot x - 0.000475 \cdot x^2; R^2 = 0.034 \tag{4.5}$$

The constant and the linear coefficient are the same for both linear and quadratic fits per CSA methods (PMJ and C2-C3). The quadratic coefficient is very small for both methods (**CSA(PMJ)**: 9.07×10^{-4}; **CSA(C2-C3)**: 4.75×10^{-4}). There is almost no quadratic trend in both cases.

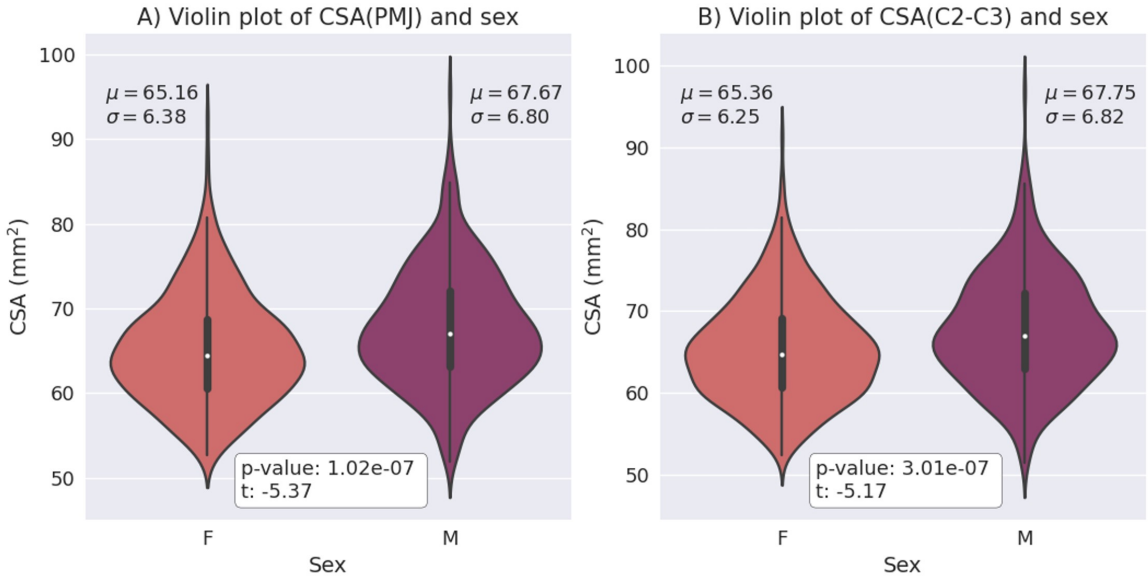

Figure 4.4 **A)** Violin plot of spinal cord CSA at 64 mm from the PMJ for female and male with mean (μ) and STD (σ) for each sex. **B)** Violin plot of spinal cord CSA at C2-C3 disc for female and male with mean (μ) and STD (σ) for each sex.

Multilinear regression

Based on the Pearson's correlation analysis presented in **Table 4.1**, the following parameters were input in the stepwise linear regression: sex, height, weight, age, brain volume, ventricular

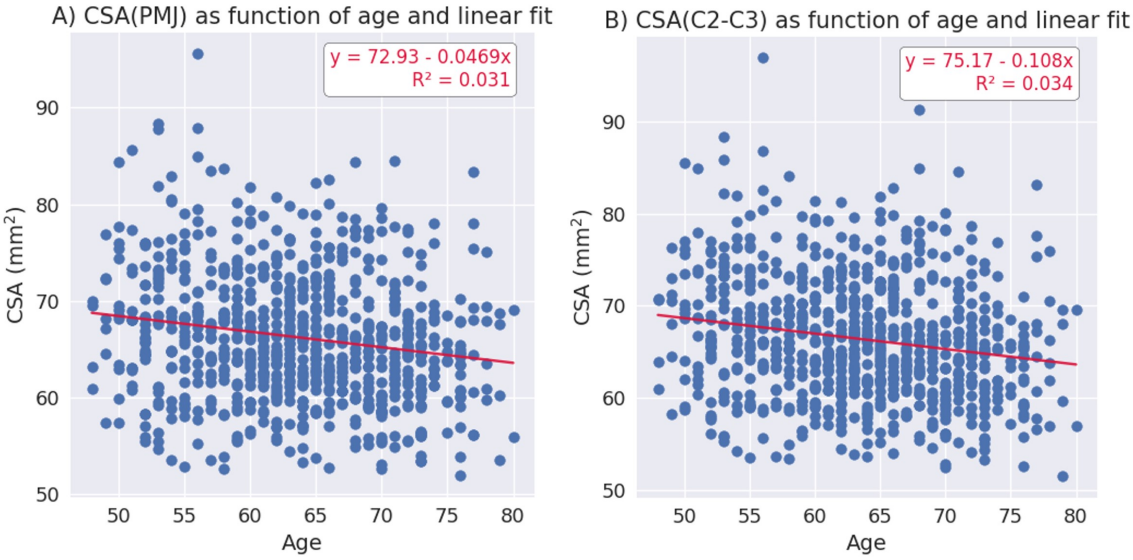

Figure 4.5 **A)** Linear fit for CSA at 64 mm from the PMJ as a function of age. **B)** Linear fit for CSA at C2-C3 disc as a function of age.

CSF volume and thalamus volume. Since brain WM volume, GM volume and brain volume have a very strong correlation (0.94 and 0.96), brain WM volume and GM volume were not included in the model to avoid collinearity.

The stepwise method yielded a model including brain volume and thalamus volume for CSA(PMJ) and CSA(C2-C3). The resulting model is shown in **Table 4.2** for CSA at 64 mm from the PMJ and at **Table 4.3** for CSA at C2-C3 disc. Adjusted R^2 is 0.265 for CSA(PMJ) and 0.271 for CSA(C2-C3). Both models show a significant association with CSA (*p-value* < 0.0001).

Table 4.2 Multilinear Regression Analysis for spinal cord CSA(PMJ) (N = 804 participants).

R^2	**R^2adj**	**F**	***p-value***	**AIC**
0.267	0.265	145.7	1.077e-54	5093
	coeff	***t***	***p-value***	
const	27.18	11.634	5.154e-29	
thalamus volume	1.99e-03	8.344	3.131e-16	
brain volume	7.56e-06	2.407	0.016	

Table 4.3 Multilinear Regression Analysis for spinal cord CSA(C2-C3) (N=804 participants).

$\mathbf{R^2}$	$\mathbf{R^2}$**adj**	**F**	***p-value***	**AIC**
0.267	0.269	148.7	1.18e-55	5072
	coeff	***t***	***p-value***	
const	27.49	11.924	2.737e-30	
thalamus volume	0.002	8.498	9.373e-17	
brain volume	7.30e-06	2.355	0.019	

4.3.3 Normalization

Brain and thalamus volumes

The presented model's coefficients led to the following normalization equation with thalamus volume and brain volume and their respective mean for CSA at 64 mm from the PMJ and at C2-C3 disc. Normalized CSA(PMJ) had a mean and STD of 66.26 mm^2 ± 5.72 mm^2 and for CSA(C2-C3), 66.40 mm^2 ± 5.64 mm^2.

CSA(PMJ):

$$CSA^i_{norm} = CSA^i_{meas} + 1.986 \cdot 10^{-3} \cdot (15266 - X^i_{TV}) + 7.56 \cdot 10^{-6} \cdot (1156171 - X^i_{BV}) \quad (4.6)$$

$$z\text{-}score = \frac{CSA_{norm} - 66.26}{5.72} \quad (4.7)$$

CSA(C2-C3):

$$CSA^i_{norm} = CSA^i_{meas} + 0.002 \cdot (15266 - X^i_{TV}) + 7.30 \cdot 10^{-6} \cdot (1156171 - X^i_{BV}) \quad (4.8)$$

$$z\text{-}score = \frac{CSA_{norm} - 66.40}{5.64} \quad (4.9)$$

`TV: thalamus volume (mm`^{3}`) ; BV: brain volume (mm`^{3}`)`

With the CSA at 64 mm from the PMJ normalization, COV went from 10.09 % (CSA^i_{meas}) to 8.64 % (CSA^i_{norm}), a reduction of 14.37 %. With the CSA at C2-C3 disc normalization, COV went from 9.96 % (CSA^i_{meas}) to 8.51 % (CSA^i_{norm}) a reduction of 14.61 %.

Brain and thalamus volumes and sex interaction with brain volume

Figure 4.6 and **Figure 4.7** show scatterplots of CSA at 64 mm from the PMJ and at the C2-C3 disc with both predictors (brain volume and thalamus volume) separated for sex.

Qualitatively, we observe that the slopes for female and male are different with the brain volume predictor, however the slopes are closer with the thalamus volume predictor. To quantitatively validate if the interaction coefficient is significant in the model, we computed the interaction of both predictors with sex. The interaction coefficient for brain volume was significant (**CSA(PMJ)**: *p-value* = 0.006; **CSA(C2-C3)**: *p-value* = 0.005) and sex was also significant when adding the interaction parameter **(CSA(PMJ)**: *p-value* = 0.005; **CSA(C2-C3)**: *p-value* = 0.004). For thalamus volume, the interaction coefficient was not significant **(CSA(PMJ)**: *p-value* = 0.227; **CSA(C2-C3)**: *p-value* = 0.218) neither was sex (**CSA(PMJ)**: *p-value* = 0.227; **CSA(C2-C3)**: *p-value* = 0.213). The interaction of brain volume and sex was therefore added to the previous model since it has a significant effect. The following equation presents the corresponding normalization equation:

CSA(PMJ):

$$\begin{aligned} CSA^i_{norm} =& CSA^i_{meas} + 1.98 \cdot 10^{-3} \cdot (15266 - X^i_{TV}) + 2.45 \cdot 10^{-6} \cdot (1156171 - X^i_{BV}) \\ & - 15 \cdot (0.437 - X^i_{sex}) + 1.26 \cdot 10^{-5} \cdot (530335 - X^i_{sex} \cdot X^i_{BV}) \end{aligned} \tag{4.10}$$

$$z\text{-}score = \frac{CSA_{norm} - 66.26}{5.59} \tag{4.11}$$

CSA(C2-C3):

$$\begin{aligned} CSA^i_{norm} =& CSA^i_{meas} + 1.98 \cdot 10^{-3} \cdot (15266 - X^i_{TV}) + 2.49 \cdot 10^{-6} \cdot (1156171 - X^i_{BV}) \\ & - 15.23 \cdot (0.437 - X^i_{sex}) + 1.26 \cdot 10^{-5} \cdot (530335 - X^i_{sex} \cdot X^i_{BV}) \end{aligned} \tag{4.12}$$

$$z\text{-}score = \frac{CSA_{norm} - 66.40}{5.61} \tag{4.13}$$

`TV: thalamus volume (mm`^{3}`) ; BV: brain volume (mm`^{3}`)`

The model was significant (*p-value* < 0.0001) for both CSA(PMJ) and CSA(C2-C3). Normalized CSA(PMJ) had a mean and STD of 66.26 mm^2 $\pm$ 5.69 mm^2 and for CSA(C2-C3), 66.40 mm^2 $\pm$ 5.61 mm^2. The COV of CSA(PMJ) went from 10.09 % to 8.59 %, a reduction of 14.85 %. The COV of CSA(PMJ) went from 9.96 % to 8.42 %, a reduction of 15.13 %. Adjusted R^2 was 0.271 for CSA(PMJ) and 0.276 for CSA(C2-C3).

Brain volume and sex interaction

Since measuring thalamus volume is not always convenient, we also proposed a model without the thalamus volume as a predictor and kept only brain volume, sex, and the interaction. Normalized CSA(PMJ) had a mean and STD of 66.26 mm^2 $\pm$ 5.94 mm^2 and for CSA(C2-

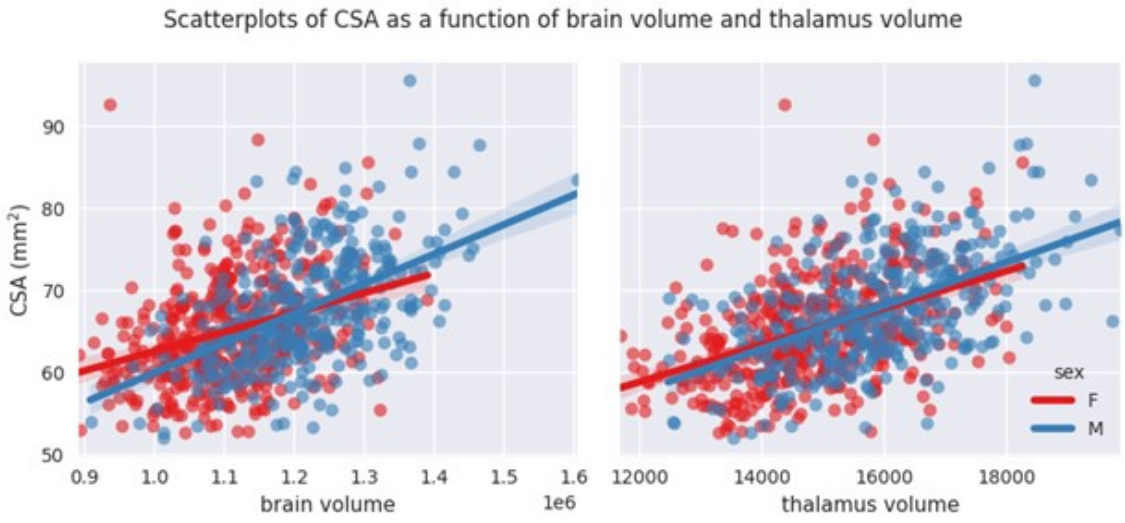

Figure 4.6 Scatterplots of CSA(PMJ) as a function of brain volume and thalamus volume separated for sex with linear fit.

C3), 66.40 mm^2 ± 5.86 mm^2. The COV went from 10.09 % to 8.96 %, a reduction of 11.22 % for CSA(PMJ) and the adjusted R^2 was 0.209. The COV went from 9.96 % to 8.88 %, a reduction of 11.39 % for CSA(C2-C3) and the adjusted R^2 was 0.212. Both models were also significant (*p-value* < 0.0001). Even if this model is less performant than the one including the thalamus volume, we present it given that thalamus volume is not often measured in neuroimaging analysis pipelines or in the presence of thalamic atrophy [83–88]. The normalization model has the following equation:

CSA(PMJ):

$$\begin{aligned} CSA^i_{norm} =& CSA^i_{meas} + 2.37 \cdot 10^{-5} \cdot (1156171 - X^i_{BV}) - 15 \cdot (0.427 - X^i_{sex}) \\ &+ 1.24 \cdot 10^{-5} \cdot (530335 - X^i_{sex} \cdot X^i_{BV}) \end{aligned} \tag{4.14}$$

$$z\text{-}score = \frac{CSA_{norm} - 66.26}{5.94} \tag{4.15}$$

CSA(C2-C3):

$$\begin{aligned} CSA^i_{norm} =& CSA^i_{meas} + 2.38 \cdot 10^{-5} \cdot (1156171 - X^i_{BV}) - 15.23 \cdot (0.427 - X^i_{sex}) \\ &+ 1.25 \cdot 10^{-5} \cdot (530335 - X^i_{sex} \cdot X^i_{BV}) \end{aligned} \tag{4.16}$$

$$z\text{-}score = \frac{CSA_{norm} - 66.40}{5.86} \tag{4.17}$$

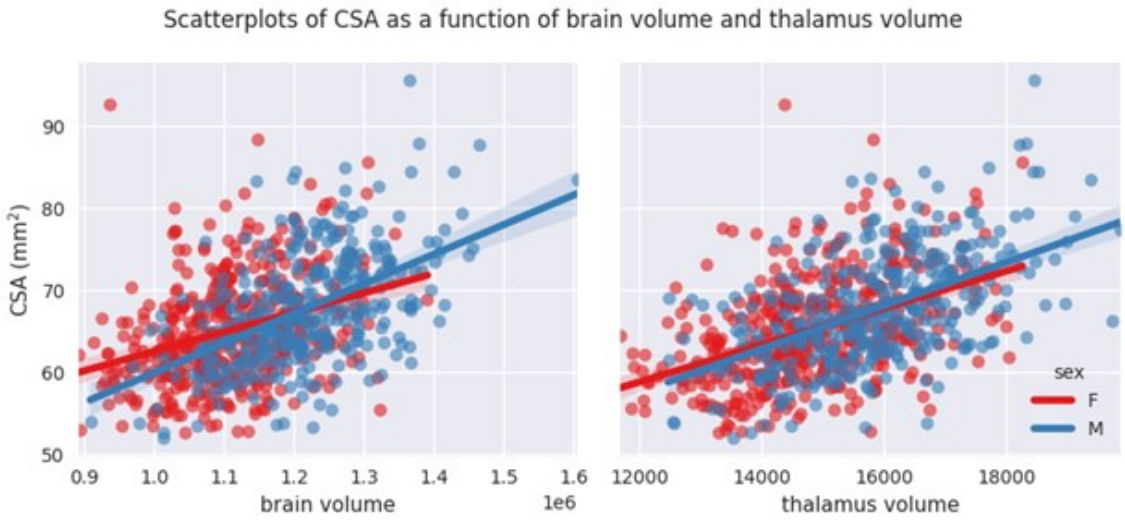

Figure 4.7 Scatterplots of CSA(C2-C3) as a function of brain volume and thalamus volume separated for sex with linear fit.

`TV: thalamus volume (mm`^{3}`) ; BV: brain volume (mm`^{3}`)`

4.4 Discussion

In this work, we quantified the contribution of various factors on inter-subject variability in cervical spinal cord CSA measurements in 804 participants with a fully-automatic processing pipeline. We implemented a measurement method for spinal cord CSA that uses the PMJ as opposed to the vertebral reference to overcome its limitations associated with the head position variability. Finally, we developed a normalization model which can reduce inter-subject variability by up to 14.85 % for CSA(PMJ) or 15.13 % for CSA(C2-C3).

4.4.1 CSA results

We obtained mean CSA values of 66.2 mm^2 and 66.4 mm^2 for PMJ-based and vertebral-based CSA respectively, which is lower than what was reported in other studies [9, 10, 71]. Lower values could be explained by various factors. Firstly, the population studied here is relatively older than in other published studies (range: 48 to 80, mean: 64). Secondly, the segmentation method has an impact on defining the boundary between the spinal cord and surrounding CSF. SCT's `sct_deepseg_sc` is more conservative than other software in defining this border, which results in a smaller CSA [89,90]. This is due to the segmentation algorithm: if we adjust the threshold for determining the boundary between the spinal cord and the background

(CSF), the produced segmentation becomes systematically scaled up/down depending on the threshold value. This translates to a systematic bias, similar to a calibration problem, which applies, in average, equally across data quality. Therefore, when it comes to using CSA values for clinical studies, it only adds an offset and does not affect the precision of the measure. Thirdly, acquisition parameters (which drive image contrast) also influence CSA values [12, 14]. Furthermore, gradient echo T1w acquisitions are prone to motion artifacts, which hamper the performance of spinal cord segmentation. COV were 9.96 % and 10.09 % (C2-C3, PMJ), which is similar to what was observed in previous studies [9, 10, 71].

4.4.2 PMJ-based CSA method

Regarding vertebral-based CSA and PMJ-based CSA, COVs are very similar (9.96 % C2-C3, 10.09 % PMJ) as for CSA values (see **Figure 4.3**). The CSA measures between the PMJ and C2-C3 disc reference were statistically different ($p\text{-}value = 0.0002$). This suggests that using the PMJ as a reference for CSA measurement is relevant to overcome the imprecise prediction of the spinal segments. This enforces the fact that vertebral levels are not a precise surrogate for spinal levels. In terms of variability, there is no clear conclusion if the PMJ-based method reduces the inter-subject variability, which is a relevant indicator in cross-sectional studies (e.g., used to assess the signature of a biomarker with different phenotypes). However, for longitudinal studies (i.e.: intra-subject COV), given that head tilting might change across sessions, it is possible that a PMJ-based method is preferred. While no clear conclusion can be drawn from the PMJ-based method in comparison with the vertebral-based method in terms of inter-subject CSA variability, this study sets the foundations, which are hard to establish, to further investigate the relevance of a PMJ-based method since it is fully-automatic and suggests promising results for longitudinal studies.

Some limitations are associated with the PMJ-based CSA method. The use of the PMJ label to interpolate with the centerline is not the exact extrapolation of the centerline. Spinal cord curvature at the PMJ varies across individuals, which adds variability to the computed distance. PMJ label positioning across participants may also differ, also affecting the measured distance.

Moreover, the absolute distance from PMJ doesn't consider the fact that the spinal cord length varies across individuals [26, 91]. Using a relative distance to predict the spinal segments from the PMJ could be relevant to overcome this limitation. Results from this study show a difference between spinal cord CSA using a vertebral-based vs PMJ-based reference, but not between the inter-subject variability. A comparison with the nerve rootlets is necessary to assess which method ensures proper prediction of the spinal segments; it will be the

subject of further investigations.

Another question remains about the robustness of the PMJ-based CSA method in the presence of lesions in the brainstem and the spinal cord. The presence of lesions in the brainstem could lower the performance of the automated identification of the PMJ, which needs to be further assessed in pathological data. The other important aspect of the PMJ-based method is the spinal cord centerline, which is extracted from the spinal cord segmentation. In the presence of lesions, the automatic segmentation could also be less reliable, requiring manual correction. Future developments of spinal cord segmentation algorithms that are robust to the presence of lesions would address this limitation.

In the case of high atrophy rate in the brainstem, we expect that it is very unlikely that the PMJ won't be easily identifiable, considering it is the only required label in the brainstem region for this method. Additionally, we don't expect that the centerline extraction will be affected by lesions in the brainstem since it only relies on the spinal cord segmentation. However, a high atrophy rate in the spinal cord would affect the spinal cord segmentation. The centerline would lose some precision since it is extracted by computing the center of mass of each slice of the spinal cord segmentation. This could result in loss of precision in the computation of the distance from the PMJ in order to compute CSA, but further investigations are needed to establish the impact of lesions in the brainstem or spinal cord on the PMJ-based CSA method.

4.4.3 Correlation with spinal cord CSA

Our analysis shows a strong correlation between brain volume, brain WM volume, brain GM volume and thalamus volume with CSA, as previous studies have reported [9, 10, 62, 66]. The highest correlation was found with thalamus volume (Pearson's r = 0.51). Numerous ascending tracts project from the spinal cord to various thalamus nuclei (spinothalamic tract), which could explain a close correlation between CSA and thalamus volume compared to other brain structures [92–94]. No significant correlation was found with ventricular CSF volume. Correlations with height and weight are low.

It would have been interesting to explore other potential regressors explaining spinal cord CSA, such as other deep GM structures, as well as brainstem structures (e.g., pons, medulla) due to their closeness to the cervical spinal cord. These additional regressors would help elucidate if the strong correlation between the thalamus volume and spinal cord CSA is unique to the thalamus or if it is also found in other structures. We found a statistical difference between spinal cord CSA between male and female; females have a significantly smaller CSA than males as previous studies have shown [9, 10, 66]. Regarding the effect of

age on spinal cord CSA, we found a decrease of CSA with age. Linear and quadratic fit gave very similar results (**CSA(PMJ)**: $R^2 = 0.031$ and **CSA(C2-C3)**: $R^2 = 0.034$ for both fits). Since the age range of the participants goes from 48 to 80 years old, it is not surprising that a linear fit is also adequate, in comparison with results reported by others [9,71]. Since CSA peaks around 45 years old [9,71], CSA values for the age range of this study are decreasing with age as we observed (see **Figure 4.5**).

4.4.4 Normalization methods

Stepwise linear regression led to thalamus volume and brain volume as predictors for spinal cord CSA. We introduce for the first time thalamus volume as a predictor for normalization of spinal cord CSA. Thalamus volume presented a high correlation with brain volume (Pearson's r = 0.79), hence some collinearity between both predictors may reduce the statistical power in the obtained model. However, we decided to keep both variables in order to preserve some potentially useful interaction measures. This model significantly reduced inter-subject variability; COV went down from 10.09 % to 8.64 %, which represents a reduction of 14.37 % for CSA(PMJ). COV went down from 9.96 % to 8.51 %, which represents a reduction of 14.61 % for CSA(C2-C3). Other parameters were not significant since they were excluded during the stepwise model ($p\text{-}value > 0.05$). Sex alone was not a significant predictor ($p\text{-}value > 0.05$) even if there is a significant difference between male and female CSA. Note the strong correlation between sex and thalamus volume (Pearson's r = 0.36) and between sex and brain volume (Pearson's r = 0.49). When adding the interaction between sex and brain volume, sex and the interaction became significant. The effect of brain volume on spinal cord CSA varies between male and female as we can observe in **Figure 4.6** and **Figure 4.7**. The interaction between thalamus volume and sex wasn't significant. The model including brain volume, thalamus volume, sex and sex/brain volume interaction led to a COV of 8.59 %, a reduction of 14.85 % for CSA(PMJ) and for CSA(C2-C3), a COV of 8.42 %, a reduction of 15.13 %. Including sex and brain volume interaction led to the best COV reduction. To our best knowledge, interaction of sex and brain volume was never considered in previous normalization models, only the fixed effect of sex on CSA was included. These findings reveal the importance to consider that factors can vary differently for males and females. We also proposed a model without the thalamus volume, given the difficulty to measure it (it requires the proper anatomical sequence with sufficient contrast and resolution) and/or in the case of abnormal thalamic atrophy, which could happen in various pathological conditions. This model reduced CSA variability less than when including thalamus volume (11.22 % of reduction for CSA(PMJ) vs 11.39 % for CSA(C2-C3)). The combination of thalamus volume, brain volume and sex better explains CSA variability.

Even if CSA at 64 mm from the PMJ and at C2-C3 disc differed significantly, the normalization analysis and obtained models did not vary and the coefficients of the models were very similar.

We obtained a smaller reduction than other models presented in previous studies [9, 71]. Kesenheimer et al. [71] obtained a reduction of COV of 23.7 % using sex, brain WM volume and spinal cord canal area, Papinutto et al. [9] obtained a reduction of 17.74 % using Vscale and axial-canal product. It is important to consider that the predictors of the normalization methods were different, mainly regarding metrics related to the spinal cord canal which could explain the smaller reduction of COV obtained with our model (CSA(PMJ): 14.85 % or CSA(C2-C3): 15.13 %). We did not include spinal cord canal metrics in our analysis because of the lack of automated methods for robust spinal cord canal segmentation combined with the large number of participants in this study. Also, the size of the cohort is larger than in the previously mentioned works, N = 60 for [71] and N = 129 for [9], which impacts the distribution and coverage of the data of the participants and affects the normalization method.

Age was not a significant predictor for spinal cord CSA. Trends for CSA and brain volume for the age range of our study were very similar. The effect may differ for younger people since brain volume decreases linearly with age while CSA increases until about 45 years old and decreases afterward [9].

We have to consider the fact that older people may be more subject to motion in the MRI than younger people (discomfort, difficulty breathing) resulting in a bias in the measured CSA (blurring, motion artifact ghosting). Further investigations are needed to validate if the model can expand to ages not included in this study.

The normalization model was generated from T1w data with a specific protocol. Subsequent studies should assess whether the model is adequate for other acquisition parameters and contrasts. It is known that the output CSA varies for different acquisition protocols [12]. However, since there is a direct relationship between CSA values from different contrasts, there would be a systematic offset in the produced CSA. Since the model is linear, it should hold for different contrasts.

It is important to note that the choice of processing software package (and its version) used to compute the brain morphometrics affects the measured brain and thalamus volumes, and hence the proposed normalization model. The proposed normalization model would then require data to be processed using the same processing software as that used for the UK Biobank analysis pipeline [81].

The model was developed from healthy participants; the question remains if it would be applicable to patients with neurodegenerative diseases such as MS. Thalamic atrophy is common in neurodegenerative diseases such as MS [83–88]. In the case of such atrophy, one should refrain from normalizing CSA with thalamus volume since the normalization would be biased. This is why we proposed a model without the thalamus volume. Also, brain volume changes have been associated with atrophy for various neurodegenerative diseases. A normalization model including brain volume may not be generalizable for those patients. As done in other studies [71], intracranial volume could be a relevant substitute for brain volume since it is not affected by neurodegenerative diseases. Including sex interaction here will also be important and can improve the normalization model. Further studies could include intracranial volume in the normalization model.

Furthermore, other confounding factors could possibly affect image acquisitions for pathological patients. Severe motor disability could induce some breathing difficulties which induces considerable motion artifacts, thus spinal cord segmentation and CSA bias.

4.4.5 SCT normalization feature

We made available the obtained normalization model in the open-source software SCT within `sct_process_segmentation`. Since thalamus volume may not be available in all spinal cord MRI studies, we made it possible for the user to normalize CSA values without thalamus volume. Even if the best model was obtained with thalamus volume, brain volume, sex and sex interaction between brain volume and sex, normalizing spinal cord CSA without thalamus volume could still reduce CSA variability. The normalization feature can be used by adding the option `-normalize` followed by the predictors and their corresponding values. For more information on usage, refer to: https://spinalcordtoolbox.com/user_section/command-line.html#sct-process-segmentation.

4.5 Conclusions

This study features an analysis of factors contributing to spinal cord CSA variability at a larger scale than what was done previously to our best knowledge using an automatic processing pipeline. We introduced a new reference in the context of CSA measurements based on a neurological reference (PMJ) to overcome vertebral reference limitations (neck flexion and extension) which sets ground for further investigation regarding the prediction of spinal segments and cervical CSA studies. We computed over a large cohort of participants spinal cord CSA at 64 mm from the PMJ on T1w scans from the UK Biobank database.

The pipeline is based on regular brain MRI scans, making it of interest for a broad range of study types, including clinical studies. No significant age trend was found while spinal cord CSA was significantly different for males and females. We present an effective normalization model including thalamus volume, brain volume, sex and sex/brain volume interaction readily usable in SCT. The most relevant factors to explain spinal cord CSA variability are related to the brain; these findings show the importance of having a brain MRI acquisition in spinal cord studies/research. Reducing inter-subject variability could improve comparison between CSA measures to increase its sensitivity and specificity to better assess pathology-related changes.

4.6 Acknowledgements

We thank Étienne Bergeron, Olivier Lupien-Morin, Benjamin Carrier and Yassine El Bouchaibi for helping with the manual correction and labeling, Nicholas Guenther and Alexandru Foias for data management with git-annex. This research was conducted using data from UK Biobank (www.ukbiobank.ac.uk). This study was funded by the Canada Research Chair in Quantitative Magnetic Resonance Imaging [950-230815], the Canadian Institute of Health Research [CIHR FDN-143263], the Canada Foundation for Innovation [32454, 34824], the Fonds de Recherche du Québec - Santé [28826], the Natural Sciences and Engineering Research Council of Canada [RGPIN-2019-07244], the Canada First Research Excellence Fund (IVADO and TransMedTech), the Courtois NeuroMod project, the Quebec BioImaging Network [5886, 35450], the Spinal Research and Wings for Life (INSPIRED project).

4.7 Conflict of Interest

None

4.8 Supplementary Material

4.8.1 Supplementary Figures and Tables

Supplementary Figures

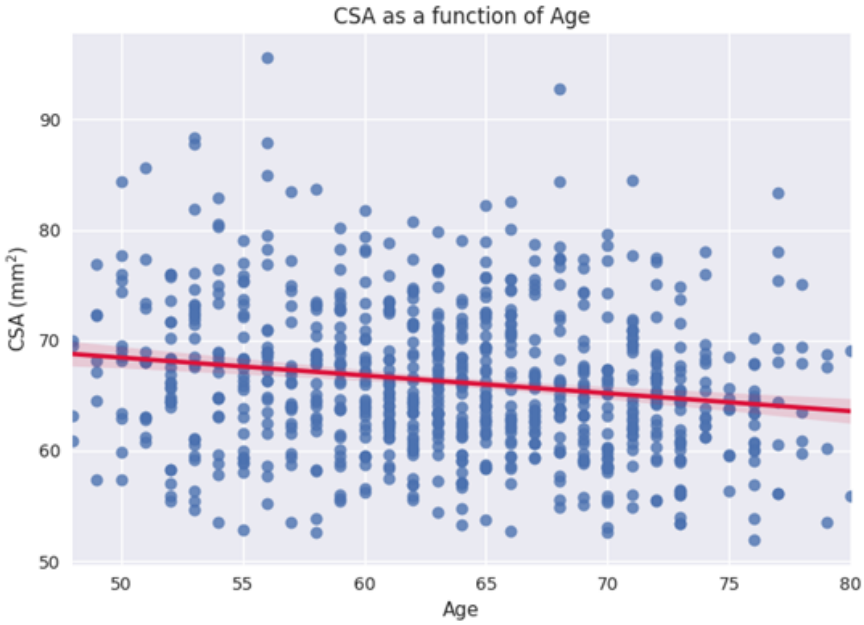

Figure 4.8 Scatterplot of CSA at 64 mm from the PMJ as a function of age.

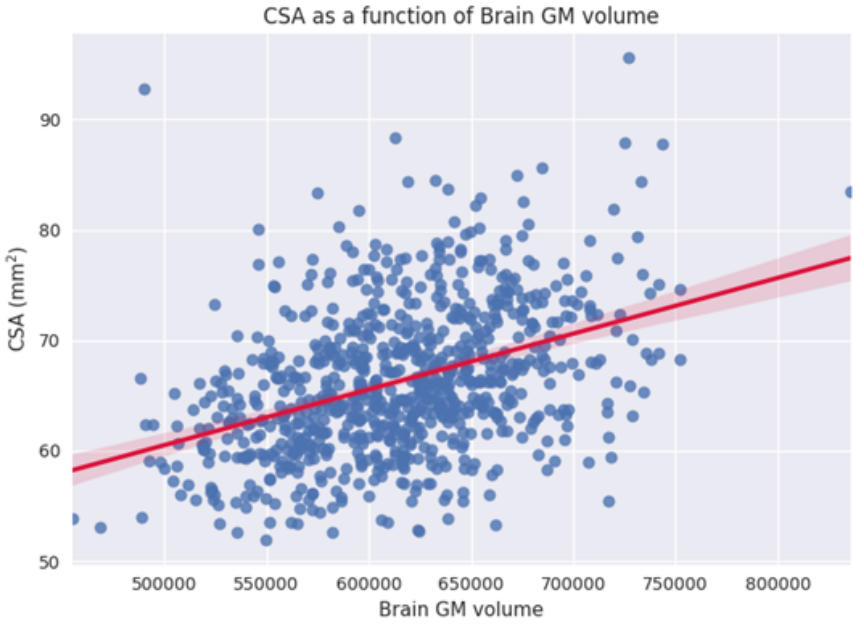

Figure 4.9 Scatterplot of CSA at 64 mm from the PMJ as a function of brain GM volume.

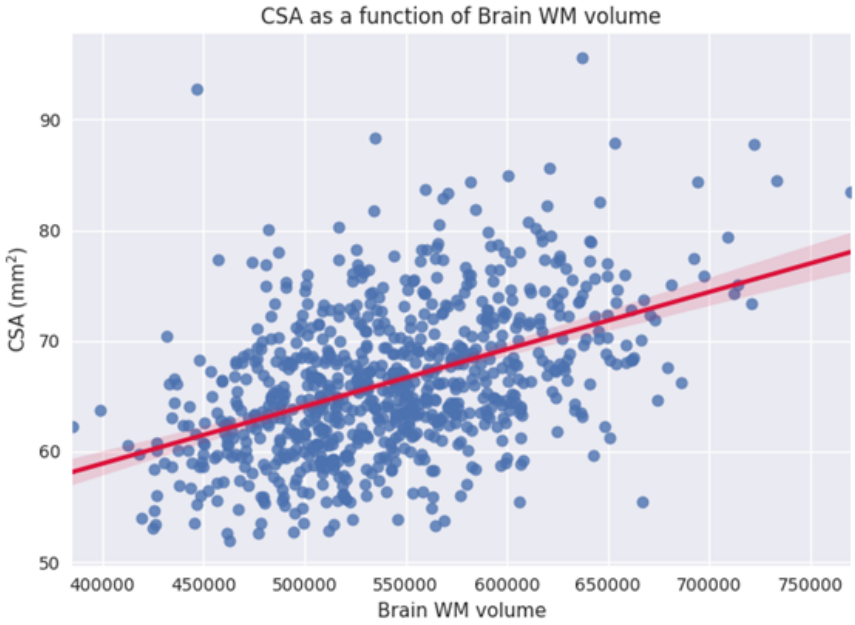

Figure 4.10 Scatterplot of CSA at 64 mm from the PMJ as a function of brain WM volume.

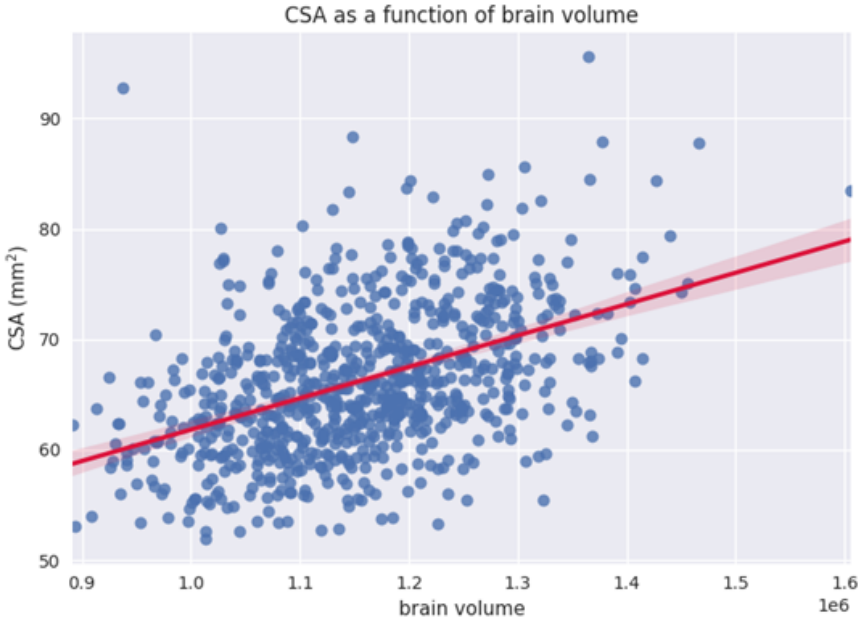

Figure 4.11 Scatterplot of CSA at 64 mm from the PMJ as a function of brain volume.

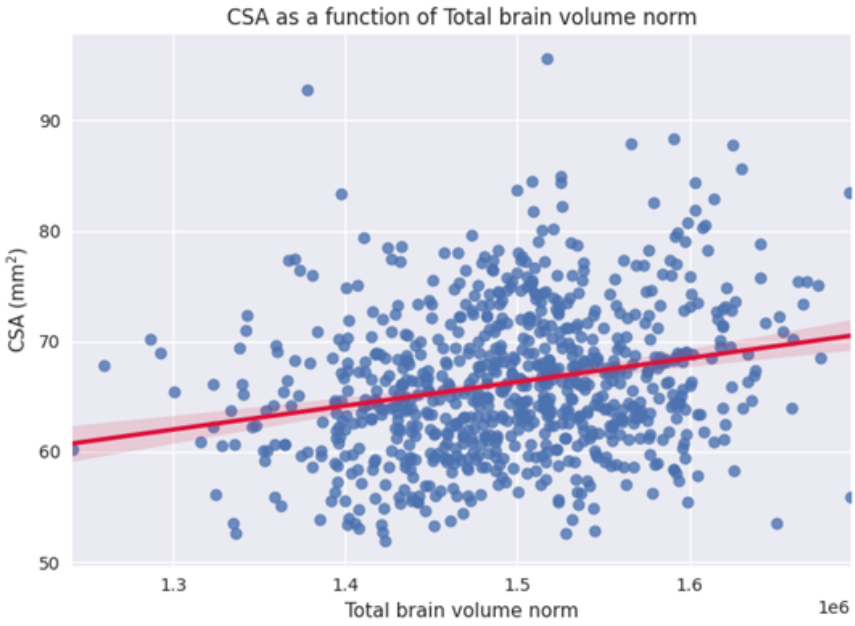

Figure 4.12 Scatterplot of CSA at 64 mm from the PMJ as a function of brain volume normalized for head size.

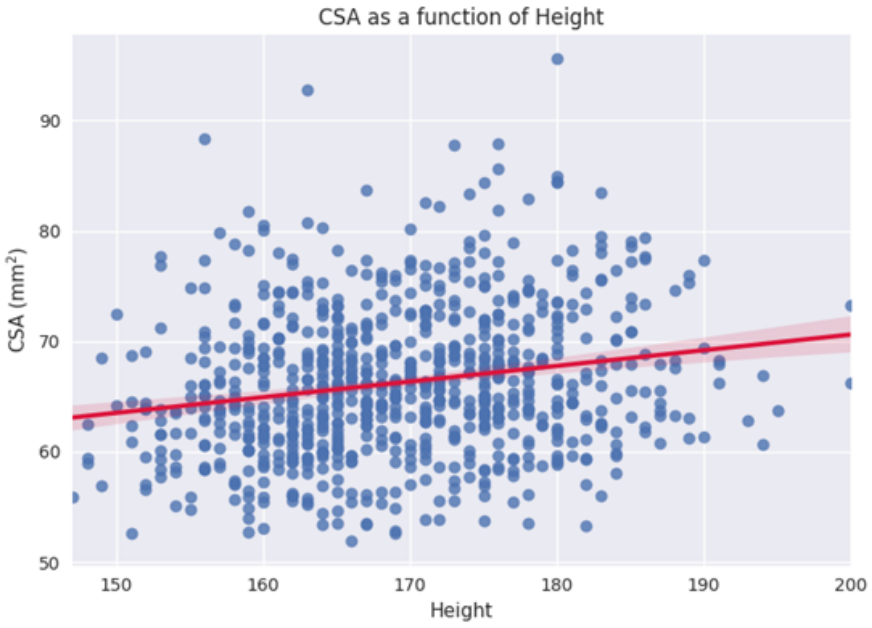

Figure 4.13 Scatterplot of CSA at 64 mm from the PMJ as a function of height.

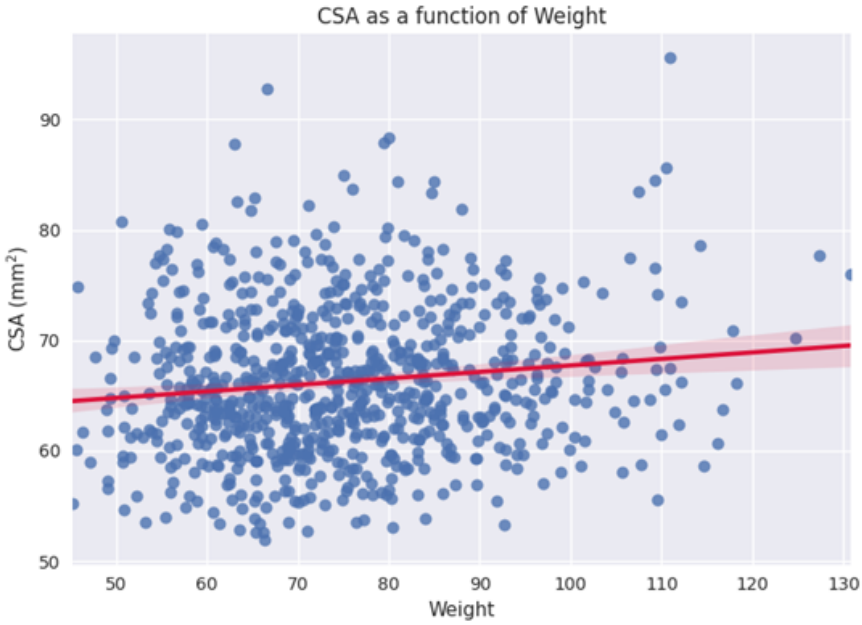

Figure 4.14 Scatterplot of CSA at 64 mm from the PMJ as a function of weight.

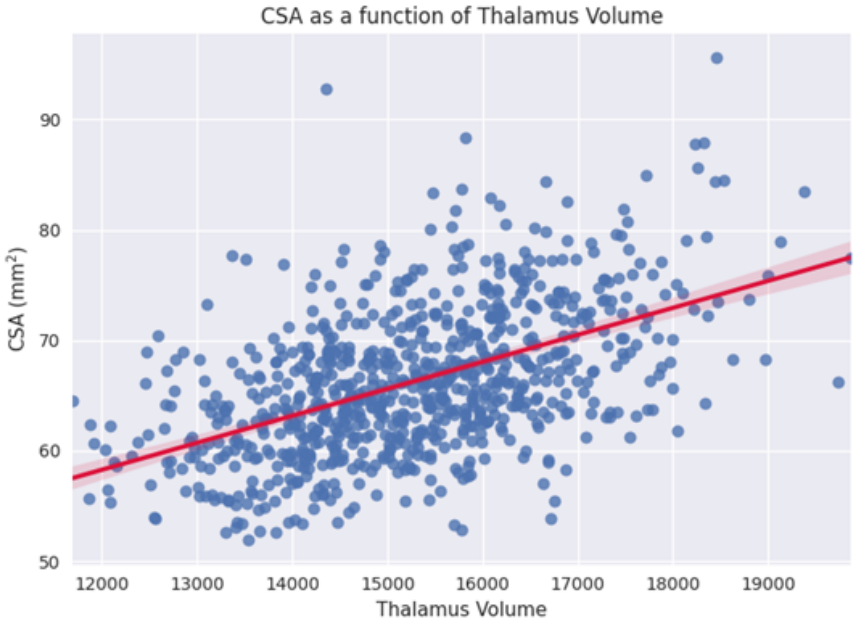

Figure 4.15 Scatterplot of CSA at 64 mm from the PMJ as a function of thalamus volume.

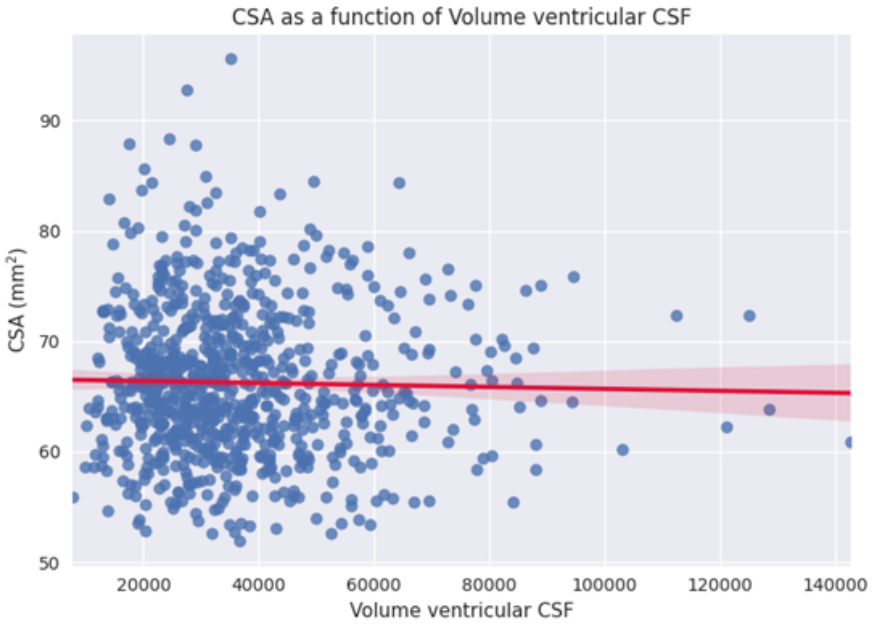

Figure 4.16 Scatterplot of CSA at 64 mm from the PMJ as a function of ventricular CSF volume

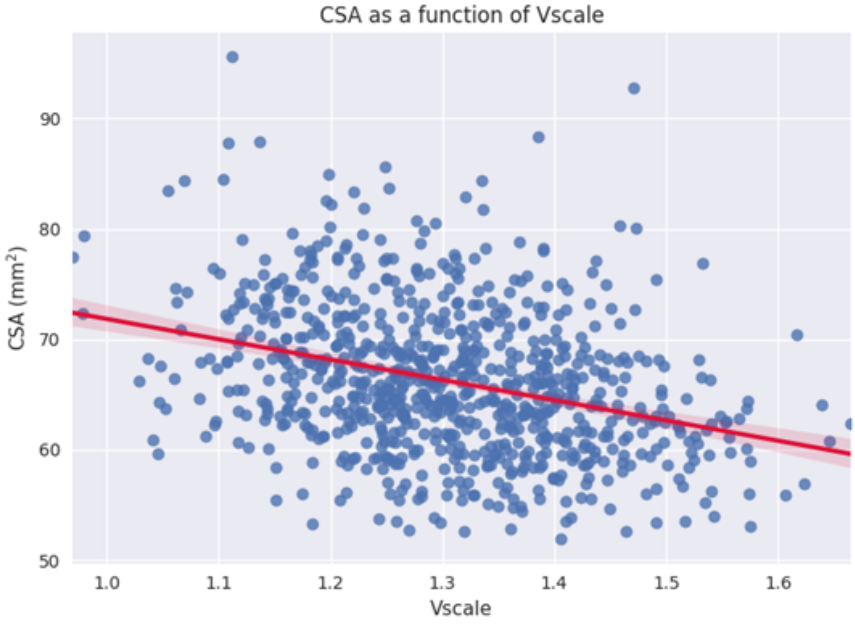

Figure 4.17 Scatterplot of CSA at 64 mm from the PMJ as a function of Vscale

CHAPTER 5 ARTICLE 2: PONTOMEDULLARY JUNCTION AS A REFERENCE FOR SPINAL CORD CROSS-SECTIONAL AREA: VALIDATION ACROSS NECK POSITIONS

Published the 19th of August 2023 in Scientific Reports, 13, 13527 (2023). https://doi.org/10.1038/s41598-023-40731-3

Title: Pontomedullary junction as a reference for spinal cord cross-sectional area: validation across neck positions.

Authors: Sandrine Bédard[1], Maxime Bouthillier[1,2] Julien Cohen-Adad[1,3,4,5]

Affiliations:

1. NeuroPoly Lab, Institute of Biomedical Imaging, Polytechnique Montréal, Montreal, Quebec, Canada.
2. Centre hospitalier de l'Université de Montréal, University of Montreal, Montreal, QC, Canada.
3. Functional Neuroimaging Unit, CRIUGM, University of Montreal, Montreal, QC, Canada.
4. Mila - Quebec AI Institute, Montreal, QC, Canada.
5. Centre de recherche du CHU Sainte-Justine, Université de Montréal, Montréal, QC, Canada

Abstract

Background: Spinal cord CSA is an important MRI biomarker to assess spinal cord atrophy in various neurodegenerative and traumatic spinal cord diseases. However, the conventional method of computing CSA based on vertebral levels is inherently flawed, as the prediction of spinal levels from vertebral levels lacks reliability, leading to considerable variability in CSA measurements. Computing CSA from an intrinsic neuroanatomical reference, the PMJ, has been proposed in previous work to overcome limitations associated with using a vertebral reference. However, the validation of this alternative approach, along with its variability across and within participants under variable neck extensions, remains unexplored. The goal of this study was to determine if the variability of CSA across neck flexions/extensions is reduced when using the PMJ, compared to vertebral levels.

Methods: Ten participants underwent a 3T MRI T2w isotropic scan at 0.6 mm^3 for 3 neck positions: extension, neutral and flexion. Spinal cord segmentation, vertebral labeling, PMJ labeling, and CSA were computed automatically while spinal segments were labeled manually.

Results: Mean COV for CSA across neck positions was 3.99 ± 2.96 % for the PMJ method vs. 4.02 ± 3.01 % for manual spinal segment method vs. 4.46 ± 3.10 % for the disc method. These differences were not statistically significant.

Conclusion: The PMJ method was slightly more reliable than the disc-based method to compute CSA at specific spinal segments, although the difference was not statistically significant. This suggests that the PMJ can serve as a valuable alternative and reliable method for estimating CSA when a disc-based approach is challenging or not feasible, such as in cases involving fused discs in individuals with spinal cord injuries.

Corresponding author:
Sandrine Bédard
Ecole Polytechnique, Pavillon Lassonde, L5626
2700, chemin de la Tour
Montréal, QC
H3T 1J4
email: sandrine.bedard@polymtl.ca

5.1 Introduction

Spinal cord CSA is a relevant biomarker to assess spinal cord atrophy in diseases like MS [77,95] and spinal cord injury [3,96,97]. Early neurodegeneration in MS requires high accuracy in detecting subtle atrophy for monitoring purposes [98]. Traditionally, CSA is measured at a specific rostro-caudal location based on vertebral levels to enable consistent comparisons through time in cross-sectional and longitudinal studies. It is important to note that there is a distinction between vertebral levels and spinal levels. Inferring the neuroanatomic position of the spinal levels with the vertebrae can introduce inaccuracies, contributing to variability in CSA measurements [16]. Cadotte et al. [16], showed that spinal segment positions differ across individuals and poorly overlap with vertebral bodies. A vertebral reference also does not account for variations in neck positioning within the MRI scanner. Spinal levels can be identified by segmenting the nerve rootlets, but it is a challenging task, and requires high resolution scans (about 0.6 mm^3) and an expert rater. Having a more precise surrogate reference for spinal levels is important to link CSA measurements with the clinical outcome.

It is important to consider neck flexion and extension from an anatomical and biomechanical standpoint. The spinal cord dura mater is a continuation of the cranial dura mater extending from the foramen magnum and the brainstem [99]. Head extension and flexion produce a change of direction of the nerve rootlets compared to a neutral posture where nerve rootlets run downwards. Neck flexion also elongates the spinal cord, with its maximum between C2-T1 nerve rootlets [100]. Neck flexion and extension also produce movement of the spinal segments relative to vertebral segments: Bilston & Thibault [32] showed during neck extension that C3 moves caudally of 5 mm vs 2 mm at C5 compared to neutral positions.

A few have introduced surrogate neuroanatomic landmarks to overcome the limitation of the vertebral reference like the PMJ [16, 17] or the *conus medullaris* [19].

We introduced in previous work an automatic pipeline to compute CSA at a distance from the PMJ in a cross-sectional study to reduce spinal cord CSA inter-subject variability [101]. CSA averaged at the C2-C3 disc and CSA at 64 mm from the PMJ gave similar COVs; no clear conclusion about the effect of the reference on CSA variability across individuals was found [101]. Further validation is necessary to evaluate the potential use of PMJ-based reference in the context of longitudinal studies.

The aim of this study is to investigate the relevance of the PMJ as an anatomical reference to mitigate intra-subject variability in CSA measurements in a longitudinal context. It involves (i) developing a pipeline to label the spinal segments using the nerve rootlets in T2w images, (ii) determining the variability of intervertebral discs and the PMJ across three neck flexion/extensions, and (iii) comparing CSA variability using the PMJ, traditional vertebral levels, and spinal segments as references.

5.2 Material and Methods

Data acquisition

Ten healthy participants (Age: mean ± STD = 22.9 ± 1.2 years old; 3 females) were scanned using a Siemens 3T Prisma-fit with a 64 head-neck coil at three neck positions (extension, neutral, and flexion), as illustrated in **Figure 5.1**. Informed consent was obtained from each participant and appropriate padding was used to maintain the head position and ensure comfort. The study was approved by the Comité d'éthique de la recherche du Regroupement Neuroimagerie Québec. All experiments were performed in accordance with the Declaration of Helsinki.

The field of view covered the top of the head down to at least the T1 vertebrae. A 3D sagittal T2w scan was acquired for each neck position with the following parameters: SPACE

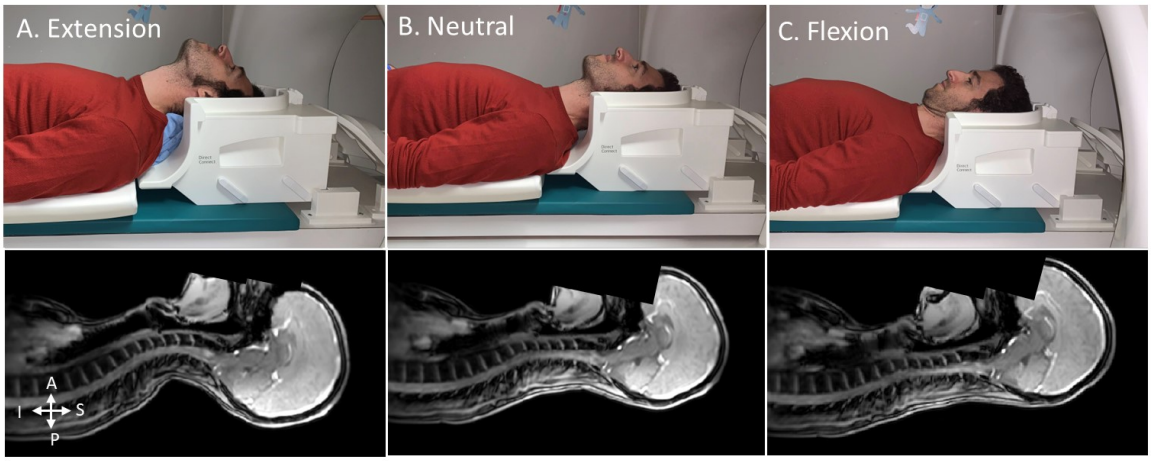

Figure 5.1 Example of the head positioning in the MRI's head coil for neck extension **(A)**, neutral **(B)** and flexion **(C)**. The bottom row shows localizers. (One of the authors is in the scanner).

sequence, TR: 1.5 s, TE: 0.12 s, matrix: 72×384, in-plane resolution: 0.6×0.6 mm^2, number of slices: 384, slice thickness: 0.6 mm, pixel bandwidth: 620 Hz/pixel).

5.2.1 Data processing

The spinal cord was automatically segmented using SCT [30] `sct_deepseg_sc` [58] and the PMJ and vertebral levels were identified.

Spinal segment labeling

Spinal segments were manually labeled on T2w images for each neck position by an expert rater (MB) using the spinal nerve rootlets to identify the mid spinal segment position (**Figure 5.2**). The standardized procedure is available on GitHub (https://github.com/sct-pipeline/pmj-based-csa/tree/r20230313#manual-labeling-of-spinal-cord-rootlets-with-fsleyes).

Briefly, to label the spinal segments, we propose straightening the spinal cord to enhance visualization of the spinal nerve rootlets, as the natural curvature of the spinal cord can impede their clear identification in the coronal view. Non-local means adaptive denoising is applied to denoise the image [102]. In summary, the non-local mean filter leverages the similarity between distinct image patches to decrease noise while preserving details. Furthermore, it integrates the spatial and frequency information present in the image to adapt the denoising process. Spinal segment labels are then placed at the center (superior-inferior) of where the rootlet emerges from the spinal cord on the corresponding axial slice in the center of the

spinal cord. The labeling convention is indicated in **Figure 5.2**, and all spinal segments with visible nerve rootlets (except C1) are labeled for all neck positions and participants. The labels are finally brought back to the curved space with the inverse transform.

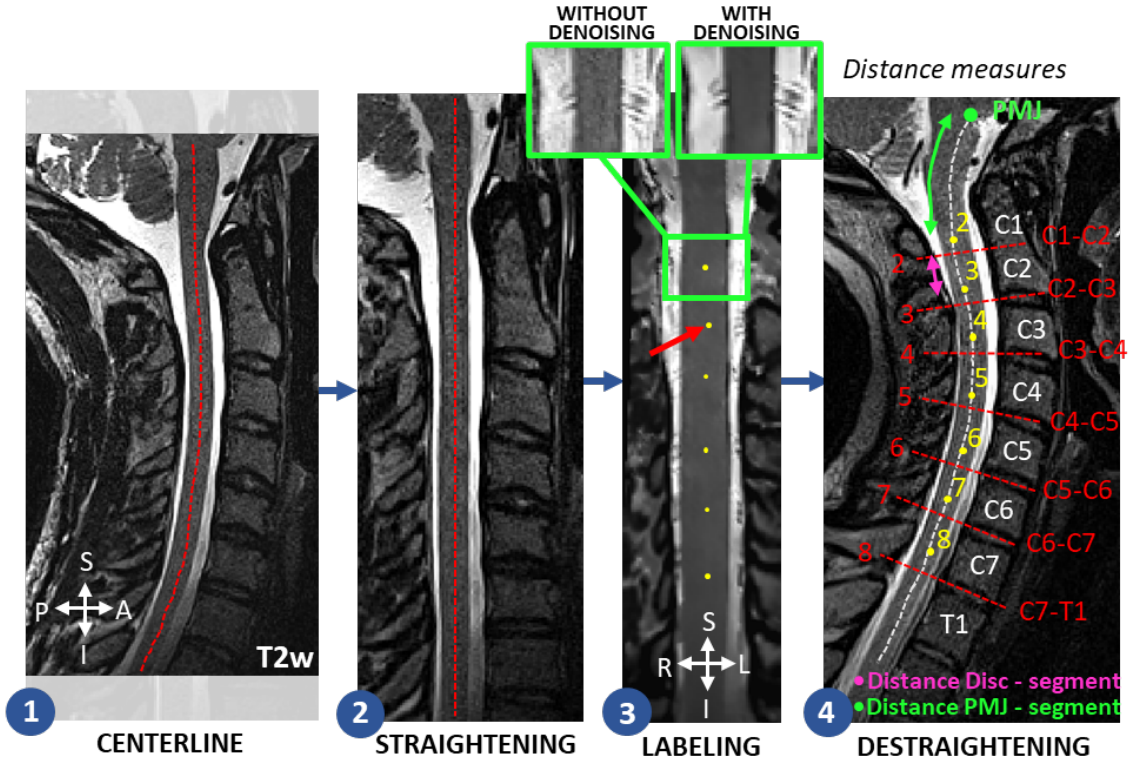

Figure 5.2 Spinal segment labeling pipeline. **(1)** spinal cord centerline is detected, **(2)** spinal cord is straightened, **(3)** denoised, and manually labeled in the coronal view. **(4)** The inverse transformation is applied on the labels. The distances between the PMJ and each spinal segment (green), and between each spinal segment and corresponding disc (pink) were computed.

Distance with PMJ, spinal segment and discs

To estimate the position of the spinal segments using the PMJ and the discs as references, we computed two types of distances along the spinal cord centerline for each participant and neck position: between the PMJ and each spinal segment (**Figure 5.2.4** green), and between each intervertebral disc and its corresponding spinal segment (**Figure 5.2.4** pink).

To assess the reliability of the spinal segment location estimation across the different neck positions, we computed the STD across neck positions for each participant. The STD was computed for each method (PMJ, discs) and for each level (2 to 7). The STD was chosen

to assess variability, as opposed to COV, because the absolute value of distances PMJ-spinal segment becomes larger for lower spinal segments, which would have influenced the COV when compared to disc-spinal segment distances. To assess if there was a significant difference between the STD of the estimated spinal segment positions measured with the PMJ and the discs, we conducted a paired two-way ANOVA test on the STD across neck positions (dependent variable) of the 10 participants. The independent variables were the methods (PMJ, discs) and levels (from 2 to 7). A significance level of $p\text{-}value = 0.05$ was set. We used the ANOVA test to detect a global effect of the independent variables rather than specific group differences. No post-hoc analysis was conducted.

CSA computation

Spinal cord CSA was computed using `sct_process_segmentation` and averaged across 3 slices using three references: *CSA PMJ*, *CSA spinal*, and *CSA discs* (**Figure 5.3**). *CSA PMJ* was computed at the distance between the PMJ and each spinal segment, averaged across the three neck positions. That distance was subject-specific. The reason we chose to average the distance across neck positions is the following. The main idea of this paper is to validate a PMJ-based method [101] as a reference for computing CSA instead of relying on intervertebral discs due to the known variability in the spatial correspondence between the spine and spinal cord. As a reminder, the PMJ-based method relies on a set distance from the PMJ along the spinal cord centerline. In the [101] paper, that distance was set to 64 mm, which corresponded to the distance to the C2-C3 disc, averaged across 804 adult participants. In the present study, instead of computing a distance between the PMJ and the C2-C3 disc, we estimate a distance between the PMJ and each spinal segment (manually identified with the nerve rootlets). That distance is calculated for each participant and for each neck position. Our hypothesis is that, for each participant, regardless of the neck extension, the PMJ-based CSA will give similar values (as opposed to the disc-based CSA, because the spinal cord moves along the superior-inferior axis relative to the discs, depending on the neck position). To verify this hypothesis, we set a subject-specific distance between the PMJ and each spinal segment to be the average across the three neck positions. Then, we compute the CSA using that distance, and we evaluate the stability of that CSA measure. *CSA spinal* is computed at the spinal segment location for spinal levels C2 to C8, and *CSA discs* at the intervertebral discs C2-C3 to C7-T1.

To estimate the variability of CSA across neck positions, we computed the COV, instead of the STD in order to aggregate the results across participants and levels, since CSA varies across participants and across spinal levels [103].

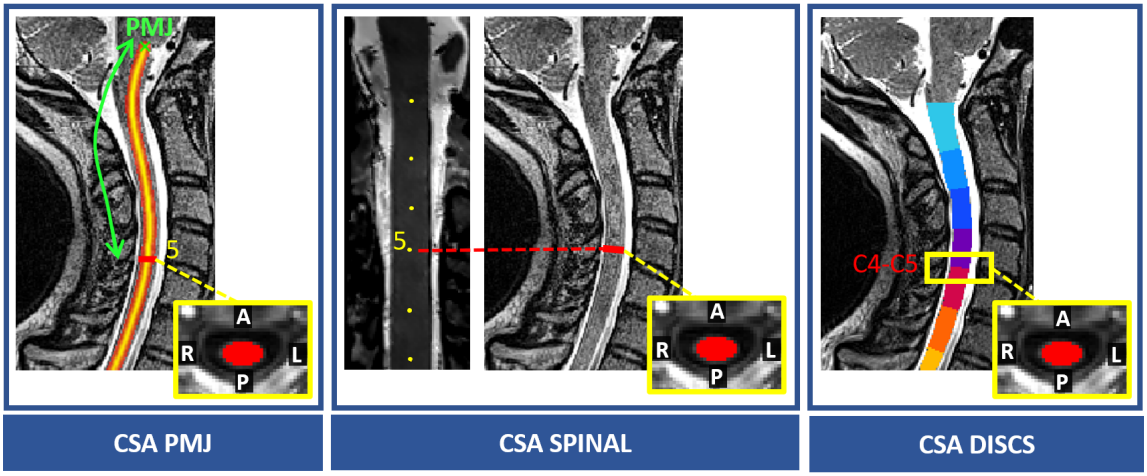

Figure 5.3 Spinal cord CSA computed with 3 references: **(A)** mean distance of each spinal rootlet from participant's PMJ, **(B)** each spinal segment, **(C)** each intervertebral disc.

The COV across neck positions was computed for each participant, method and level as following:

$$COV[i] = STD(neck\ position\ n = 3)/MEAN(n = 3) \tag{5.1}$$

A paired 3-way ANOVA test was performed to evaluate if CSA computed using the 3 different references (PMJ, Spinal, and Disc) yielded equivalent measures per participant. The independent variables examined in our analysis were the methods (PMJ, Spinal, and Disc), levels, and neck positions. Note that the ANOVA test was specifically conducted on the CSA rather than on the COV, in order to be able to account for the neck position as an independent variable. Furthermore, due to the paired nature of the ANOVA test, COV was not relevant.

Neck angle

The angle of the spinal cord was computed for each neck position in the right-left axis. The angle was computed between the C1-C2 and C4-C5 intervertebral discs (**Figure S5.71**) [104, 105]. The C4-C5 disc was chosen instead of the C6-C7 disc as done in the previous studies [104,105] since one participant presented a smaller field-of-view in the superior inferior direction resulting in the absence of the C5-C6 and lower discs.

Quality control

After running analysis, the quality of all spinal cord segmentations, vertebral labeling and PMJ labeling were visually assessed. Problematic segmentations (under- segmentation/leaking) and labels were identified in SCT's quality control report and manually corrected using ITK-SNAP. Disc labels were placed at the posterior tip of the disc for C1-C2 to C7-T1 and the PMJ was identified in the mid-sagittal plane. Corrections were added to the source dataset and the analysis was run again using the corrections instead of automatic labeling.

Code availability

The processing pipeline uses SCT v5.4 and is available on GitHub https://github.com/sct-pipeline/pmj-based-csa/releases/tag/r20230313 with its documentation: https://github.com/sct-pipeline/pmj-based-csa/tree/r20230313#readme.

5.3 Results

All data is accessible on OpenNeuro in the BIDS format [106]; manually corrected segmentations and PMJ, disc and spinal segment labels are also available: https://openneuro.org/datasets/ds004507/versions/1.0.1.

5.3.1 Spinal segment labeling

Spinal nerve rootlets looked similar across neck positions in the straightened space per participant (**Figure 5.4**). However, the center of spinal segments was more difficult to label in flexion due to motion artifacts, as seen in sub-003 (**Figure 5.4A.3**) resulting in less defined nerve rootlets. In contrast, sub-007 (**Figure 5.4B**) had good data quality with no motion artifacts and clear nerve rootlets.

5.3.2 Distance with PMJ, spinal segment and discs

To estimate the position of the spinal segments using the PMJ and discs, we computed the distance PMJ-spinal segment and the distance disc-spinal segment. Next, we compared the reliability of estimating the spinal segments position across neck positions for each method (PMJ, discs). To assess this, we computed the STD of the distances across neck positions for both the PMJ and discs methods. Results are presented visually with a boxplot (**Figure 5.5**), numerically (**Table 5.1**), and statistically (**Table 5.4**).

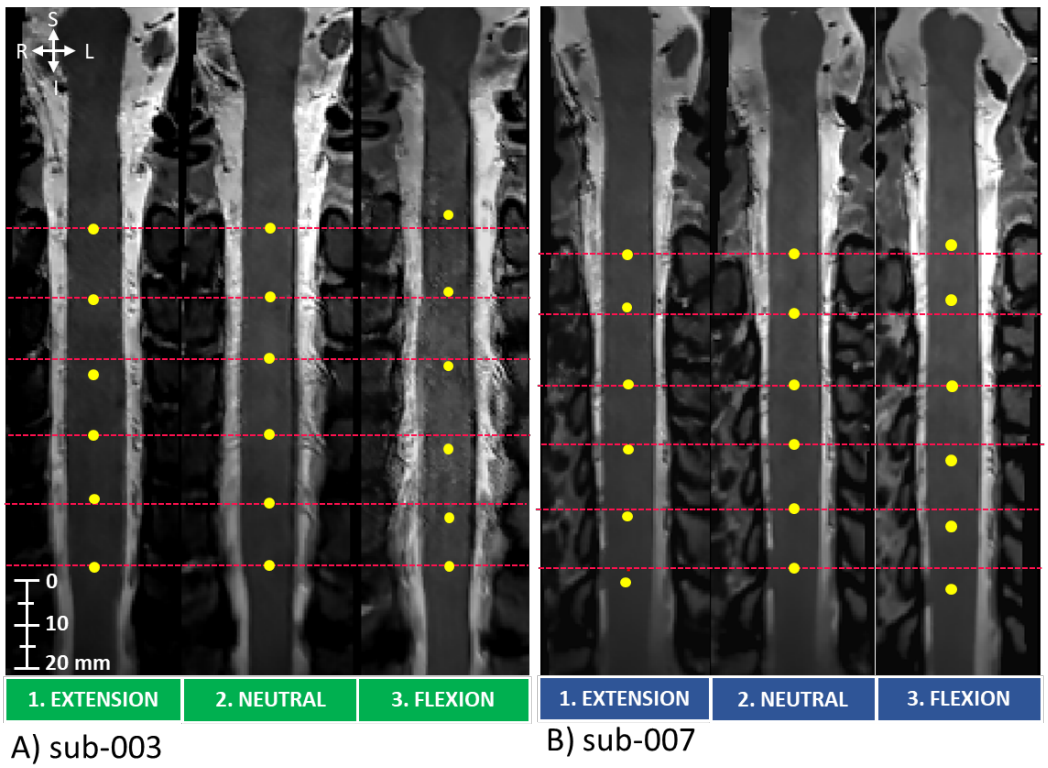

Figure 5.4 Example of challenging **(A)** and easy **(B)** spinal segment labeling in the straightened space in two representative participants. In the more challenging participants, motion and CSF flow likely contributed to the less apparent nerve rootlets.

Figure S5.8 shows scatterplots of the STD across neck positions of the distance PMJ-spinal segment **(a)** and the distance disc-spinal segment **(b)** for each participant.

Table 5.1 aggregates the STD across neck positions of the distance PMJ-spinal segment and disc-spinal segment between all participants and levels. The mean STD is lower when measuring from the PMJ than from the discs (1.06 ± 0.33 mm vs. 1.40 ± 0.26 mm).

To validate if there was a significant difference between the STDs across neck positions of the PMJ and discs method, we performed a paired two-way ANOVA test on the STD of distances across neck positions. Independent variables were methods (PMJ, Disc) and levels. Results are presented in **Table 5.4**. The analysis found no significant difference between the STD of PMJ and disc methods ($p\text{-value} > 0.05$), but a significant difference across levels ($p\text{-value} = 0.0386$). We did not conduct any further post-hoc analysis across levels. Our main focus was to investigate whether there were differences in the variability of the estimated spinal segment positions between the PMJ and discs-based estimation methods.

Table 5.1 STD of distance between spinal segments and PMJ or discs per level.

	Distances STD (mm)	
	PMJ	***DISC***
Levels	**mean ± std**	**mean ± std**
2	0.59 ± 0.31	1.19 ± 0.73
3	0.77 ± 0.51	1.14 ± 0.75
4	1.04 ± 0.63	1.37 ± 0.84
5	1.43 ± 1.42	1.85 ± 1.26
6	1.23 ± 1.00	1.35 ± 0.87
7	1.31 ± 1.10	1.52 ± 0.73
MEAN	**1.06 ± 0.33**	**1.40 ± 0.26**

Table 5.2 Paired Two-way ANOVA of STD of distance PMJ-spinal segment and disc-spinal segment across neck positions.

	F value	***Num DF***	***Den DF***	***p-value***
Method	0.795	1	8	0.399
Levels	2.618	5	40	**0.0386***
Method × Levels	0.405	5	40	0.843

*p-*value* < 0.05. *Method*: PMJ or Disc. *Levels*: 2, 3, 4, 5, 6, 7. ×: interaction. *F value*: F value of Fisher's exact Test. *Num DF*: Degrees of freedom of numerator. *Den DF*: Degrees of freedom of denominator. *p-value*: p-value of Fisher Test.

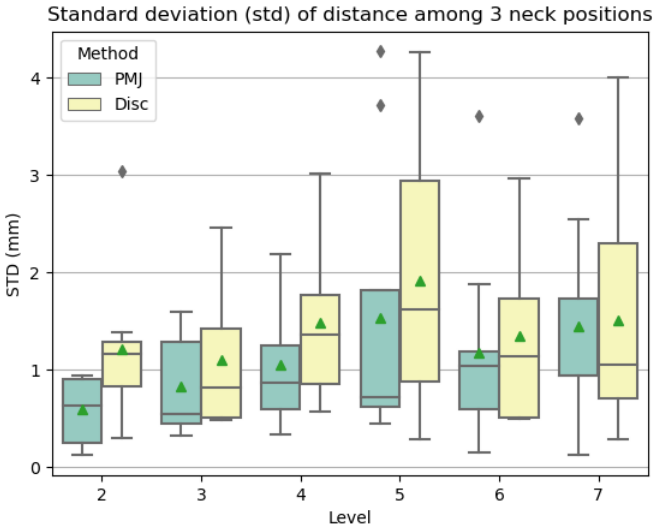

Figure 5.5 Boxplots (25-75 percentiles) of STD across neck positions per participant of the distance between the spinal segment and PMJ (green) and spinal segment and corresponding discs (yellow). Green triangles show the mean and gray diamonds outliers. No post-hoc analysis was performed beyond the ANOVA described in Table 5.4.

5.3.3 CSA computation

CSA was computed from 3 anatomical references: PMJ, spinal segments, and discs. It was averaged on 3 slices per level and the COV across neck positions was computed for each participant, method, and level. **Figure 5.6** shows boxplots of COV of CSA across neck positions for each method and level for a visual representation of the results. Mean CSA values across neck positions and participants for each method and level can be found in **Table S5.5**.

A scatterplot of COV for each participant and method is presented in **Figure S5.9**. The mean CSA COV across participants, levels and methods is presented at **Table 5.3.**

We performed a paired 3-way ANOVA test on spinal cord CSA to assess statistical differences between methods (PMJ, Spinal, Discs), levels, and neck positions. Results are presented in **Table 5.4**. The ANOVA test results revealed no significant differences in CSA between methods or neck positions ($p\text{-}value > 0.05$). However, the test did indicate a significant difference in CSA across levels for all methods and neck positions ($p\text{-}value = 0.000004$). There was also a significant interaction between method, levels, and neck position on CSA ($p\text{-}value = 0.0205$), indicating that the relationship between methods and levels differed across neck positions.

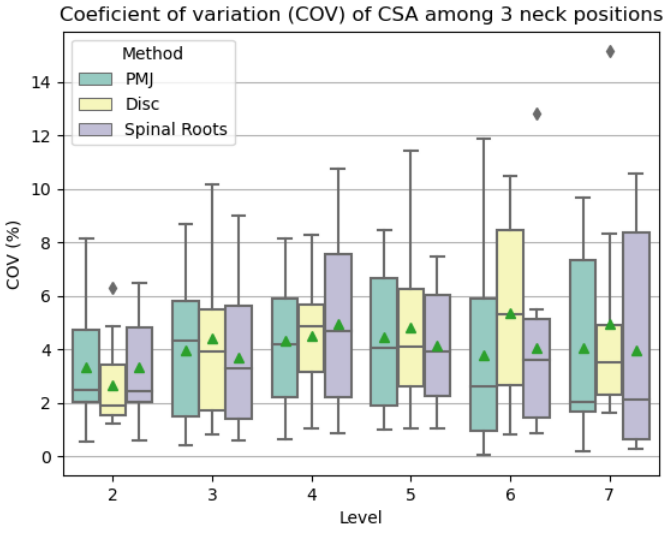

Figure 5.6 Boxplot of CSA COV per level based on discs C1-C2 to C7-T1, on spinal segments C2 to C8, and on the mean distance between the PMJ and each spinal segment. Green triangles represent the mean, and gray diamonds represent outliers.

Table 5.3 Mean COV of CSA per level across participants using PMJ, spinal segments and Discs as a reference and averaged on 3 slices.

	COV (%)		
	PMJ	***Spinal***	***Discs***
Levels	**mean ± std**	**mean ± std**	**mean ± std**
2	3.36 ± 2.44	3.32 ± 2.01	2.67 ± 1.74
3	3.97 ± 2.76	3.69 ± 2.76	4.43 ± 3.32
4	4.33 ± 2.53	4.97 ± 3.32	4.50 ± 2.39
5	4.45 ± 2.91	4.12 ± 2.26	4.82 ± 3.20
6	3.77 ± 3.64	4.04 ± 3.60	5.38 ± 3.62
7	4.07 ± 3.49	3.95 ± 4.10	4.95 ± 4.34
MEAN	3.99 ± 2.96	4.02 ± 3.01	**4.46 ± 3.10**

Table 5.4 Paired Three-way ANOVA on spinal cord CSA.

	F value	***Num DF***	***Den DF***	***p-value***
Method	2.413	2	18	0.118
Levels	26.269	3	27	**0.000004***
Neck position	2.695	2	18	0.0947
Method × Levels	0.999	6	54	0.435
Method × Neck position	0.561	4	36	0.692
Levels × Neck position	0.823	6	54	0.557
Method × Levels × Neck position	2.131	12	108	**0.0205***

*p-value < 0.05. *Method*: PMJ, Spinal, Discs. *Levels*: 2, 3, 4, 5. *Neck position*: Extension, Neutral, Flexion. ×: interaction. *F value*: F value of Fisher's exact Test. *Num DF*: Degrees of freedom of numerator. Den DF: Degrees of freedom of denominator. *p-value*: p-value of Fisher Test

5.3.4 Neck angle

We computed the neck angle between the C1-C2 and C4-C5 intervertebral discs (**Figure S5.7**) to evaluate if the variation of neck angle had an impact on the observed variability between discs/PMJ and spinal segments. **Table S5.6** displays participant neck angles for each neck position, with mean values of 18.45 ± 3.82 ° for extension, 11.14 ± 3.02 ° for neutral, and 4.79 ± 3.01° for flexion.

Table S5.7 presents the correlation between neck angle variation and spinal segment position variation (from PMJ or disc) between neck flexion and extension and **Table S5.8** per level. **Figure S5.10** presents a scatterplot of neck angle variation vs variation of the distance spinal segment-PMJ and spinal segment-disc.

5.4 Discussion

In this study, we evaluated the reliability of computing CSA using spinal segment positions, from intervertebral discs vs. from the PMJ in human participants across different neck positions (extension, neutral, flexion). The variability of the estimated spinal segments across neck positions using the PMJ vs. the discs did not differ significantly, although we noted a trend of lower variability (STD) for the PMJ method. Additionally, we compared spinal cord CSA across 3 references (PMJ, intervertebral discs, and spinal segment) and we did not find any significant difference between CSA variability when using the PMJ as a reference, although the PMJ method yielded lower COV.

5.4.1 Spinal segment manual labeling

Identifying nerve rootlets to label spinal segments is highly dependent on image quality, and even with high-resolution scans, it can be difficult, time-consuming and is not realistic for large scale studies. This highlights the need for a surrogate reference and further improvement of data acquisition quality. Flexion presented worse data quality of nerve rootlets due to increased artifacts caused by participants' movement (swallowing is difficult). The difficulty of accurately identifying nerve rootlets adds variability to distance and CSA measures. AI-based labeling methods could potentially increase the reliability of the labels in the future.

5.4.2 Distance with PMJ, spinal segments and discs

The PMJ method was slightly more reliable than the disc-based method to estimate spinal segment position (STD PMJ: 1.06 mm vs. Disc 1.40 mm), although the difference was not statistically significant. However, it is important to consider the limitations of our study, such as the small number of participants and neck positions, as well as the variability in manual labeling (**Figure 5.5**).

We observed higher disc vs. spinal segments discrepancies between neck positions than in a previous study [16], possibly due to different acquisition parameters and the use of three positions in our study.

5.4.3 CSA computation

The PMJ method has a 0.5 % lower COV than the disc-based method on the CSA measures across neck positions, although that difference was not significant. A better COV helps reduce the minimum sample size required to detect atrophy in longitudinal studies, as demonstrated by Bautin et al [20]. However, we still observed a 4 % intra-subject variability between the neck positions, corresponding to a 3.08 mm^2 difference at C5 (CSA of 77 mm^2), corresponding to the cervical enlargement, and a 2.60 mm^2 difference at C7 (CSA of 65 mm^2).

The observed difference of 2.5-3 mm^2, when compared to pathological cohorts, falls within the expected effect size for such cohorts. For example, in a systematic review, Casserly et al. [39] reported an estimated atrophy rate of 1.78 % per year in all MS patients, with a mean CSA at C2-C5 of 73.07 mm^2, corresponding to a 1.3 mm^2. It is important to consider that CSA measurements can be influenced by factors such as the segmentation method, acquisition parameters, scanner, and inter-individual differences (sex, age) [9, 12, 14, 20, 101].

This variability could be attributed to image quality, and over-segmentation of the spinal

cord due to residual segmentation errors (inclusion of spinal nerve rootlets). Depending on the neck position, the fanning in/out of the nerve rootlets at the proximity of the spinal cord would be more or less tangential to the spinal cord and could be more or less included in the automatic segmentation, resulting in variability of CSA across neck extensions. Some studies have also reported significantly smaller CSA and anterior-posterior diameter in neck flexion than neutral position with the elongation of the cord [33], which could also contribute to the observed variability.

5.4.4 Limitations & Perspective

Limitations of this study include imprecise manual spinal segment labeling, which may explain why PMJ-based CSA had lower COV than when using spinal segments as a reference.

Measuring CSA based on the PMJ does not consider inter-subject spinal cord length variability as discussed by Bédard et al. [101]. Hence, the PMJ-based approach, if not normalized, would be more suitable for longitudinal studies where participants would be their own controls. Metrics like cervical enlargement or total spinal cord length could be suitable candidates for normalization, but further investigation is needed as no clear link of the spinal segments' location related to other anatomical references has yet emerged [107].

Neck positioning can also vary in different clinical contexts [108]. For example, for spinal cord compressions such as for patients with cervical myelopathy, studies have shown an increase in the severity of spinal cord compression with the extension of the neck. It was found to be better correlated with clinical deficits than in a neutral position [104, 109]. The variation of the spinal segments relative to the intervertebral discs is therefore important to consider when computing spinal cord morphometrics such as CSA when varying neck position. Furthermore, measuring at the precise location of the compression instead of averaging morphometrics across vertebral levels when using a distance from the PMJ could provide better monitoring of the compression and increase the sensitivity of myelopathy detection. Kinetic MRI is another example where the patient in a weight-bearing position can take various head flexion-extension positions; it can reveal abnormalities not shown by traditional supine or neutral MRI, mainly in spinal cord injuries [110, 111].

5.5 Conclusion

In this study, we investigated the use of the PMJ as an anatomical reference for computing spinal cord CSA instead of relying on intervertebral discs. We compared the estimation of the spinal segments position and CSA measures using the PMJ vs. intervertebral discs as a

reference. This comparison was performed across three neck positions using high isotropic resolution T2w scans. Our findings show that the PMJ method was slightly more reliable than the disc-based method to compute CSA at specific spinal segments, although the difference was not statistically significant. This suggests that the PMJ can serve as a valuable alternative and reliable method for estimating CSA when a disc-based approach is challenging or not feasible, such as in cases involving fused discs in individuals with spinal cord injuries. Moreover, utilizing an anatomical reference based on the central nervous system could prove beneficial for studies investigating peripheral motor functions, dermatomes, and functional MRI studies.

5.6 Acknowledgements

We thank Hugues Leblond for insightful conversations. This study was funded by the Canada Research Chair in Quantitative Magnetic Resonance Imaging [950-230815], the Canadian Institute of Health Research [CIHR FDN-143263], the Canada Foundation for Innovation [32454, 34824], the Fonds de Recherche du Québec - Santé [28826], the Natural Sciences and Engineering Research Council of Canada [RGPIN-2019-07244], the Canada First Research Excellence Fund (IVADO and TransMedTech), the Courtois NeuroMod project, the Quebec BioImaging Network [5886, 35450], the Spinal Research and Wings for Life (INSPIRED project).

5.7 Author contributions

SB and JCA designed the study and performed the experiments. MB performed manual labeling on the experimental data and drafted the manuscript introduction. SB processed the experimental data, performed the analysis, drafted the manuscript, and designed the figures. JCA supervised the project. JCA and SB discussed the results and contributed to the final manuscript.

5.8 Data availability statement

The datasets generated during and/or analyzed during the current study are available in the Spinal Cord Head Position MRI repository: https://openneuro.org/datasets/ds004507/versions/1.0.1

5.9 Additional Information

5.9.1 Competing interests

The authors declare no competing interests.

5.10 Supplementary material

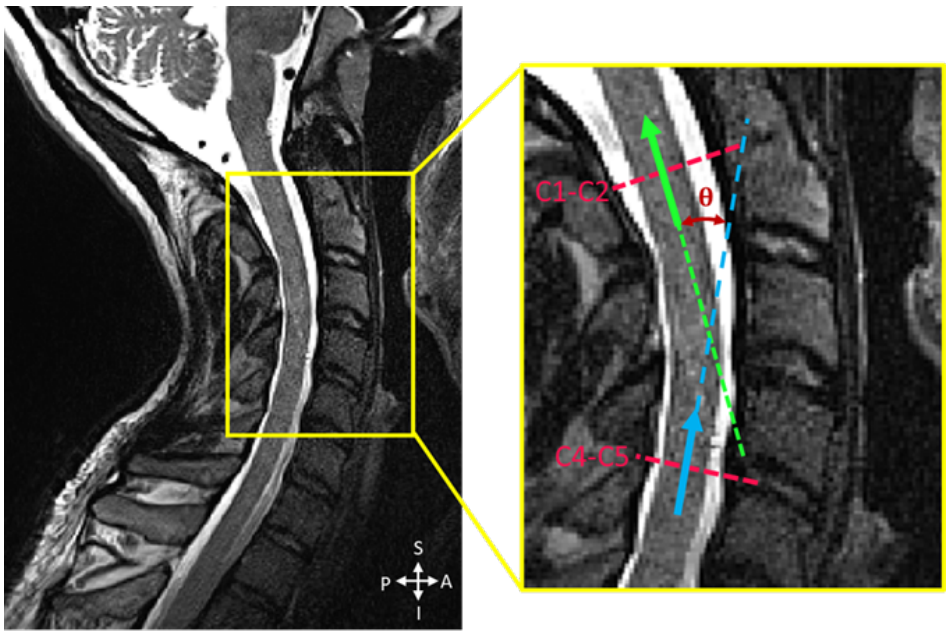

Figure 5.7 Neck angle measurement. The neck angle was computed in the right-left direction between the C1-C2 and C4-C5 intervertebral discs.

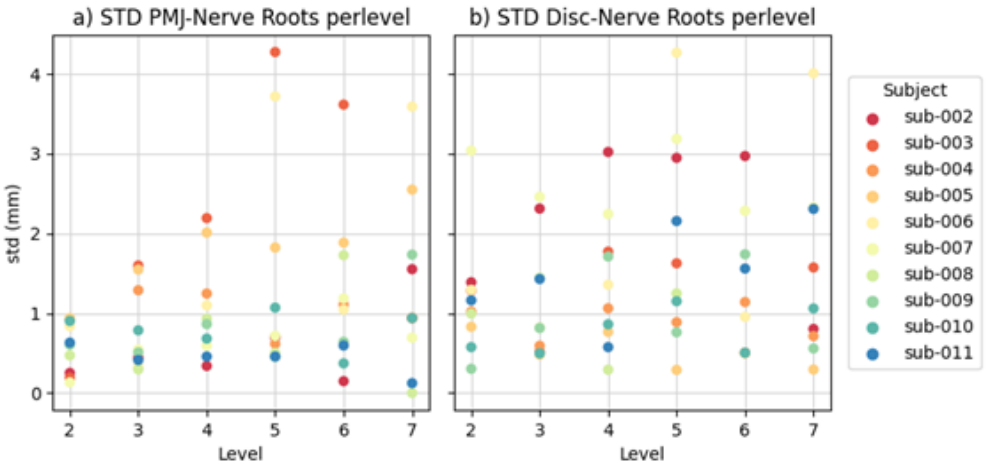

Figure 5.8 STD across neck positions of the distance between the PMJ and spinal segments (a) and between each disc and spinal segment (b) per participant.

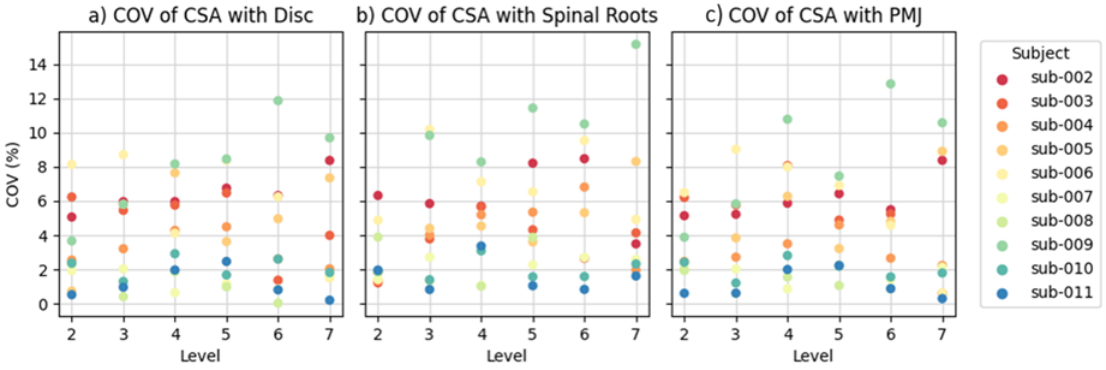

Figure 5.9 a) Scatterplot of COV of CSA perlevel based on intervertebral discs C1-C2 to C7-T1. b) Scatterplot of COV of CSA per level based on spinal segments C3 to T1. c) Scatterplot of COV of CSA per level based on the mean distance between the PMJ and each spinal segment. CSA is averaged on 3 slices.

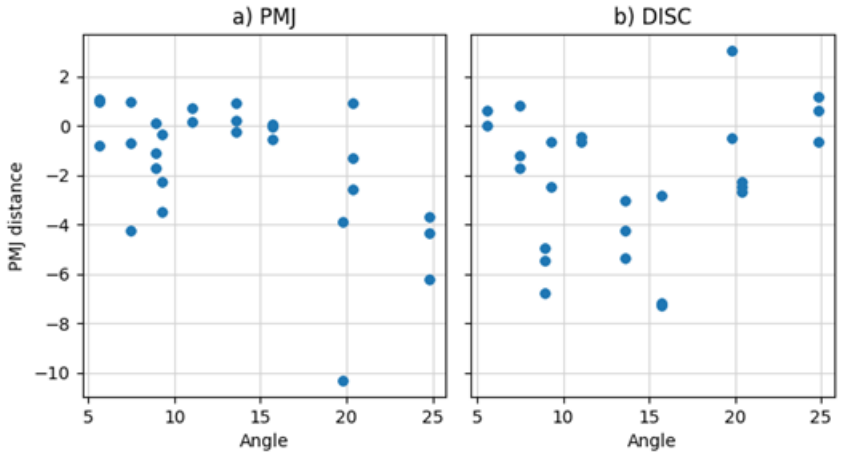

Figure 5.10 Each dot corresponds to a participant position and angle. For each participant, we calculated the angle between the spinal cord centerline at C2-C3 and C4-C5 levels, and we took the difference of that angle between the neck extension and flexion: this is what is represented in the abscissa. The ordinate represents the difference of distance, between extension and flexion, between the PMJ and the corresponding spinal segment (PMJ-segment C2 ; PMJ-segment C3, etc.) (a) and the difference of distance between the corresponding disc and the corresponding spinal segment (disc C2 - segment C2; disc C3 - segment C3, etc.) (b).

Table 5.5 Spinal cord CSA results across neck positions per method and level.

	CSA *(mm^2)*		
	PMJ	***Spinal***	***Discs***
Levels	**mean ± std**	**mean ± std**	**mean ± std**
2	71.98 ± 4.58	72.31 ± 4.50	72.65 ± 4.70
3	71.66 ± 4.68	71.62 ± 4.74	70.75 ± 5.57
4	75.29 ± 5.62	74.71 ± 5.62	73.98 ± 5.09
5	77.17 ± 4.04	77.32 ± 4.03	77.00 ± 4.79
6	73.58 ± 5.17	73.81 ± 4.92	74.30 ± 4.55
7	65.04 ± 8.69	65.23± 8.38	64.50 ± 7.32
MEAN	**72.45 ± 4.18**	**72.50 ± 4.09**	**72.20 ± 4.30**

Table 5.6 Neck angle of the 3 neck positions per participant.

	Angles (°)		
Participants	***Extension***	***Neutral***	***Flexion***
sub-002	20.57	14.85	4.85
sub-003	16.54	6.10	-3.27
sub-004	23.46	7.52	3.11
sub-005	28.84	14.46	4.01
sub-006	20.02	14.18	8.99
sub-007	11.90	9.34	2.97
sub-008	17.63	14.46	8.34
sub-009	16.46	12.53	9.02
sub-010	13.42	6.54	7.82
sub-011	15.68	11.46	2.11
MEAN	**18.45**	**11.14**	**4.79**
STD	**3.82**	**3.02**	**3.01**

Table 5.7 Correlation between neck angle variation and variation of distance of the spinal segment and PMJ/discs between neck flexion and extension.

	Δ *angles*	***level***	**Δ *distance_pmj***	**Δ *distance_disc***
Δ *angles*	1	0.024	-0.503	0.164
level	-	1	-0.419	-0.096
Δ *distance_pmj*	-	-	1	-
Δ *distance_disc*	-	-	-	1

Δ *: variation between neck flexion and extension position*

Table 5.8 Correlation between neck angle variation and distance of the spinal segment variation between neck flexion and extension for PMJ and discs per level.

	Correlation with Δ angle	
Level	Δ ***distance_pmj***	Δ ***distance_disc***
2	**0.084**	-0.709
3	-0.897	**0.796**
4	**-0.426**	-0.454
5	-0.657	**0.584**
6	**-0.069**	-0.594
7	-0.518	**0.321**

BOLD*: minimum absolute correlation.*

CHAPTER 6 GENERAL DISCUSSION

In this discussion, we elaborate on the methodology developed in this study, alongside the principal findings from **Chapters 4** and **5**.

6.1 Research Objectives & Hypotheses

In this study, we developed an automatic pipeline to compute spinal cord CSA at a specific distance from the PMJ and applied this pipeline to a large database. Additionally, we intergrated the method into the SCT software where it can be used from the command line. However, our results did not support the main hypothesis that the PMJ provides a more accurate estimation of the spinal segments' position. The validation of spinal segment position estimation (Chapter 5) was constrained by the limited number of participants (n=10) and of neck positions (n=3). Due to the imprecision in manual labeling of spinal segments, we refrained from collecting additional data. Future research could explore the use of more accurate spinal segment labels. For example, the automatic segmentation of nerve rootlets proposed by Valosek et al. [112] could provide more accurate spinal segments labeling and facilitate further analyses.

Using the PMJ as a reference for CSA computation did not show any significant differences in inter-subject variability compared to using vertebral levels. Further investigations should consider a form of normalization with the spinal cord length.

Using the PMJ for CSA computation across different neck positions produced CSA values similar to those obtained using manual spinal segments and intervertebral disc levels. It is essential to increase the sample size and the range of neck positions to further validate these results. Moreover, the poor precision in manual spinal segment labeling limited the scope of this study; improving the reliability of these labels is warranted.

6.2 PMJ based-CSA Method

This research introduces an automatic approach for calculating spinal cord CSA at a specific distance from the PMJ. This method requires a spinal cord segmentation and a single point label of the PMJ, which can both be obtained automatically. However, it is important to note that the accuracy of CSA measurements depends on the quality of both the segmentation and the PMJ label. Manual corrections can be made as required, and to facilitate this, we provided a comprehensive quality control workflow. This includes a tutorial on how to correct

segmentation and PMJ labeling, available at: https://github.com/sct-pipeline/ukbiobank-spinalcord-csa?tab=readme-ov-file#quality-control.

The methodology involves extracting the centerline of the spinal cord from its segmentation and then interpolating between the top of the centerline and the PMJ, as the centerline often does not extend to the PMJ. We also provide a quality control report of this centerline. Some errors may be introduced when interpolating between the PMJ and the centerline, affecting the measured distance. We did not compare the extracted centerline to any ground truths, but the centerlines were visually assessed.

The PMJ was proposed as reference for distance measurements by Stroman et al. [17] and [16] although not specifically in the context of CSA computation. It was selected due to its role in the central nervous system and its visibility on structural MRI scans, including both T1w and T2w. The PMJ also has the advantage of requiring only a single point label, unlike vertebral labels.

Directly using spinal segment labels would avoid using a proxy reference like the PMJ for CSA computation. Yet, spinal segment labeling presents major challenges as discussed in section 6.5. The automatic segmentation of nerve rootlets, as suggested by Valosek et al. [112], opens new research avenues to derive their corresponding spinal segment. Future investigations could include computing the CSA at specific spinal levels derived from automatic nerve rootlet segmentation and comparing these measurements to those obtained using the PMJ as a reference.

Using an anatomical reference for CSA or other morphometric computation is typically preferred over registration-based methods. Spinal cord registration to templates typically relies on intervertebral discs and the spinal cord, presenting the same limitations in accurately correlating vertebrae with spinal segments. Registration can also introduce errors, further complicating these measurements [8].

6.3 CSA Measurements

In this study, CSA was calculated automatically from the PMJ across two datasets using T1w and T2w MRI contrasts. Specifically, **Chapter 4** details the computation of PMJ-based CSA and CSA at the C2-C3 vertebral levels for T1w images of 804 healthy adults from the UK Biobank dataset. PMJ-based CSA and CSA at C2-C3 vertebral levels differed significantly.

Further exploration in **Chapter 5** involved analyzing the spinal cord CSA on T2w images from 10 healthy participants, using 3 distinct references: the PMJ, cervical intervertebral

discs, and cervical spinal segments. We obtained very similar CSA values between all 3 references across subjects and neck positions. Additionally, CSA values at C2-C3 vertebral levels from this study were higher than those reported in the study on the UK Biobank. This discrepancy could be attributed to several factors, including the difference in MRI contrasts (T2w vs. T1w) [61] and variations in the age range of the study populations [9].

This study focused only on spinal cord CSA measures; although the method can also be used with other morphometric measures provided by `sct_process_segmentation`, such as the anteroposterior diameter, transverse diameter, eccentricity, and solidity. These metrics could undergo the same analyses as those performed for CSA to compare their variability using the PMJ vs. a vertebral reference.

6.4 Impact of PMJ Reference on CSA Variability

The initial investigation on inter-subject variability, detailed in **Chapter 4**, involved calculating CSA at 64 mm from the PMJ for all 804 individuals. This distance was chosen based on the average location of the C2-C3 intervertebral discs within the cohort. However, this fixed distance does not account for individual differences in spinal cord length, which could have influenced the observed inter-subject variability.

Interestingly, our findings did not reveal any significant differences in CSA inter- and intra-subject variability, regardless of whether vertebral or spinal levels or the PMJ were used as references. This may also be attributed to the fact that the variability between the spinal vs. vertebral level is lower at the upper cervical levels compared to lower levels.

In **Chapter 5**, the position of the spinal segments was estimated using both the PMJ and intervertebral discs. We reported the STD across 3 neck positions for 6 different cervical levels. For the PMJ and intervertebral discs, we observed a lower variability across neck positions for higher levels (C2-C3) than lower levels. For both methods, the estimation of the spinal segment C5 had the highest intra-subject variability. This level was shown to be particularly affected by neck curvature changes, in terms of CSA and position [32].

When investigating the impact of using the PMJ instead of vertebral levels for CSA computation on intra-subject variability (**Chapter 5**), we did not find any significant differences between the two methods. The limited number of neck positions (n = 3) and subjects (n = 10) may have contributed to the lack of statistical power.

The variability in CSA measurements is influenced by several factors, including the precision of image segmentation and the accuracy of the labels (whether intervertebral discs, PMJ, or spinal segments). Image artifacts, such as motion blur and ghosting, can also affect

the delineation of the spinal cord from the surrounding CSF, highlighting the necessity for quality control, particularly with automatic processing methods. This would result in a reduced precision of CSA measures. Given the small size of the spinal cord, subtle atrophy may not be detected: even minor inaccuracies in CSA measurements can significantly impact the utility of CSA as a biomarker for disease prognosis and monitoring.

The evaluation conducted in this study was limited to healthy subjects, where CSA variations within a few millimeters are minimal. As discussed in Chapter 5, CSA was computed only over a 3 mm extent. It would be beneficial to replicate this study in patients with spinal cord compression, where CSA variations are expected to be more pronounced at the site of compression.

For the application of the PMJ-based method in cross-sectional studies, an additional reference is necessary to account for variations in spinal cord length. Measuring the total length of the spinal cord is however challenging, as it requires scanning the entire spinal cord. Alternative references, such as the position of the cervical enlargement, could also be considered for normalization. However, the extent and size of the cervical enlargement varies among individuals which complicates its identification across individuals [27]. Another approach could involve using the distance between the rostral nerve rootlet of C1 to C8 as the length of the cervical region for normalization.

This concept of using a reference from the central nervous system could be translated to the lumbar spinal cord, where there is a notable discrepancy between spinal cord segments and vertebral levels. For example, the conus medullaris could serve as a potential reference.

Further validation could be conducted on a patient population to monitor atrophy over time, comparing PMJ-based CSA measurements with those based on vertebral levels. This would provide additional validation for the proposed method.

6.5 Spinal Segment Labeling

In **Chapter 5**, we introduced a pipeline for labeling spinal segments in T2w high-resolution images, which involved spinal cord straightening and denoising. Despite these enhancements, accurately identifying spinal segments using nerve rootlets remains challenging. Our findings indicated increased CSA variability when using spinal segment labels compared to the PMJ, highlighting the necessity for more precise spinal segment identification methods.

In this sense, Valosek et al. [112] recently introduced a deep learning model to segment spinal nerve rootlets and determining their respective spinal levels. Such segmentation could lead to a more accurate labeling of the spinal levels, offering personalized identification of these

levels for each subject. This approach becomes particularly crucial for lower spinal levels, where discrepancies between spinal and vertebral levels tends to increase, emphasizing the need for a precise identification of the spinal segments.

6.6 Data and Code Availability

The methodology for computing CSA based on the PMJ is integrated in the open-source software SCT, complete with a detailed tutorial and the normalization model. Significant efforts were made to thoroughly document the methodologies and findings of both chapters (4 and 5), with all associated code made accessible via GitHub. Additionally, the T2w images captured at various neck positions, along with the spinal cord segmentations and labels, are publicly available: the dataset, titled *Spinal Cord Head Position MRI*, is hosted on OpenNeuro and can be accessed at https://openneuro.org/datasets/ds004507/. This dataset is valuable for further explorations of intra-subject variability, particularly concerning the identification of spinal segments.

6.7 Perspectives

Using the PMJ as a reference for spinal cord CSA computations offers a reliable alternative in situations where vertebral labeling is difficult or impossible due to conditions like disc fusions or disc malformations. This approach simplifies the labeling process by requiring only a single reference point, as opposed to the multiple labels necessary for vertebral-based references, thereby facilitating quicker and simpler manual corrections. Additionally, the ability to customize the extent of CSA measurements according to user specifications makes this method particularly useful for localized assessments, such as evaluating spinal cord compressions.

Additionally, computing distances along the spinal cord centerline from the PMJ holds potential beyond CSA measurement. It could be beneficial for other applications, such as localizing lesions, spinal cord compressions, or nerve rootlets [112].

CHAPTER 7 CONCLUSION

7.1 Summary of Works

The main objective of this project was to evaluate the impact of using the PMJ as a reference for spinal cord CSA measurements on both inter- and intra-subject variability. Initially, we developed an automatic pipeline for calculating CSA at a specified distance from the PMJ (**O1)**, which is incorporated into the open-source software SCT. Our findings indicated that CSA variability was consistent, irrespective of whether the PMJ or vertebral levels were used as a reference point. Further analysis within a large subset of the UK Biobank dataset **(O2)** revealed that factors such as sex, brain volume, and thalamus volume significantly influenced CSA variability, as determined through a stepwise linear regression. We proposed a normalization model for CSA incorporating theses significant factors as covariates. Subsequently, we evaluated the impact of the PMJ as a reference for CSA measures on intra-subject variability **(O3)** by acquiring high-resolution MRI images from 10 healthy individuals across 3 neck positions (flexion, neutral, extension). Although intra-subject variability was marginally lower with the PMJ reference compared to vertebral levels or manual spinal segment labels, this difference was not statistically significant. Overall, we demonstrated that using the PMJ as a reference for CSA computation offers comparable performance in term of inter- and intra-subject variability to using the vertebral levels as a reference, suggesting its utility in scenarios where vertebral labeling is challenging.

7.2 Limitations

PMJ-based CSA presents a few limitations. In cross-sectional studies, using the PMJ as a reference without normalization fails to account for inter-subject variability in spinal cord length [26]. However, in the UK Biobank dataset, discussed in Chapter 4, we did not have access to these measurements, as the field-of-view in the images was limited to the upper cervical cord. Although height was considered as a potential covariate in the stepwise analysis, it was not significant. It is important to note that the length of the spinal cord may also not correlate directly with an individual's height, as the length of the legs also contributes to overall height. Additionally, interpolating between the PMJ label and the spinal cord centerline may not approximate the exact centerline between the PMJ and spinal cord, thus introducing errors in the distance measures.

This study focused on the cervical spinal cord, examining C2-C3 vertebral levels in **Chapter**

4 and extending to the entire cervical region (C2-C7) in **Chapter 5**. Lower levels, such as thoracic or lumbar, where discrepancies between spinal and vertebral levels are potentially more pronounced, were not included.

Here, we focused on the variability of CSA to evaluate the impact of using the PMJ as an anatomical reference compared to vertebral levels. Using the COV as a measure of variability does not account for potential biases introduced by the choice of anatomical references. Therefore, additional validation, particularly in patient populations to detect atrophy, is essential. It is important to clarify that the validation of the PMJ-based CSA method is detailed in Chapter 5 while Chapter 4 explores the application of the method on a large population. Additionally, other anatomical references closer to the region of interest could also be explored.

In this study, we only explored demographic factors, anatomical factors, and vertebral reference contributing to CSA variability, without diving into the potential impact of MRI contrast, segmentation techniques, or MRI equipment, all of which are important considerations for multi-center studies. Moreover, our analyses did not include metrics related to the size of the spinal canal or the length of the spinal cord.

7.3 Future Research

Further research is needed to reduce CSA variability. Using the PMJ did not show any significant difference in terms of CSA intra- and inter-subject variability compared to a traditional vertebral reference. This underscores the need for the development of automatic tools for precise spinal level identification. Additionally, the observed variability of spinal levels in a healthy population requires further investigations on MRI data as the majority of the studies reporting this variability are on *ex vivo* data. Moreover, we did not explore other potential factors contributing to CSA variability, such as MRI contrasts and segmentation techniques. Future research will address these limitations and focus on developing automatic tools for spinal canal measurement and spinal levels identification, which could serve as a potential normalization factor for CSA.

REFERENCES

[1] C. Lukas, M. H. Sombekke, B. Bellenberg, H. K. Hahn, V. Popescu, K. Bendfeldt, E. W. Radue, A. Gass, S. J. Borgwardt, L. Kappos, Y. Naegelin, D. L. Knol, C. H. Polman, J. J. G. Geurts, F. Barkhof, and H. Vrenken, "Relevance of spinal cord abnormalities to clinical disability in multiple sclerosis: MR imaging findings in a large cohort of patients," *Radiology*, vol. 269, no. 2, pp. 542–552, Nov. 2013.

[2] R. Bonacchi, M. Filippi, and M. A. Rocca, "Role of artificial intelligence in MS clinical practice," *Neuroimage Clin*, vol. 35, p. 103065, May 2022.

[3] C. Trolle, E. Goldberg, and C. Linnman, "Spinal cord atrophy after spinal cord injury - a systematic review and meta-analysis," *Neuroimage Clin*, vol. 38, p. 103372, Mar. 2023.

[4] J. Cohen-Adad and C. Wheeler-Kingshott, *Quantitative MRI of the Spinal Cord*, J. C.-A. C. Wheeler-Kingshott, Ed. Academic Press, Jan. 2014.

[5] C. Walton, R. King, L. Rechtman, W. Kaye, E. Leray, R. A. Marrie, N. Robertson, N. La Rocca, B. Uitdehaag, I. van der Mei, M. Wallin, A. Helme, C. Angood Napier, N. Rijke, and P. Baneke, "Rising prevalence of multiple sclerosis worldwide: Insights from the atlas of MS, third edition," *Mult. Scler.*, vol. 26, no. 14, pp. 1816–1821, Dec. 2020.

[6] N. A. Losseff, S. L. Webb, J. I. O'Riordan, R. Page, L. Wang, G. J. Barker, P. S. Tofts, W. I. McDonald, D. H. Miller, and A. J. Thompson, "Spinal cord atrophy and disability in multiple sclerosis. a new reproducible and sensitive MRI method with potential to monitor disease progression," *Brain*, vol. 119 (Pt 3), pp. 701–708, Jun. 1996.

[7] R. Zivadinov, A. C. Banas, V. Yella, N. Abdelrahman, B. Weinstock-Guttman, and M. G. Dwyer, "Comparison of three different methods for measurement of cervical cord atrophy in multiple sclerosis," *AJNR Am. J. Neuroradiol.*, vol. 29, no. 2, pp. 319–325, Feb. 2008.

[8] J. Valošek, S. Bédard, M. Keřkovský, T. Rohan, and J. Cohen-Adad, "A database of the healthy human spinal cord morphometry in the PAM50 template space," *Imaging Neuroscience*, Jan. 2024.

[9] N. Papinutto, C. Asteggiano, A. Bischof, T. J. Gundel, E. Caverzasi, W. A. Stern, S. Bastianello, S. L. Hauser, and R. G. Henry, "Intersubject variability and normalization strategies for spinal cord total Cross-Sectional and gray matter areas," *J. Neuroimaging*, vol. 30, no. 1, pp. 110–118, Jan. 2020.

[10] L. Solstrand Dahlberg, O. Viessmann, and C. Linnman, "Heritability of cervical spinal cord structure," *Neurol Genet*, vol. 6, no. 2, p. e401, Apr. 2020.

[11] M. C. Yiannakas, A. M. Mustafa, B. De Leener, H. Kearney, C. Tur, D. R. Altmann, F. De Angelis, D. Plantone, O. Ciccarelli, D. H. Miller, J. Cohen-Adad, and C. A. M. Gandini Wheeler-Kingshott, "Fully automated segmentation of the cervical cord from t1-weighted MRI using PropSeg: Application to multiple sclerosis," *Neuroimage Clin*, vol. 10, pp. 71–77, 2016.

[12] J. Cohen-Adad, E. Alonso-Ortiz, M. Abramovic, C. Arneitz, N. Atcheson, L. Barlow, R. L. Barry, M. Barth, M. Battiston, C. Büchel, M. Budde, V. Callot, A. J. E. Combes, B. De Leener, M. Descoteaux, P. L. de Sousa, M. Dostál, J. Doyon, A. Dvorak, F. Eippert, K. R. Epperson, K. S. Epperson, P. Freund, J. Finsterbusch, A. Foias, M. Fratini, I. Fukunaga, C. A. M. Gandini Wheeler-Kingshott, G. Germani, G. Gilbert, F. Giove, C. Gros, F. Grussu, A. Hagiwara, P.-G. Henry, T. Horák, M. Hori, J. Joers, K. Kamiya, H. Karbasforoushan, M. Keřkovský, A. Khatibi, J.-W. Kim, N. Kinany, H. H. Kitzler, S. Kolind, Y. Kong, P. Kudlička, P. Kuntke, N. D. Kurniawan, S. Kusmia, R. Labounek, M. M. Laganà, C. Laule, C. S. Law, C. Lenglet, T. Leutritz, Y. Liu, S. Llufriu, S. Mackey, E. Martinez-Heras, L. Mattera, I. Nestrasil, K. P. O'Grady, N. Papinutto, D. Papp, D. Pareto, T. B. Parrish, A. Pichiecchio, F. Prados, À. Rovira, M. J. Ruitenberg, R. S. Samson, G. Savini, M. Seif, A. C. Seifert, A. K. Smith, S. A. Smith, Z. A. Smith, E. Solana, Y. Suzuki, G. Tackley, A. Tinnermann, J. Valošek, D. Van De Ville, M. C. Yiannakas, K. A. Weber, Ii, N. Weiskopf, R. G. Wise, P. O. Wyss, and J. Xu, "Open-access quantitative MRI data of the spinal cord and reproducibility across participants, sites and manufacturers," *Sci Data*, vol. 8, no. 1, p. 219, Aug. 2021.

[13] J. Cohen-Adad, E. Alonso-Ortiz, M. Abramovic, C. Arneitz, N. Atcheson, L. Barlow, R. L. Barry, M. Barth, M. Battiston, C. Büchel, M. Budde, V. Callot, A. J. E. Combes, B. De Leener, M. Descoteaux, P. L. de Sousa, M. Dostál, J. Doyon, A. Dvorak, F. Eippert, K. R. Epperson, K. S. Epperson, P. Freund, J. Finsterbusch, A. Foias, M. Fratini, I. Fukunaga, C. A. M. G. Wheeler-Kingshott, G. Germani, G. Gilbert, F. Giove, C. Gros, F. Grussu, A. Hagiwara, P.-G. Henry, T. Horák, M. Hori, J. Joers,

K. Kamiya, H. Karbasforoushan, M. Keřkovský, A. Khatibi, J.-W. Kim, N. Kinany, H. Kitzler, S. Kolind, Y. Kong, P. Kudlička, P. Kuntke, N. D. Kurniawan, S. Kusmia, R. Labounek, M. M. Laganà, C. Laule, C. S. Law, C. Lenglet, T. Leutritz, Y. Liu, S. Llufriu, S. Mackey, E. Martinez-Heras, L. Mattera, I. Nestrasil, K. P. O'Grady, N. Papinutto, D. Papp, D. Pareto, T. B. Parrish, A. Pichiecchio, F. Prados, À. Rovira, M. J. Ruitenberg, R. S. Samson, G. Savini, M. Seif, A. C. Seifert, A. K. Smith, S. A. Smith, Z. A. Smith, E. Solana, Y. Suzuki, G. Tackley, A. Tinnermann, J. Valošek, D. Van De Ville, M. C. Yiannakas, K. A. Weber, 2nd, N. Weiskopf, R. G. Wise, P. O. Wyss, and J. Xu, "Generic acquisition protocol for quantitative MRI of the spinal cord," *Nat. Protoc.*, vol. 16, no. 10, pp. 4611–4632, Oct. 2021.

[14] N. Papinutto and R. G. Henry, "Evaluation of intra-and interscanner reliability of MRI protocols for spinal cord gray matter and total cross-sectional area measurements," *J. Magn. Reson. Imaging*, vol. 49, no. 4, pp. 1078–1090, 2019.

[15] C. Chien, V. Juenger, M. Scheel, A. U. Brandt, and F. Paul, "Considerations for mean upper cervical cord area implementation in a longitudinal MRI setting: Methods, interrater reliability, and MRI quality control," *AJNR Am. J. Neuroradiol.*, vol. 41, no. 2, pp. 343–350, Feb. 2020.

[16] D. W. Cadotte, A. Cadotte, J. Cohen-Adad, D. Fleet, M. Livne, J. R. Wilson, D. Mikulis, N. Nugaeva, and M. G. Fehlings, "Characterizing the location of spinal and vertebral levels in the human cervical spinal cord," *AJNR Am. J. Neuroradiol.*, vol. 36, no. 4, pp. 803–810, Apr. 2015.

[17] P. W. Stroman, C. R. Figley, and C. M. Cahill, "Spatial normalization, bulk motion correction and coregistration for functional magnetic resonance imaging of the human cervical spinal cord and brainstem," *Magn. Reson. Imaging*, vol. 26, no. 6, pp. 809–814, Jul. 2008.

[18] M. Amann, S. Pezold, Y. Naegelin, K. Fundana, M. Andělová, K. Weier, C. Stippich, L. Kappos, E.-W. Radue, P. Cattin, and T. Sprenger, "Reliable volumetry of the cervical spinal cord in MS patient follow-up data with cord image analyzer (cordial)," *J. Neurol.*, vol. 263, no. 7, pp. 1364–1374, Jul. 2016.

[19] C. Tsagkas, A. Altermatt, U. Bonati, S. Pezold, J. Reinhard, M. Amann, P. Cattin, J. Wuerfel, D. Fischer, K. Parmar, and A. Fischmann, "Reliable and fast volumetry of the lumbar spinal cord using cord image analyser (cordial)," *Eur. Radiol.*, vol. 28, no. 11, pp. 4488–4495, Nov. 2018.

[20] P. Bautin and J. Cohen-Adad, "Minimum detectable spinal cord atrophy with automatic segmentation: Investigations using an open-access dataset of healthy participants," *Neuroimage Clin*, vol. 32, p. 102849, Oct. 2021.

[21] M. K. Ganapathy, V. Reddy, and P. Tadi, "Neuroanatomy, spinal cord morphology," in *StatPearls*. Treasure Island (FL): StatPearls Publishing, Oct. 2022.

[22] O. Bican, A. Minagar, and A. A. Pruitt, "The spinal cord: a review of functional neuroanatomy," *Neurol. Clin.*, vol. 31, no. 1, pp. 1–18, Feb. 2013.

[23] R. S. Tubbs, M. Loukas, J. B. Slappey, M. M. Shoja, W. J. Oakes, and E. G. Salter, "Clinical anatomy of the C1 dorsal root, ganglion, and ramus: a review and anatomical study," *Clin. Anat.*, vol. 20, no. 6, pp. 624–627, Aug. 2007.

[24] E. Diaz and H. Morales, "Spinal cord anatomy and clinical syndromes," *Semin. Ultrasound CT MR*, vol. 37, no. 5, pp. 360–371, Oct. 2016.

[25] A. Mendez, R. Islam, T. Latypov, P. Basa, O. J. Joseph, B. Knudsen, A. M. Siddiqui, P. Summer, L. J. Staehnke, P. J. Grahn, N. Lachman, A. J. Windebank, and I. A. Lavrov, "Segment-Specific orientation of the dorsal and ventral roots for precise therapeutic targeting of human spinal cord," *Mayo Clin. Proc.*, vol. 96, no. 6, pp. 1426–1437, Jun. 2021.

[26] N. Boonpirak and W. Apinhasmit, "Length and caudal level of termination of the spinal cord in thai adults," *Acta Anat.*, vol. 149, no. 1, pp. 74–78, 1994.

[27] B. De Leener, V. S. Fonov, D. L. Collins, V. Callot, N. Stikov, and J. Cohen-Adad, "PAM50: Unbiased multimodal template of the brainstem and spinal cord aligned with the ICBM152 space," *Neuroimage*, vol. 165, pp. 170–179, Jan. 2018.

[28] J. K. Mai and G. Paxinos, *The Human Nervous System*. Academic Press, Dec. 2011.

[29] A. Frostell, R. Hakim, E. P. Thelin, P. Mattsson, and M. Svensson, "A review of the segmental diameter of the healthy human spinal cord," *Front. Neurol.*, vol. 7, p. 238, Dec. 2016.

[30] B. De Leener, S. Lévy, S. M. Dupont, V. S. Fonov, N. Stikov, D. Louis Collins, V. Callot, and J. Cohen-Adad, "SCT: Spinal cord toolbox, an open-source software for processing spinal cord MRI data," *Neuroimage*, vol. 145, no. Pt A, pp. 24–43, Jan. 2017.

[31] C. Gros, B. De Leener, S. M. Dupont, A. R. Martin, M. G. Fehlings, R. Bakshi, S. Tummala, V. Auclair, D. G. McLaren, V. Callot, J. Cohen-Adad, and M. Sdika, "Automatic spinal cord localization, robust to MRI contrasts using global curve optimization," *Med. Image Anal.*, vol. 44, pp. 215–227, Feb. 2018.

[32] L. E. Bilston and L. E. Thibault, "Biomechanics of cervical spinal cord injury in flexion and extension: A physical model to estimate spinal cord deformations," *Int. J. Crashworthiness*, vol. 2, no. 2, pp. 207–218, Jan. 1997.

[33] P. Sudres, M. Evin, P.-J. Arnoux, and V. Callot, "Cervical canal morphology: Effects of neck flexion in normal condition: New elements for biomechanical simulations and surgical management," *Spine*, vol. 45, no. 16, pp. 1102–1109, Aug. 2020.

[34] Y. Mina, S. Azodi, T. Dubuche, F. Andrada, I. Osuorah, J. Ohayon, I. Cortese, T. Wu, K. R. Johnson, D. S. Reich, G. Nair, and S. Jacobson, "Cervical and thoracic cord atrophy in multiple sclerosis phenotypes: Quantification and correlation with clinical disability," *Neuroimage Clin*, vol. 30, p. 102680, Apr. 2021.

[35] M. Horáková, T. Horák, J. Valošek, T. Rohan, E. Koriťáková, M. Dostál, J. Kočica, T. Skutil, M. Keřkovský, Z. Kadaňka, Jr, P. Bednařík, A. Svátková, P. Hluštík, and J. Bednařík, "Semi-automated detection of cervical spinal cord compression with the spinal cord toolbox," *Quant. Imaging Med. Surg.*, vol. 12, no. 4, pp. 2261–2279, Apr. 2022.

[36] M. A. Rocca, P. Valsasina, A. Meani, C. Gobbi, C. Zecca, À. Rovira, X. Montalban, H. Kearney, O. Ciccarelli, L. Matthews, J. Palace, A. Gallo, A. Bisecco, A. Gass, P. Eisele, C. Lukas, B. Bellenberg, F. Barkhof, H. Vrenken, P. Preziosa, G. Comi, M. Filippi, and MAGNIMS Study Group, "Clinically relevant cranio-caudal patterns of cervical cord atrophy evolution in MS," *Neurology*, vol. 93, no. 20, pp. e1852–e1866, Nov. 2019.

[37] A. R. Martin, B. De Leener, J. Cohen-Adad, D. W. Cadotte, S. Kalsi-Ryan, S. F. Lange, L. Tetreault, A. Nouri, A. Crawley, D. J. Mikulis, and Others, "Clinically feasible microstructural MRI to quantify cervical spinal cord tissue injury using DTI, MT, and t2*-weighted imaging: assessment of normative data and reliability," *AJNR Am. J. Neuroradiol.*, vol. 38, no. 6, pp. 1257–1265, 2017.

[38] V. P. B. Grover, J. M. Tognarelli, M. M. E. Crossey, I. J. Cox, S. D. Taylor-Robinson, and M. J. W. McPhail, "Magnetic resonance imaging: Principles and techniques: Lessons for clinicians," *J. Clin. Exp. Hepatol.*, vol. 5, no. 3, pp. 246–255, Sep. 2015.

[39] C. Casserly, E. E. Seyman, P. Alcaide-Leon, M. Guenette, C. Lyons, S. Sankar, A. Svendrovski, S. Baral, and J. Oh, "Spinal cord atrophy in multiple sclerosis: A systematic review and meta-analysis," *J. Neuroimaging*, vol. 28, no. 6, pp. 556–586, Nov. 2018.

[40] J. Galley, R. Sutter, C. Germann, F. Wanivenhaus, and D. Nanz, "High-resolution in vivo MR imaging of intraspinal cervical nerve rootlets at 3 and 7 tesla," *Eur. Radiol.*, vol. 31, no. 7, pp. 4625–4633, Jul. 2021.

[41] J. Cohen-Adad, E. Alonso-Ortiz, S. Alley, M. M. Lagana, F. Baglio, S. J. Vannesjo, H. Karbasforoushan, M. Seif, A. C. Seifert, J. Xu, J.-W. Kim, R. Labounek, L. Vojtíšek, M. Dostál, J. Valošek, R. S. Samson, F. Grussu, M. Battiston, C. A. M. Gandini Wheeler-Kingshott, M. C. Yiannakas, G. Gilbert, T. Schneider, B. Johnson, and F. Prados, "Comparison of multicenter MRI protocols for visualizing the spinal cord gray matter," *Magn. Reson. Med.*, vol. 88, no. 2, pp. 849–859, Aug. 2022.

[42] Y. Liu, X. Zhou, J. Ma, Y. Ge, and X. Cao, "The diameters and number of nerve fibers in spinal nerve roots," *J. Spinal Cord Med.*, vol. 38, no. 4, pp. 532–537, Jul. 2015.

[43] D. Ravi, Alzheimer's Disease Neuroimaging Initiative, F. Barkhof, D. C. Alexander, L. Puglisi, G. J. M. Parker, and A. Eshaghi, "An efficient semi-supervised quality control system trained using physics-based MRI-artefact generators and adversarial training," *Med. Image Anal.*, vol. 91, p. 103033, Jan. 2024.

[44] N. Papinutto, R. Bakshi, A. Bischof, P. A. Calabresi, E. Caverzasi, R. T. Constable, E. Datta, G. Kirkish, G. Nair, J. Oh, D. Pelletier, D. L. Pham, D. S. Reich, W. Rooney, S. Roy, D. Schwartz, R. T. Shinohara, N. L. Sicotte, W. A. Stern, I. Tagge, S. Tauhid, S. Tummala, R. G. Henry, and North American Imaging in Multiple Sclerosis Cooperative(NAIMS), "Gradient nonlinearity effects on upper cervical spinal cord area measurement from 3D T1 -weighted brain MRI acquisitions," *Magn. Reson. Med.*, vol. 79, no. 3, pp. 1595–1601, Mar. 2018.

[45] F. Barkhof, M. Filippi, D. H. Miller, P. Scheltens, A. Campi, C. H. Polman, G. Comi, H. J. Adèr, N. Losseff, and J. Valk, "Comparison of MRI criteria at first presentation to predict conversion to clinically definite multiple sclerosis," *Brain*, vol. 120 (Pt 11), pp. 2059–2069, Nov. 1997.

[46] A. R. Martin, B. De Leener, J. Cohen-Adad, D. W. Cadotte, A. Nouri, J. R. Wilson, L. Tetreault, A. P. Crawley, D. J. Mikulis, H. Ginsberg, and M. G. Fehlings, "Can microstructural MRI detect subclinical tissue injury in subjects with asymptomatic

cervical spinal cord compression? a prospective cohort study," *BMJ Open*, vol. 8, no. 4, p. e019809, Apr. 2018.

[47] A. R. Martin, B. De Leener, J. Cohen-Adad, S. Kalsi-Ryan, D. W. Cadotte, J. R. Wilson, L. Tetreault, A. Nouri, A. Crawley, D. J. Mikulis, H. Ginsberg, E. M. Massicotte, and M. G. Fehlings, "Monitoring for myelopathic progression with multiparametric quantitative MRI," *PLoS One*, vol. 13, no. 4, p. e0195733, Apr. 2018.

[48] A. R. Martin, B. De Leener, J. Cohen-Adad, D. W. Cadotte, S. Kalsi-Ryan, S. F. Lange, L. Tetreault, A. Nouri, A. Crawley, D. J. Mikulis, H. Ginsberg, and M. G. Fehlings, "A novel MRI biomarker of spinal cord white matter injury: T2*-Weighted white matter to gray matter signal intensity ratio," *AJNR Am. J. Neuroradiol.*, vol. 38, no. 6, pp. 1266–1273, Jun. 2017.

[49] S. Garg and S. R. Bhagyashree, "Spinal cord MRI segmentation techniques and algorithms: A survey," *SN Computer Science*, vol. 2, no. 3, p. 229, Apr. 2021.

[50] M. Moccia, S. Ruggieri, A. Ianniello, A. Toosy, C. Pozzilli, and O. Ciccarelli, "Advances in spinal cord imaging in multiple sclerosis," *Ther. Adv. Neurol. Disord.*, vol. 12, p. 1756286419840593, Apr. 2019.

[51] E. Ullmann, J. F. Pelletier Paquette, W. E. Thong, and J. Cohen-Adad, "Automatic labeling of vertebral levels using a robust template-based approach," *Int. J. Biomed. Imaging*, vol. 2014, p. 719520, Jul. 2014.

[52] W. Mbarki, M. Bouchouicha, S. Frizzi, F. Tshibasu, L. B. Farhat, and M. Sayadi, "Lumbar spine discs classification based on deep convolutional neural networks using axial view MRI," *Interdisciplinary Neurosurgery*, vol. 22, p. 100837, Dec. 2020.

[53] M. Vania and D. Lee, "Intervertebral disc instance segmentation using a multistage optimization mask-RCNN (MOM-RCNN)," *Finite Elem. Anal. Des.*, vol. 8, no. 4, pp. 1023–1036, Jun. 2021.

[54] L. Rouhier, F. P. Romero, J. P. Cohen, and J. Cohen-Adad, "Spine intervertebral disc labeling using a fully convolutional redundant counting model," Mar. 2020.

[55] A. Bozorgpour, B. Azad, R. Azad, Y. Velichko, U. Bagci, and D. Merhof, "HCA-Net: Hierarchical context attention network for intervertebral disc semantic labeling," Nov. 2023.

[56] A. Jamaludin, T. Kadir, and A. Zisserman, "SpineNet: Automated classification and evidence visualization in spinal MRIs," *Med. Image Anal.*, vol. 41, pp. 63–73, Oct. 2017.

[57] R. Azad, L. Rouhier, and J. Cohen-Adad, "Stacked hourglass network with a multi-level attention mechanism: Where to look for intervertebral disc labeling," in *Machine Learning in Medical Imaging*. Springer International Publishing, 2021, pp. 406–415.

[58] C. Gros, B. De Leener, A. Badji, J. Maranzano, D. Eden, S. M. Dupont, J. Talbott, R. Zhuoquiong, Y. Liu, T. Granberg, R. Ouellette, Y. Tachibana, M. Hori, K. Kamiya, L. Chougar, L. Stawiarz, J. Hillert, E. Bannier, A. Kerbrat, G. Edan, P. Labauge, V. Callot, J. Pelletier, B. Audoin, H. Rasoanandrianina, J.-C. Brisset, P. Valsasina, M. A. Rocca, M. Filippi, R. Bakshi, S. Tauhid, F. Prados, M. Yiannakas, H. Kearney, O. Ciccarelli, S. Smith, C. A. Treaba, C. Mainero, J. Lefeuvre, D. S. Reich, G. Nair, V. Auclair, D. G. McLaren, A. R. Martin, M. G. Fehlings, S. Vahdat, A. Khatibi, J. Doyon, T. Shepherd, E. Charlson, S. Narayanan, and J. Cohen-Adad, "Automatic segmentation of the spinal cord and intramedullary multiple sclerosis lesions with convolutional neural networks," *Neuroimage*, vol. 184, pp. 901–915, Jan. 2019.

[59] H. Kearney, M. C. Yiannakas, K. Abdel-Aziz, C. A. M. Wheeler-Kingshott, D. R. Altmann, O. Ciccarelli, and D. H. Miller, "Improved MRI quantification of spinal cord atrophy in multiple sclerosis," *J. Magn. Reson. Imaging*, vol. 39, no. 3, pp. 617–623, Mar. 2014.

[60] G. Kim, F. Khalid, V. V. Oommen, S. Tauhid, R. Chu, M. A. Horsfield, B. C. Healy, and R. Bakshi, "T1- vs. t2-based MRI measures of spinal cord volume in healthy subjects and patients with multiple sclerosis," *BMC Neurol.*, vol. 15, no. 1, p. 124, Jul. 2015.

[61] S. Bédard, N. K. Enamundram, C. Tsagkas, E. Pravatà, C. Granziera, A. Smith, K. A. Weber, II, and J. Cohen-Adad, "Towards contrast-agnostic soft segmentation of the spinal cord," Oct. 2023.

[62] C. Engl, P. Schmidt, M. Arsic, C. C. Boucard, V. Biberacher, M. Röttinger, T. Etgen, S. Nunnemann, N. Koutsouleris, M. Reiser, E. M. Meisenzahl, and M. Mühlau, "Brain size and white matter content of cerebrospinal tracts determine the upper cervical cord area: evidence from structural brain MRI," *Neuroradiology*, vol. 55, no. 8, pp. 963–970, Aug. 2013.

[63] W. Rashid, G. R. Davies, D. T. Chard, C. M. Griffin, D. R. Altmann, R. Gordon, R. Kapoor, A. J. Thompson, and D. H. Miller, "Upper cervical cord area in early

relapsing-remitting multiple sclerosis: cross-sectional study of factors influencing cord size," *J. Magn. Reson. Imaging*, vol. 23, no. 4, pp. 473–476, Apr. 2006.

[64] A. C. Laing, E. C. Brenneman, A. Yung, J. Liu, P. Kozlowski, and T. Oxland, "The effects of age on the morphometry of the cervical spinal cord and spinal column in adult rats: an MRI-based study," *Anat. Rec.*, vol. 297, no. 10, pp. 1885–1895, Oct. 2014.

[65] M. Yanase, Y. Matsuyama, K. Hirose, H. Takagi, M. Yamada, H. Iwata, and N. Ishiguro, "Measurement of the cervical spinal cord volume on MRI," *J. Spinal Disord. Tech.*, vol. 19, no. 2, pp. 125–129, Apr. 2006.

[66] N. Papinutto, R. Schlaeger, V. Panara, A. H. Zhu, E. Caverzasi, W. A. Stern, S. L. Hauser, and R. G. Henry, "Age, gender and normalization covariates for spinal cord gray matter and total Cross-Sectional areas at cervical and thoracic levels: A 2D phase sensitive inversion recovery imaging study," *PLoS One*, vol. 10, no. 3, p. e0118576, 2015.

[67] M. Ishikawa, M. Matsumoto, Y. Fujimura, K. Chiba, and Y. Toyama, "Changes of cervical spinal cord and cervical spinal canal with age in asymptomatic subjects," *Spinal Cord*, vol. 41, no. 3, pp. 159–163, Mar. 2003.

[68] F. Kato, Y. Yukawa, K. Suda, M. Yamagata, and T. Ueta, "Normal morphology, age-related changes and abnormal findings of the cervical spine. part II: magnetic resonance imaging of over 1,200 asymptomatic subjects," *Eur. Spine J.*, vol. 21, no. 8, pp. 1499–1507, 2012.

[69] S. Terao, G. Sobue, Y. Hashizume, N. Shimada, and T. Mitsuma, "Age-related changes of the myelinated fibers in the human corticospinal tract: a quantitative analysis," *Acta Neuropathol.*, vol. 88, no. 2, pp. 137–142, 1994.

[70] M. P. Sanfilipo, R. H. B. Benedict, R. Zivadinov, and R. Bakshi, "Correction for intracranial volume in analysis of whole brain atrophy in multiple sclerosis: the proportion vs. residual method," *Neuroimage*, vol. 22, no. 4, pp. 1732–1743, Aug. 2004.

[71] E. M. Kesenheimer, M. J. Wendebourg, M. Weigel, C. Weidensteiner, T. Haas, L. Richter, L. Sander, A. Horvath, M. Barakovic, P. Cattin, C. Granziera, O. Bieri, and R. Schlaeger, "Normalization of spinal cord total Cross-Sectional and gray matter areas as quantified with radially sampled averaged magnetization inversion recovery acquisitions," *Front. Neurol.*, vol. 12, p. 637198, Mar. 2021.

[72] S. Narayanan, D. L. Collins, S. Francis, and D. L. Arnold, "Spinal cord cross-sectional area correlates with brain and intra-cranial volume," *Proc. Intl. Soc. Mag. Reson. Med.*, vol. 11, p. 270, 2003.

[73] D. H. Mathalon, E. V. Sullivan, J. M. Rawles, and A. Pfefferbaum, "Correction for head size in brain-imaging measurements," *Psychiatry Res.*, vol. 50, no. 2, pp. 121–139, Jun. 1993.

[74] J. Oh, M. Seigo, S. Saidha, E. Sotirchos, K. Zackowski, M. Chen, J. Prince, M. Diener-West, P. A. Calabresi, and D. S. Reich, "Spinal cord normalization in multiple sclerosis," *J. Neuroimaging*, vol. 24, no. 6, pp. 577–584, Nov. 2014.

[75] B. C. Healy, A. Arora, D. L. Hayden, A. Ceccarelli, S. S. Tauhid, M. Neema, and R. Bakshi, "Approaches to normalization of spinal cord volume: application to multiple sclerosis," *J. Neuroimaging*, vol. 22, no. 3, pp. e12–9, Jul. 2012.

[76] S. Ruggieri, M. Petracca, L. De Giglio, F. De Luca, C. Giannì, F. Gurreri, N. Petsas, S. Tommasin, C. Pozzilli, and P. Pantano, "A matter of atrophy: differential impact of brain and spine damage on disability worsening in multiple sclerosis," *J. Neurol.*, May 2021.

[77] R. Bonacchi, E. Pagani, A. Meani, L. Cacciaguerra, P. Preziosa, E. De Meo, M. Filippi, and M. A. Rocca, "Clinical relevance of multiparametric MRI assessment of cervical cord damage in multiple sclerosis," *Radiology*, vol. 296, no. 3, pp. 605–615, Sep. 2020.

[78] L. Fradet, P.-J. Arnoux, J.-P. Ranjeva, Y. Petit, and V. Callot, "Morphometrics of the entire human spinal cord and spinal canal measured from in vivo high-resolution anatomical magnetic resonance imaging," *Spine*, vol. 39, no. 4, pp. E262–9, Feb. 2014.

[79] K. L. Miller, F. Alfaro-Almagro, N. K. Bangerter, D. L. Thomas, E. Yacoub, J. Xu, A. J. Bartsch, S. Jbabdi, S. N. Sotiropoulos, J. L. R. Andersson, L. Griffanti, G. Douaud, T. W. Okell, P. Weale, I. Dragonu, S. Garratt, S. Hudson, R. Collins, M. Jenkinson, P. M. Matthews, and S. M. Smith, "Multimodal population brain imaging in the UK biobank prospective epidemiological study," *Nat. Neurosci.*, vol. 19, no. 11, pp. 1523–1536, Nov. 2016.

[80] M. F. Glasser, S. N. Sotiropoulos, J. A. Wilson, T. S. Coalson, B. Fischl, J. L. Andersson, J. Xu, S. Jbabdi, M. Webster, J. R. Polimeni, D. C. Van Essen, and M. Jenkinson, "The minimal preprocessing pipelines for the human connectome project," *Neuroimage*, vol. 80, pp. 105–124, Oct. 2013.

[81] F. Alfaro-Almagro, M. Jenkinson, N. K. Bangerter, J. L. R. Andersson, L. Griffanti, G. Douaud, S. N. Sotiropoulos, S. Jbabdi, M. Hernandez-Fernandez, E. Vallee, D. Vidaurre, M. Webster, P. McCarthy, C. Rorden, A. Daducci, D. C. Alexander, H. Zhang, I. Dragonu, P. M. Matthews, K. L. Miller, and S. M. Smith, "Image processing and quality control for the first 10,000 brain imaging datasets from UK biobank," *Neuroimage*, vol. 166, pp. 400–424, Feb. 2018.

[82] Toutenburg, H., Draper, N., and H. Smith, *Applied regression analysis*, J. W. . Sons, Ed. New York: Wiley, 1969, vol. 11.

[83] M. A. Rocca, S. Mesaros, E. Pagani, M. P. Sormani, G. Comi, and M. Filippi, "Thalamic damage and long-term progression of disability in multiple sclerosis," *Radiology*, vol. 257, no. 2, pp. 463–469, Nov. 2010.

[84] A. Eshaghi, F. Prados, W. J. Brownlee, D. R. Altmann, C. Tur, M. J. Cardoso, F. De Angelis, S. H. van de Pavert, N. Cawley, N. De Stefano, M. L. Stromillo, M. Battaglini, S. Ruggieri, C. Gasperini, M. Filippi, M. A. Rocca, A. Rovira, J. Sastre-Garriga, H. Vrenken, C. E. Leurs, J. Killestein, L. Pirpamer, C. Enzinger, S. Ourselin, C. A. M. G. Wheeler-Kingshott, D. Chard, A. J. Thompson, D. C. Alexander, F. Barkhof, O. Ciccarelli, and MAGNIMS study group, "Deep gray matter volume loss drives disability worsening in multiple sclerosis," *Ann. Neurol.*, vol. 83, no. 2, pp. 210–222, Feb. 2018.

[85] C. J. Azevedo, S. Y. Cen, S. Khadka, S. Liu, J. Kornak, Y. Shi, L. Zheng, S. L. Hauser, and D. Pelletier, "Thalamic atrophy in multiple sclerosis: A magnetic resonance imaging marker of neurodegeneration throughout disease," *Ann. Neurol.*, vol. 83, no. 2, pp. 223–234, Feb. 2018.

[86] S. Schönecker, C. Neuhofer, M. Otto, A. Ludolph, J. Kassubek, B. Landwehrmeyer, S. Anderl-Straub, E. Semler, J. Diehl-Schmid, C. Prix, C. Vollmar, J. Fortea, Deutsches FTLD-Konsortium, H.-J. Huppertz, T. Arzberger, D. Edbauer, B. Feddersen, M. Dieterich, M. L. Schroeter, A. E. Volk, K. Fließbach, A. Schneider, J. Kornhuber, M. Maler, J. Prudlo, H. Jahn, T. Boeckh-Behrens, A. Danek, T. Klopstock, and J. Levin, "Atrophy in the thalamus but not cerebellum is specific for c9orf72 FTD and ALS patients - an Atlas-Based volumetric MRI study," *Front. Aging Neurosci.*, vol. 10, p. 45, Mar. 2018.

[87] E. Finegan, S. L. Hi Shing, R. H. Chipika, M. C. McKenna, M. A. Doherty, J. C. Hengeveld, A. Vajda, C. Donaghy, R. L. McLaughlin, S. Hutchinson, O. Hardiman,

and P. Bede, "Thalamic, hippocampal and basal ganglia pathology in primary lateral sclerosis and amyotrophic lateral sclerosis: Evidence from quantitative imaging data," *Data Brief*, vol. 29, p. 105115, Apr. 2020.

[88] H. Foo, E. Mak, T. T. Yong, M. C. Wen, R. J. Chander, W. L. Au, Y. Y. Sitoh, L. C. S. Tan, and N. Kandiah, "Progression of subcortical atrophy in mild parkinson's disease and its impact on cognition," *Eur. J. Neurol.*, vol. 24, no. 2, pp. 341–348, Feb. 2017.

[89] C. Lukas, B. Bellenberg, F. Prados, P. Valsasina, K. Parmar, I. Brouwer, D. Pareto, À. Rovira, J. Sastre-Garriga, C. A. Gandini Wheeler-Kingshott, L. Kappos, M. A. Rocca, M. Filippi, M. Yiannakas, F. Barkhof, and H. Vrenken, "Quantification of cervical cord Cross-Sectional area: Which acquisition, vertebra level, and analysis software? a multicenter repeatability study on a traveling healthy volunteer," 2021.

[90] M. M. Weeda, S. M. Middelkoop, M. D. Steenwijk, M. Daams, H. Amiri, I. Brouwer, J. Killestein, B. M. J. Uitdehaag, I. Dekker, C. Lukas, B. Bellenberg, F. Barkhof, P. J. W. Pouwels, and H. Vrenken, "Validation of mean upper cervical cord area (MUCCA) measurement techniques in multiple sclerosis (MS): High reproducibility and robustness to lesions, but large software and scanner effects," *Neuroimage Clin*, vol. 24, p. 101962, Aug. 2019.

[91] J. Lang and C. T. Bartram, "Fila radicularia of the ventral and dorsal radices of the human spinal cord," *Gegenbaurs Morphol. Jahrb.*, vol. 128, no. 4, pp. 417–462, 1982.

[92] T. J. Torrico and S. Munakomi, "Neuroanatomy, thalamus," https://europepmc.org/article/nbk/nbk542184, accessed: 2022-9-27.

[93] G. J. Giesler, Jr, H. R. Spiel, and W. D. Willis, "Organization of spinothalamic tract axons within the rat spinal cord," *J. Comp. Neurol.*, vol. 195, no. 2, pp. 243–252, Jan. 1981.

[94] C. J. Hodge, Jr and A. V. Apkarian, "The spinothalamic tract," *Crit. Rev. Neurobiol.*, vol. 5, no. 4, pp. 363–397, 1990.

[95] N. Cawley, C. Tur, F. Prados, D. Plantone, H. Kearney, K. Abdel-Aziz, S. Ourselin, C. A. G. Wheeler-Kingshott, D. H. Miller, A. J. Thompson, and O. Ciccarelli, "Spinal cord atrophy as a primary outcome measure in phase II trials of progressive multiple sclerosis," *Mult. Scler.*, vol. 24, no. 7, pp. 932–941, Jun. 2018.

[96] S. Schading, M. Seif, T. Leutritz, M. Hupp, A. Curt, N. Weiskopf, and P. Freund, "Reliability of spinal cord measures based on synthetic t1-weighted MRI derived from multiparametric mapping (MPM)," *Neuroimage*, vol. 271, p. 120046, May 2023.

[97] M. Seif, T. Leutritz, S. Schading, T. Emmengger, A. Curt, N. Weiskopf, and P. Freund, "Reliability of multi-parameter mapping (MPM) in the cervical cord: A multi-center multi-vendor quantitative MRI study," *Neuroimage*, vol. 264, p. 119751, Dec. 2022.

[98] K. Abdel-Aziz, T. Schneider, B. S. Solanky, M. C. Yiannakas, D. R. Altmann, C. A. M. Wheeler-Kingshott, A. L. Peters, B. L. Day, A. J. Thompson, and O. Ciccarelli, "Evidence for early neurodegeneration in the cervical cord of patients with primary progressive multiple sclerosis," *Brain*, vol. 138, no. Pt 6, pp. 1568–1582, Jun. 2015.

[99] S. Szotek, J. Dawidowicz, M. Geniusz, M. Kozak, R. Łukomski, and A. Czogalla, "The biomechanical characteristics of spinal dura mater in the context of its basic morphology," *Acta Bioeng. Biomech.*, vol. 23, no. 4, 2021.

[100] J. D. Reid, "Effects of flexion-extension movements of the head and spine upon the spinal cord and nerve roots," *J. Neurol. Neurosurg. Psychiatry*, vol. 23, no. 3, pp. 214–221, Aug. 1960.

[101] S. Bédard and J. Cohen-Adad, "Automatic measure and normalization of spinal cord cross-sectional area using the pontomedullary junction," *Front. Neuroimaging*, vol. 1, Nov. 2022.

[102] P. Coupe, P. Yger, S. Prima, P. Hellier, C. Kervrann, and C. Barillot, "An optimized blockwise nonlocal means denoising filter for 3-D magnetic resonance images," *IEEE Trans. Med. Imaging*, vol. 27, no. 4, pp. 425–441, Apr. 2008.

[103] J. L. Sherman, P. Y. Nassaux, and C. M. Citrin, "Measurements of the normal cervical spinal cord on MR imaging," *AJNR Am. J. Neuroradiol.*, vol. 11, no. 2, pp. 369–372, Mar. 1990.

[104] R. J. V. Bartlett, C. A. Rowland Hill, A. S. Rigby, S. Chandrasekaran, and H. Narayanamurthy, "MRI of the cervical spine with neck extension: is it useful?" pp. 1044–1051, 2012.

[105] M. P. Bazylewicz, F. Berkowitz, and A. Sayah, "3D T2 MR Imaging–Based measurements of the posterior cervical thecal sac in flexion and extension for cervical puncture," *AJNR Am. J. Neuroradiol.*, vol. 37, no. 3, pp. 579–583, Mar. 2016.

[106] S. Bédard and J. Cohen-Adad, "PMJ BIDS dataset," 2023.

[107] S. Mesbah, A. Herrity, B. Ugiliweneza, C. Angeli, Y. Gerasimenko, M. Boakye, and S. Harkema, "Neuroanatomical mapping of the lumbosacral spinal cord in individuals with chronic spinal cord injury," *Brain Commun*, vol. 5, no. 1, p. fcac330, 2023.

[108] B. Schatlo, L. Remonda, P. Gruber, J. Fandino, V. Rohde, A.-R. Fathi, and J. Berberat, "Cervical spine prospective feasibility study : Dynamic Flexion-Extension Diffusion-Tensor weighted magnetic resonance imaging," *Clin. Neuroradiol.*, vol. 29, no. 3, pp. 523–532, Sep. 2019.

[109] L. Nigro, P. Donnarumma, R. Tarantino, M. Rullo, A. Santoro, and R. Delfini, "Static and dynamic cervical MRI: two useful exams in cervical myelopathy," *J Spine Surg*, vol. 3, no. 2, pp. 212–216, Jun. 2017.

[110] E. L. Lord, R. Alobaidan, S. Takahashi, J. R. Cohen, C. J. Wang, B. J. Wang, and J. C. Wang, "Kinetic magnetic resonance imaging of the cervical spine: a review of the literature," *Global Spine J*, vol. 4, no. 2, pp. 121–128, Jun. 2014.

[111] G. Michelini, A. Corridore, S. Torlone, F. Bruno, C. Marsecano, R. Capasso, F. Caranci, A. Barile, C. Masciocchi, and A. Splendiani, "Dynamic MRI in the evaluation of the spine: state of the art," *Acta Biomed.*, vol. 89, no. 1-S, pp. 89–101, Jan. 2018.

[112] J. Valosek, T. Mathieu, R. Schlienger, O. S. Kowalczyk, and J. Cohen-Adad, "Automatic segmentation of the spinal cord nerve rootlets," Feb. 2024.

APPENDIX A MY CONTRIBUTIONS

The research conducted throughout my Master's studies extended beyond the scope of this thesis. Due to constraints on space, certain projects could not be included. Below is an overview of the publications and work submitted during my Master's studies.

A.1 Scientific Publications

* Co-first authorship

Published Articles

- Valošek, J.*, **Bédard, S.***, et al., (2024). *A database of the healthy human spinal cord morphometry in the PAM50 template space.* Imaging Neuroscience, https://doi.org/10.1162/imag_a_00075.
- **Bédard, S.**, Bouthillier, M. & Cohen-Adad, J. (2023). *Pontomedullary junction as a reference for spinal cord cross-sectional area: validation across neck positions.* Sci Rep 13, 13527. https://doi.org/10.1038/s41598-023-40731-3
- **Bédard, S.**, & Cohen-Adad, J. (2022). *Automatic measure and normalization of spinal cord cross-sectional area using the pontomedullary junction*, Frontiers in Neuroimaging, 1. https://doi.org/10.3389/fnimg.2022.1031253

Articles Under Review

- **Bédard, S. ***, Valošek, J.*, *et al* (2024). *Normalizing Spinal Cord Compression Morphometric Measures: Application in Degenerative Cervical Myelopathy.* Journal of Neurosurgury: Spine. [Submitted], https://doi.org/10.1101/2024.03.13.24304177
- Muhammad, F., Weber, K.A., **Bédard, S.**, *et al.* (2024). *Cervical Spinal Cord Morphometrics in Degenerative Cervical Myelopathy: Quantification using Semi-automated Normalized Technique and Correlation with Neurological Dysfunctions.* The Spine Journal. [Submitted].
- **Bédard, S.***, Kartik, N.* *et al.* (2023), *Towards contrast-agnostic soft segmentation of the spinal cord.* Medical Image Analysis, [Under review]. https://doi.org/10.48550/arXiv.2310.15402.

A.2 Conference Abstracts

- **Bédard, S.** *et al.* (2024 - May 4-9). *Automatic spinal cord segmentation: Generalization across MR parameters, sites, vendors, and pathologies.* [Oral presentation]. 2024 ISMRM & ISMRT Annual Meeting & Exhibition ISMRM, Singapore.

- Valošek, J*, **Bédard, S.*** *et al.* (2024 - May 4-9). *Interactive database of spinal cord morphometry.* [Poster]. 2024 ISMRM & ISMRT Annual Meeting & Exhibition ISMRM, Singapore.

- **Bédard, S.***, Oliva, V.* *et al.* (2024). *Simultaneous brain-spinal cord functional MRI with a force-matching task.* [Poster]. 2024 Annual Meeting of the Organization for Human Brain Mapping (OHBM), Seoul, Korea.

- Oliva, V., **Bédard, S.***, *et al.* (2024). *Investigating full neuraxis correlates of hand dexterity* [Poster]. 2024 Annual Meeting of the Organization for Human Brain Mapping (OHBM), Seoul, Korea.

- Pfyffer, D., Kaptan, M., Law C., Weber, K., Oliva, V., **Bédard, S.** *et al.* (2024). *Corticospinal pain processing and modulation in fibromyalgia: a combined brain-cord fMRI study. dexterity.* [Poster]. 2024 Annual Meeting of the Organization for Human Brain Mapping (OHBM), Seoul, Korea.

- Pfyffer, D., Kaptan, M., Law C., Weber, K., Oliva, V., **Bédard, S.** *et al.* (2024). *Imaging Corticospinal Correlates of Aberrant Pain Processing and Modulation in Fibromyalgia Using Combined Brain-Spinal Cord Functional Magnetic Resonance Imaging.* [Poster] 2024 USASP Annual Scientific Meeting, Seattle, WA, USA.

- **Bédard, S.** *et al.* (2023 - June 3-8). *Contrast-agnostic segmentation of the spinal cord using deep learning.* [Oral presentation]. 2023 ISMRM & ISMRT Annual Meeting & Exhibition ISMRM, Toronto, ON, Canada.

- **Bédard, S.** et al. (2023 - July 22-26) *Normalizing Maximum Spinal Cord Compression for Robust Assessment of Spinal Cord Injury.* [Poster]. 2023 Annual Meeting of the Organization for Human Brain Mapping (OHBM), Montréal, QC, Canada.

- **Bédard, S.** *et al.* (2023 - July 22-26) *Contrast-agnostic segmentation of the spinal cord: Validation in a multi-center cohort.* [Poster]. 2023 Annual Meeting of the Organization for Human Brain Mapping (OHBM), Montréal, QC, Canada.

- Valošek, J., **Bédard, S.**, *et al.* (2023 - July 22-26) *Spinal cord cross-sectional area using a standardized protocol in multiple sclerosis.* [Poster]. 2023 Annual Meeting of the Organization for Human Brain Mapping (OHBM), Montréal, QC, Canada.

- **Bédard, S.**, *et al.* (May 2023) *Normative spinal cord MRI morphometrics database in a standard space.* [Oral presentation]. QBIN Scientific Day 2023, Québec, QC, Canada.

- Blostein, N., Banerjee, R., **Bédard, S.**, Shahrampour, S., De Leener, B., Mohamed, F. B., Middleton, D., Krisa, L., & Cohen-Adad, J. (May 2023). *Multimodal pediatric spinal cord template.* [Oral presentation]. QBIN Scientific Day 2023, Québec, QC, Canada.

A.3 Other Contributions

Throughout my Master's studies at Neuropoly Lab, I have contributed and helped maintaining two open source datasets: *Spine Generic* and *Spinal Cord Head Position MRI*. Briefly, I curated the datasets according to the BIDS convention and updated the preprocessing pipelines and associated data. I also helped maintain and curate other internal datasets. I also assisted my colleagues in the development of processing pipelines.

I actively contributed to the Spinal Cord Toolbox (SCT) software, developed at Neuropoly Lab. Briefly, I attended the developers' meetings, I helped users on the forum, helped fix bugs and developed new features. I was also a tutor for two SCT courses (2020, 2023), where I assisted researchers and clinicians in tailoring the software to their specific research needs.

Additionally, I had the opportunity to do a research internship at the Systems Neuroscience and Pain Lab at Stanford University for 5 months (Fall 2023). During that time, I used advanced MRI techniques to assess brain and spinal cord function and structure in participants with chronic cervical radiculopathy and healthy volunteers. I developed an automatic analysis pipeline for the spinal cord and integrated a quality control workflow. I also worked on a pilot study of simultaneous brain and spinal cord tasks functional MRI. This study involved the acquisition simultaneous brain-spine functional MRI during hand grip and finger tapping tasks. Additionally, I collected physiological and behavioral data and developed a processing pipeline for the spinal cord. From this internship work, I have two accepted conference abstracts (OHBM 2024) and I am preparing a manuscript.

A.4 Supervision

During my time as a Master's student, I had the opportunity to co-supervise two students with their 3rd individual project of their bachelors in biomedical engineering, William Sirois and Louis-Thomas Lapointe. William is working on the development of an automatic deep learning method for the segmentation of the spinal canal. Louis-Thomas is working on automatic segmentation of the nerve rootlets. I also supervised 4 engineering bachelor students during a summer internship regarding manual corrections of spinal cord segmentations in 2021.